October 2019

Behavior of Prestressed Concrete Bridges with Closure Pour Connections and Diaphragms

Gercelino Ramos

BEHAVIOR OF PRESTRESSED CONCRETE BRIDGES WITH CLOSURE POUR CONNECTIONS AND DIAPHRAGMS

A Thesis Presented

by

GERCELINO RAMOS

Submitted to the Graduate School of the
University of Massachusetts Amherst in partial fulfillment
of the requirements for the degree of

MASTER OF SCIENCE IN CIVIL ENGINEERING

SEPTEMBER 2019

Civil and Environmental Engineering

BEHAVIOR OF PRESTRESSED CONCRETE BRIDGES WITH CLOSURE POUR CONNECTIONS AND DIAPHRAGMS

A Thesis Presented

by

GERCELINO RAMOS

Approved as to style and content by:

_____
Sergio F. Brena, Chairperson

_____
Kara D. Peterman, Member

_____
John E. Tobiason, Department Head
Civil and Environmental Engineering Department

ACKNOWLEDGEMENTS

I would like to express my gratitude to the individuals who supported and helped me complete this project. Thank you to my advisor, Dr. Sergio Brena, for his support and guidance throughout the project. I am grateful to my committee member, Dr. Kara Peterman, for her assistance and feedback on the research. Thank you to Mark Gauthier and Jorge Rivera for their help during the experiments. Additionally, I would like to thank my family for their tremendous support throughout my years in graduate school.

ABSTRACT

BEHAVIOR OF PRESTRESSED CONCRETE BRIDGES WITH CLOSURE POUR CONNECTIONS AND DIAPHRAGMS

SEPTEMBER 2019

GERCELINO RAMOS, B.S., UNIVERSITY OF MASSACHUSETTS AMHERST

M.S.C.E., UNIVERSITY OF MASSACHUSETTS AMHERST

Directed by: Professor Sergio F. Brena

Accelerated Bridge Construction (ABC) has gained substantial popularity in new bridge construction and bridge deck replacement because it offers innovative construction techniques that result in time and cost savings when compared to traditional bridge construction practice. One technology commonly implemented in ABC to effectively execute its projects is the use of prefabricated bridge components (precast/prestressed bridge components). Precast/prestressed bridge components are fabricated offsite or near the site and then connected on-site using small volume closure pour connections. Diaphragms are also commonly used to strengthen the connection between certain prefabricated components used in ABC, such as beam elements. Bridges containing closure pour connections and diaphragms can be designed using AASHTO LRFD live-load distribution factor formulas under the condition that the bridge must be sufficiently connected. However, these formulas were developed using analytical models that did not account for the effects of closure pours and diaphragms on live-load distribution. This research study investigates live-load distribution characteristics of precast/prestressed concrete bridges with closure pour connections and diaphragms. The investigation was conducted using finite element bridge models with closure pour joints that were

calibrated using experimental data and different configuration of diaphragms. The concrete material used for the closure pour connections was developed as part of a larger project intended to develop high early-strength concrete mixtures that specifically reach strength in only 12 hours, a critical requirement for ABC projects.

TABLE OF CONTENTS

Page

LIST OF TABLES

Table Page

LIST OF FIGURES

Figure Page

CHAPTER 1

INTRODUCTION

1.1 Motivation for Study

Accelerated Bridge Construction (ABC) has become increasingly popular in bridge deck replacement and new bridge construction because of its innovative construction methodologies. ABC utilizes new and advanced construction techniques in a cost-effective manner that results in reduction of on-site construction when compared to conventional practice. Limiting on-site construction improves work-zone safety for the traveling public and contractor personnel and reduces environmental impacts (Culmo 2011). Because of these and other advantages, application of ABC has gained significant momentum in the United States.

One important feature used in ABC that contributes to reducing on-site activities is prefabricated bridge elements and systems. This new system removes the cast-in place construction phase off the critical path of the project and allows it to occur at an offsite location under controlled environment. It also allows the components to be built adjacent to the bridge alignment alongside other construction activities. This process accelerates field construction time relative to the traditional method and results in lower construction costs (Garcia 2017). After offsite manufacturing, the prefabricated elements are transported to the construction site and joined using small volume closure pours with high performance materials. In addition to the closure pour connections, diaphragms are also commonly used to improve the connection between certain prefabricated

components such as beam elements. An illustration of closure pour connection and diaphragm connecting two prefabricated beam elements is shown in Figure 1-1.

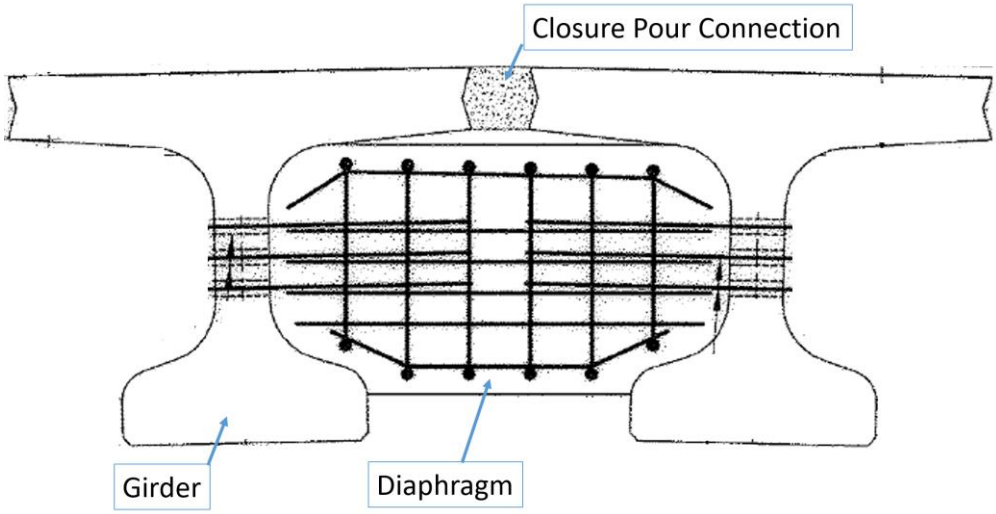

Figure 1-1: Illustration of closure pour connection and diaphragm

Closure pour connections are designed to provide continuity in the deck and ensure adequate transfer of forces between adjacent units. Diaphragms are added to reinforce the connection and provide stability. Assuming the structure behaves monolithically, engineers perform live load analysis for bridges with closure pours and diaphragms using the distribution factors from AASHTO LRFD. AASHTO LRFD distribution factors simplify live load analysis for engineers by enabling them to approximate live load effects in each girder without the use of complex 3D analyses. Using recommended code equations, designers are able to assign a portion of live load moment caused by one or more lanes of load to the individual girders.

In the development of the code formulas, finite element analysis (FEA) was used as an accurate method to evaluate the results from AASHTO LRFD equations. Analyses were carried out on a number of bridge models that considered several key parameters

that affected bridge response to live loads. Some of these parameters included girder spacing, span length, and slab thickness. The FEA assumed that the slab was continuous in the transverse direction of the bridge. This assumption eliminated the potential interference in transverse load distribution that could possibly be caused by the presence of closure pour joints in bridge decks. Effects of diaphragms was also ignored in those models.

AASHTO allows bridges with longitudinal closure pour joints and diaphragms to be designed using the AASHTO LRFD distribution factors under the condition that the bridge must be sufficiently connected. However, limited research has been done on these type of bridges to determine if the presence of the longitudinal joints affects distribution of live loads, in particularly concrete joints. As mentioned, closure pours are designed to provide adequate load transfer between the prefabricated components and allow engineers to analyze the structure assuming a continuous deck bridge. But with the limited attention given to studying its influence on load distribution, these joints could potentially bring undesirable damage to the structure. Therefore, a need to study the behavior of concrete bridges containing concrete closure pour joints has emerged.

A typical concrete closure pour connection detail can be seen in Figure 1-2. The connection consists of steel reinforcing bars and a high strength concrete mixture. The steel reinforcing bars found in the connection are the transverse reinforcement from the adjacent bridge components that project a certain distance into the joint as shown in Figure 1-2a. The bridge components are aligned to satisfy the overlap lap length and spacing of the reinforcing bars in the connection. After the components have been properly positioned, the concrete mixture is poured into the joint as seen in Figure 1-2b.

(a) (b)

Figure 1-2: (a) joint reinforcing bars (PCIMidwest) (b) concrete material (S. Brena)

Unlike the limited research dedicated to studying the influence of closure pour joints, the effects of diaphragms has been studied since the 1960s. Although there has been numerous papers published since then on the effectiveness of diaphragms, the role of intermediate diaphragms is still controversial. AASHTO separates diaphragms into two categories: end diaphragms and intermediate diaphragms. End diaphragms (EDs) are used over supports and intermediate diaphragms (IDs) are located within the span as seen in Figure 1-3. End diaphragms are typically used in practice and are known to improve load sharing characteristics of bridges. But the influence of intermediate diaphragms on bridge performance and justification for their existence is debatable among different states. Their contribution is still being studied due to inconsistency in practice for their design.

Figure 1-3: Intermediate and end diaphragms in a concrete bridge (Weeks 2011)

An advantage of using IDs is that they connect bridge girders together and prevent accidental overturning of the girders during construction. Research has shown that if designed properly, IDs can also improve lateral and vertical load distribution. However, a number of other studies disagree on the effectiveness of IDs in distribution of live loads. Some studies have indicated that IDs can actually make girders more vulnerable to damage from an impact caused by over height trucks; they can transfer the damage from the lateral impact to the other girders. Other research has shown that IDs do not always reduce maximum moment in girders and in some cases they can cause an increase in the maximum moment.

The controversy over the effectiveness of IDs is one of the reasons the models used to validate the distribution factor equations did not consider the effects of diaphragms. Another reason is that it is difficult to include effects of diaphragms in the simplified formulas since the number, type, spacing, and layout of diaphragms varies with different bridge systems. Modeling diaphragms can also be challenging as several

different parameters must be taken into account. For example, when modeling concrete diaphragms, designers must consider composite and non-composite action between diaphragms and slab, variation in stiffness due to diaphragm cracking, and connection between diaphragms and girders. There are not many research data available that provides recommendations on accurate concrete diaphragm stiffness and diaphragm-girder connections to be used in modeling. Most of the studies conducted on the influence of IDs did not account for all of these parameters which could be one of the possible reasons for the inconsistency in the results of the different research.

One important factor that is influenced by the usage of IDs addressed in research is cost. Some studies showed that the addition of IDs in precast girder bridges adds additional costs to the construction process that could be avoided. Studies claimed that although there are noticeable differences in the results from bridges with and without diaphragms, the displacements and stresses a bridge without IDs would experience fall within code design requirements. Hence, the addition of IDs comes with unnecessary construction and maintenance costs. Other research proposed increasing prestressing strands in prestressed concrete girders to resist the load rather than using IDs to avoid the additional costs. Despite these findings and recommendations on economic savings, many designs still use IDs in concrete bridges. Because of the existing controversy, this thesis incorporates a study on the role of IDs in addition to investigating the influence of closure pour connections in precast concrete bridges.

1.2 Research Objective

The objective of this study is to determine if the transverse distribution of live loads is affected by the presence of narrow concrete closure pour connections and diaphragms between girders. Geometry of a real bridge with closure pour joints and diaphragms was used in this study. This research focuses only on moment distribution factors for interior and exterior girders. The results from this project will provide the design community a better understanding of transverse load distribution between precast prestressed concrete bridge girders connected by longitudinal concrete joints as well as diaphragms.

1.3 Scope of Work

This thesis focuses on precast, prestressed Decked Bulb Tee girder bridges with concrete closure pours and diaphragms. A typical cross-section of Decked Bulb Tee girder bridge system can be seen in Figure 1-4. The study is limited to simply supported straight bridges. Analysis of the bridges was carried out using three-dimensional finite element modeling. Bridge details from Manhan Bridge, located in Massachusetts, was used to develop the models. These models were defined with the girder's material and section properties provided in the construction drawings. The longitudinal joint in the bridge was modeled explicitly in the finite element models after calibration using data from laboratory tests that were conducted at UMass Amherst as part of this study.

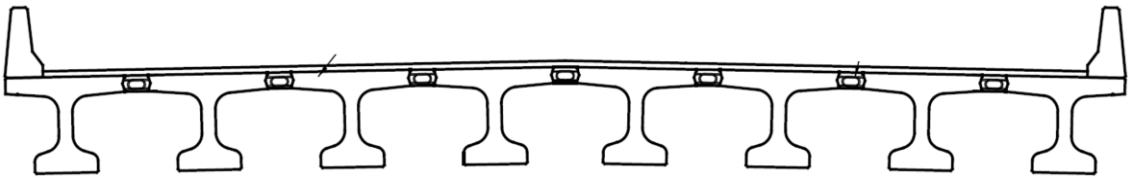

Figure 1-4: Typical Decked Bulb Tee girder bridge cross-section (PCI Northeast)

The laboratory tests were performed on a narrow closure pour comprised of steel and concrete that were conducted as part of a larger project aimed at developing high-early strength concrete mixtures for accelerated bridge construction. Narrow joints are designed to reduce the required expensive concrete material and accelerate on-site construction. Transverse load distribution between the adjacent girders relies on the closure pour developing the required strength, so this study also includes analysis performed to validate the performance of narrow concrete joints.

The analysis was initiated with a simplified model of the bridge that was created with the objective of assessing the accuracy of the selected modeling technique to be used in this study. This approach ensured that the chosen modeling method is capable of including all the important parameters that would affect the behavior of the bridge and reproduce accurate and practical results. After validating the simplified model, analysis was performed on the full-scale bridge models. A total of four full-scale models was developed in this study. Each model consisted of closure pour joints but had variation in diaphragm configuration. The models were subjected to dead and live loads given in AASHTO LRFD (2012).

Live load analysis was performed to evaluate how live load was distributed transversely between the girders via longitudinal joints and diaphragms. The maximum moment experienced by each girder was determined based on one lane, two lanes, and three lanes loaded conditions. Moment live load distribution factors were calculated from the model and compared to those from AASHTO LRFD (2012). Based on the results obtained, design implications are presented for precast/prestressed concrete bridges, specifically for moment live-load distribution factors in Decked Bulb Tee girder bridges.

1.4 Thesis Organization

This Master's thesis is composed of 8 chapters. Chapter 2 presents a literature review on AASHTO LRFD distribution factors, past studies on diaphragms in concrete bridges, and research on Decked Bulb Tee girder bridges. A description of the selected bridge and development of the finite element models are discussed in Chapter 3. Design of specimens and testing procedure of the experiment conducted on the concrete closure pour are presented in Chapter 4. Chapter 5 describes the analysis and results from the simplified model. Chapter 6 discusses moment distribution factors from the full-scale model and AASHTO LRFD along with the analysis performed to investigate the behavior of concrete closure pours. Analysis performed on the full-scale models with different diaphragm configurations and a comparison of the distribution factors are presented in Chapter 7. A summary and conclusion of the study is provided in Chapter 8. Design implication and future work in line with this project are also presented in Chapter 8.

CHAPTER 2

LITERATURE REVIEW

2.1 AASHTO LRFD Live-Load Distribution Factors

AASHTO LRFD live-load distribution factors (LLDFs) formulas were developed under the National Cooperative Highway Research Program (NCHRP) 12-26 Project. This project was initiated to evaluate the previous AASHTO LFD formula and develop more accurate equations. LFD simple formula (S/D) allowed engineers to calculate distribution factors based on girder spacing and bridge type without considering span length and stiffness properties. The S/D formulas produced valid results for nonskewed, simply supported bridges but did not always provide accurate estimates for other bridges such as skewed, curved, and relatively short and long bridges. AASHTO LRFD factors provide higher accuracy and include more parameters such as girder stiffness, span length, skew and girder spacing (Zokaie 2000).

A bridge database stored with several parameters extracted from bridges part of the National Highway Inventory across the United States was studied to identify the key parameters. Using mean values from the database, a hypothetical bridge was created for each bridge type. Finite-element or grillage analysis was carried out to assist in the development of the LLDF formulas. Important parameters considered in the analyses included different bridge types, span lengths, edge-to-edge widths, skew angles, number of girders, girder depths, slab thickness, overhangs, curb to curb widths, year of construction, girder eccentricity, girder moment of inertia, and girder area. A sensitivity study was performed to identify the key parameters for live-load distribution (Zokaie 2000).

The results from the sensitivity study were represented in plots for visual examination of the importance of the parameters. After examining the results, it was determined that the key parameters were girder spacing, span length, girder stiffness, and slab thickness. The simplified formulas were established after identifying these parameters. The finite element models used to validate the formulas assumed a continuous bridge deck system. Although providing better reliability than S/D formulas, the new formulas do not include all of the important factors that could affect LLDFs such as the effects of end and intermediate diaphragms. Zokaie (2000) stated that the formula were developed to produce results that are generally within 5% of a detailed analysis. For bridges that fall outside the range of applicability of the simple formula, a grillage or finite element analysis was recommended.

Many studies reported that AASHTO LRFD formulas are much more accurate than the AASHTO LFD factors, but the new equations may also be conservative for certain bridges analyzed using refined methods of analysis. Ypisof and Hindi (2007) identified limitations of the LRFD formulas in analysis performed on simple span slab-on-girders concrete bridges. In the study, they investigated the range of applicability limit specified in the LRFD equations for span length, slab thickness, girder spacing, and longitudinal stiffness by comparing LLDFs based on LRFD and FEA. The models were created using AASHTO-PCI concrete girders Types I-VI. End diaphragms were included in the models. The following conclusions were made from the study:

- AASHTO LRFD was over conservative in calculating LLDFs when compared to FEA for many cases, in particularly when the lever rule was used to determine LLDFs for exterior girders.

- For certain cases, the LRFD factors were lower when compared to FEA, giving a maximum of about 20% less than the FEA.
- The formulas seems to give valid results for parameters within the intermediate range of the specified limitations but tend to deviate within the extreme ranges.
- LLDFs obtained from two lanes loaded do not necessarily govern the design compared to three lanes loaded as proven for spans longer than 31 m with slab thickness and girder spacing ranging from 190-240 and 2,200-2,940 mm, respectively. FEA was recommended when the bridge is designed for three loaded lanes.

2.2 Effect of Diaphragms in Concrete Bridges

Barr et al. (2001) evaluated the accuracy of finite-element modeling techniques and code equations for determining flexural live load distribution factors for prestressed concrete girder bridges. The study also investigated the effects of lifts, IDs, EDs, continuity, skew angle, and load type. The evaluation was based on the response of a live-load test on a bridge designed by the Washington Department of Transportation. The experiment was used to ensure that moment obtained from finite element model corresponded to the observe behavior of the prototype bridge.

A series of progressively more detailed models were then developed to study the influence of the diaphragms and the other parameters on the live load distribution factors. The results showed that live load distribution factors calculated from AASHTO LRFD Specifications (1998) tend to be conservative when compared to FEA. Adding EDs reduced LLDFs for both interior and exterior girders. The addition of IDs caused a slight reduction in the distribution factors for interior girders. For exterior girders, the presence

of IDs led to a moderate increase in the distribution factors for straight and low skew angles bridges.

Cai et al. (2002) examined the effect of diaphragms on live load distribution factors and maximum strain through numerical predictions and comparisons with load testing for six prestressed concrete bridges. The bridges included different AASHTO girder types, skew angles, span lengths, diaphragm layouts, and number of lanes. These bridges were analyzed using slab-on-grid finite element technique with four different cases. In each case, the bridges were analyzed differently to consider effects of end and intermediate diaphragms. In all the cases, EDs were modeled integral with the beam ends and assuming stiffness based on uncracked sections. For IDs, full composite action with the beam was not assumed since reinforcing bars are discontinuous at the interface of the two members. Different stiffness levels were used in modeling the IDs as a result of cracking assumed to develop in the concrete. Composite behavior between IDs and the slab was also assumed in some of the models.

Results from the analyses showed that LLDFs calculated from code were conservative. AASHTO LRFD formulas overestimated the LLDFs from 14% to 40% for the six bridges tested in the study. The results obtained from the FEA proved that changing diaphragm conditions can significantly change the distribution factors. When comparing models with both EDs and IDs to the model with only EDs, the distribution factors for five of the six bridges decreased. The distribution factor increased slightly for the bridge referred to as Bridge No. 720252 for the case in which the diaphragm was modeled non-composite with the slab.

Assuming full composite diaphragm-slab action resulted in a lower distribution factor when compared to non-composite behavior. LLDFs for model with full diaphragm stiffness were smaller than those from the model with reduced stiffness. However, when comparing the models with full stiffness and those with one-third the stiffness to the data from field tests, there was a discrepancy in LLDFs, indicating that the actual diaphragm stiffness conditions of the field bridges was uncertain. The stresses on the diaphragm predicted from linear FEA were larger than the tensile strength of the concrete. Therefore, concrete cracking was assumed to have occurred in the diaphragms.

The group performed further analyses to investigate the effects of diaphragms for different number of diaphragms and skew angles. It was found that diaphragm effect on LLDFs and maximum strain were more pronounced for 0° skew angle than for 60° skew angle. By analyzing the plots for bridges with zero skew angle and with and without diaphragms, it can be noticed IDs significantly affected the shape of strain distribution. For cases without IDs, skew angle reduced LLDFs and the maximum strain.

When full stiffness IDs was introduced, the increase of skew angle increased both LLDFs and maximum strain for some of the interior girders. In the AASHTO LRFD specifications, a skew-angle factor is used to reduce LLDFs. The authors recognize the complexity of analyzing bridges with diaphragms and different skew angles and recommended that further study is needed. It was also observed that the addition of more IDs from one to three did not have a significant effect on distribution of loads. This result implied that when developing LLDFs formula that includes the effects of diaphragms, only diaphragm at critical section (near mid-span) can be considered instead of considering the total number of diaphragms.

Sengupta and Breen (1973) investigated the influence of IDs in prestressed concrete bridges using four 1/5.5 scale microconcrete simply supported models. Physical models of the bridges were tested under static and dynamic loads. Variables included in the tests were span lengths, skew angles, stiffness, number and location of diaphragms. Experimental results were used to validate a computer program for analysis of the bridge which was then used to study, the general effect of diaphragms in load distribution of a variety of bridge models.

Sengupta and Breen found that IDs assisted in distributing concentrated loads more evenly across the bridge, but with no significant reduction in governing design moment. In term of cost effectiveness, results indicated that it is more economical to increase girder strength with extra strands instead of depending on IDs to decrease the controlling distribution factor (improvement of load distribution), which would result in a reduction in girder design moment. The existence of IDs increased the intensity of girder damages from lateral impacts and made the girders more vulnerable. Therefore it was suggested that intermediate diaphragms be eliminated in simply supported prestressed concrete girder and slab bridges. EDs were found to play an important role in supporting the free edge of the transverse slab for reliable serviceability.

Wong and Gamble (1973) carried out an investigation to study the effects of diaphragms on load distribution characteristics of continuous, straight slab and girder highway bridges. The study focused on the influence of change in diaphragm stiffness and location on the variation of maximum positive and negative moments. The results of load distribution from continuous bridges were compared to those from simply supported bridges. It was found that when diaphragm stiffness exceeded the optimum stiffness,

exterior beams experienced a higher maximum moment than the absolute maximum moments in the beams of the bridge without IDs. Increasing diaphragm stiffness reduced the moments in the interior girders and increased the moments in the edge girders.

The difference in load determined for interior and exterior girders indicated that diaphragms are generally more effective in reducing moments for interior girders than exterior girders. After looking at the results, the authors concluded that only bridges with large girder spacing to span length ratio could benefit from the presence of diaphragms. However, it would be more cost effective to design the girder to resist the additional load it would take without the presence of diaphragms by increasing the number of prestressing strands in the concrete girders. The recommendation was not to include IDs in straight highway bridges with the exception of diaphragms needed for temporary erection purposes.

Cai (2005) conducted a study on slab-on-girder bridges with the goal of developing a new formula that would improve AASHTO LRFD live load distribution factors and propose a modification factor to quantify the effects of IDs. Their proposed formula included the same parameters as AASHTO LRFD (1998) but with a different format. When comparing the results obtained from the proposed formula and those from LRFD, the maximum difference was about 7%, and the average difference was about 1%. These formulas were also compared to results of distribution factors from finite element analyses of six prestressed concrete bridges used in previous studies. The comparison was between models with and without IDs. The models also accounted for different factors that could change results: reduction in stiffness due to cracking, and non-composite and full composite action between the diaphragms and slab.

The results from FEA were used in developing the modification factor for effects of diaphragms. The distribution factors calculated from LRFD and the new proposed formula predicted close results, but were conservative when compared with the values from field tests and FEA. When considering the diaphragm reduction factor, the distribution factors decreased for five of the six bridges. The results from assuming full diaphragm-slab composite action had more pronounced effects on load distribution when compared to non-composite diaphragm-slab model. The models with reduced diaphragm stiffness, one-third of the full stiffness, experienced a slight increase in LLDFs. The reduction in stiffness was less significant for straight bridges. Even though the proposed formulas provided reasonable agreement with AASHTO LRFD (1998), the authors recommended additional studies in order to develop a complete new formula for live load distribution factors.

Green et al. (2002) utilized finite element analysis to investigate the effect of IDs on bridge superstructure performance, in combination with the actual bearing stiffness and thermal changes. The analyses were performed on Florida Bulb Tee 78 girders. The study included presence of end and intermediate diaphragms, rise and drops in temperature, and increase in bearing stiffness. The results of the analyses showed that the existence of IDs is beneficial for prestressed concrete bridges in reducing maximum delfection. IDs reduced maximum deflection for straight bridges by about 17%. The reduction was less pronounced for skewed bridge, ranging from 4% to 6%. Positive thermal change in the girders magnified the benefits of IDs in decreasing deflection. Negative thermal change minimized the benefits because there was an overall increase in maximum deflection.

Green et al. (2004) investigated further into effect of IDs, bearing stiffness, and thermal changes in prestressed concrete. In this study, the effect of bridge skew was also analyzed. Results reaffirmed that IDs reduced maximum deflection likely because of a better distribution of overall bridge stiffness. The maximum deflection was reduced by about 19% for straight bridges, about 11% for 15 to 30° skew bridges, and about 6% for 60° skew bridges. The combination of IDs and positive temperature change showed to be beneficial in stiffening the girders and reducing maximum deflection. Change in negative temperature was also beneficial to the girder in reducing deflection, but at a lesser extent when compared to the positive temperature changes.

Results from a survey of design agencies conducted by Abendroth et al. (1995) showed that most of the agencies that responded to the survey specify IDs for precast concrete girder bridges, but at different locations. Ninety six percent indicated they use cast-in-place diaphragms. A smaller percentage of those agencies claimed to also have used steel channels. Approximately 50% of the respondents place diaphragms at the mid-span of the bridge, while 30% locate IDs one-third points along the span. Ten percent of the agencies put diaphragms at the one-quarter points of the span.

Abendroth et al. (1995) investigated prestressed concrete bridge response to vertical and horizontal load for various types and locations of IDs. The study included the survey on usage of diaphragm among the different design agencies, analytical and experimental investigations of a full-scale precast girder-slab bridge model. The developed models were based on several bridges with and without IDs. The models with IDs included different type and locations of diaphragms. Results indicated that vertical

load distribution is independent of diaphragm type and location, while the horizontal load distribution was a function of the intermediate diaphragm type and location.

Sithichaikasem and Gamble (1972) conducted a parametric study on the effects of the number, stiffness, and locations of IDs for simply supported, straight prestressed concrete bridges. They observed that the addition of diaphragms in these bridges does not always reduce maximum moments. In some cases, the diaphragms increased the maximum moments which can introduce harmful effects in the bridges. The presence of diaphragms in long span bridges (with a span length greater than 60 to 70 feet) is likely to produce either no reduction or an increase in maximum moment. Short span bridges with relatively wide beam spacing may benefit from IDs if properly designed.

Results also showed that only diaphragms located at or near the section of maximum moment will cause a significant change in the controlling moment. One flexible diaphragm properly placed seemed to be more advantageous to the bridge than two stiffer diaphragms at locations other than the maximum moment section. When located at the same location, a stiff diaphragm may cause an increase in maximum moment while a flexible diaphragm may decrease it. According to these results, the group made the following recommendation to designers: It is important to note that when designing a diaphragm, a flexible diaphragm can be more effective in lowering the controlling moment in certain a girder when compared to a stiff diaphragm. Therefore, designer must be careful in selecting an appropriate flexural stiffness in order for diaphragms to be effective in improving bridge performance.

Chandolu (2005) assessed the need and effectiveness for IDs in prestressed concrete girder bridges and studied if steel diaphragms is as effective as reinforced

concrete diaphragms. Parametric studies for various bridge configurations were carried out with the aid of simplified and solid finite element models calibrated under live loads. The study was based on simply supported, continuous, right, and skewed bridges. According to the results obtained, IDs decreased the load distribution factors for interior girders and increased the distribution factors for exterior girders.

The results also showed that IDs decreased the deflection for interior girders and increased the deflection marginally for exterior girders. The deflections were observed to be within the permissible limits for bridges with and without IDs which indicated that deflection is not as an important criterion affecting the decision to eliminate IDs or replace it with steel diaphragms. It was also found that steel IDs provided the same amount of stability as reinforced IDs, so if IDs were needed only for the purpose of providing stability, a steel ID would be suitable for this purpose. The steel ID was found to be adequate in carrying different loads coming onto the girders.

2.3 Decked Precast, Prestressed Concrete Girder Bridges

Distribution factors for multi-beam precast concrete bridge systems was not addressed in the design specification until the mid-1960s (Milliam 2004). In the ninth edition of AASHTO (1965) specification, distribution factors were provided for multi-beam precast girders. However, the factors were not accurate for all multi-beam sections such as decked precast prestressed concrete (DPPC) girders. After the first edition, there were other studies on LLDFs for this category of bridges to improve the first equation and cover a broader range of multi-beam sections.

A study at University of Washington in 1986, provided a new set of equations for distribution factors published in NCHRP Report 287 to serve as guidance on the design

of multi-beam precast bridges (Stanton and Mattock 1986). This study was the latest where simplified equations for live load distribution factors of DPPC girder bridges had been developed prior to the change to AASHTO LRFD according to Milliam (2004). The Washington study modified the AASHTO S/D equation for application to precast stemmed multi-beam bridge systems. But limitations encountered with the S/D formula led to the development of the LRFD LLDF equations. As discussed above, the new formulas used in the AASHTO LRFD did not provide accurate LLDFs for some bridge systems such as in the case for DPPC girder bridges.

In order to better understand LLDFs for DPPC girder bridges, some transportation agencies have funded research projects to investigate live load distribution for these bridges. Alaska DOT funded a project that examined load distribution for one lane vehicle loading in DPPC girder bridges. Alaska, having a much shorter construction season than other states, uses DPPC to accelerate highway bridge construction. The DOT uses AASHTO LRFD to design and evaluate Alaskas's highway bridges.

In the study sponsored by Alaska DOT, a new set of distribution factor equations was developed to describe the behavior of DPPC girder bridge system under a single-lane loading condition [Millian and Ma (2005)]. The study compared LLDFs from FEA to the simple S/D equation for interior girders. The S/D formula could be applied to DPPC bridges if the girders are connected to prevent relative vertical displacement at their interface. In the PCI Northeast Deck Bulb Tee (NEDBT) Guidelines, it is recommended that distribution factors be calculated using cross section (J) in AASHTO LRFD, assuming that the deck is sufficiently connected to act as a unit. This thesis focuses on these equations and not the S/D formula.

Millian and Ma (2005) addressed the limitation of the S/D factor for one lane loaded in DPPC girder bridges. The study was done through field tests, grillage modeling, and 3D finite element analysis. Eight bridges were tested in a field experiment. These bridges were located in Alaska and had different geometry of DPPC girder bridges. The top flange of the girders were connected with a shear key. The shear key consists of grout and steel angles welded together by steel plates as shown in Figure 2-1. The spacing of the connectors were typically 1.22 m (4 ft.) throughout the length of the bridge (Ma et al. 2007). Intermediate steel diaphragms were present in these bridges.

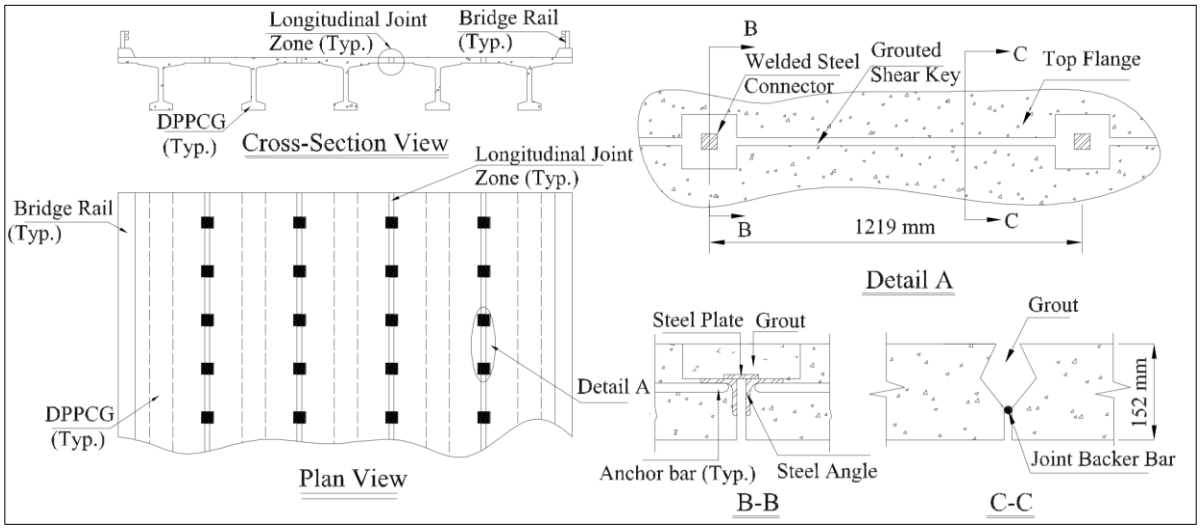

Figure 2-1: Grouted shear key (Li et al. 2010)

In the grillage model, transverse beam elements were used to approximate the behavior of the longitudinal joint. Two types of conditions were implemented to define the connection. First, a rigid connection, in which the connection is fully fixed and has full transverse continuity. The second, a hinged connection, in which the joint is released in flexure in the transverse direction. They estimated that the joint behaved somewhere between the two extreme conditions. The grillage model could not accurately

approximate the effects of intermediate steel diaphragms, so four 3D FE models were created that included the influence of the diaphragms.

One of the 3D FE models approximated the longitudinal joint as a hinged connection without the presence of diaphragms. Another model included the same hinged connection but with steel diaphragms represented using truss elements. The other two models were developed with the same properties as the first two but with the joint modeled with a rigid connection. Similar results for distribution factors were obtained from the grillage and FE models with a hinged connection and without the steel diaphragms. The presence of steel diaphragms in the model with hinged connection reduced LLDFs and behaved more closely to the rigid FE and grillage models. It was concluded that these models better approximated the experimental data for shear and moment distribution.

A parametric study was then conducted to determine which parameters had the biggest effect on the distribution factors. A set of grillage models were used in the parametric study. Some of the parameters varied were girder height, girder spacing, deck thickness, span length, and the rigidity of the longitudinal joint. The model with a 6-in. deck and hinged connections was compared to the S/D formula. It was determined that the parameters that had the most influence on the bridge distribution factors were girder spacing, bridge length, and girder moment of inertia. Based on the results obtained, the group proposed new equations for single-lane live load distribution factors for DPPC girder bridges. Comparison of the values from the proposed formulas and the results from the parametric study showed that the recommended equations were more accurate than

the AASHTO LRFD equation. The proposed equations were also closer to the distribution factors derived from the field test data than those from code.

Millian and Ma (2005) also observed that the presence of intermediate diaphragms in DPPC girder bridges influences the distribution factors and recommended a further study on its impact. Ma et al. (2007) carried out parametric studies to study the effect of shear connectors and intermediate diaphragms on live load distribution and connector forces. Three-dimensional finite element models were developed and calibrated with field tests to perform the analysis. The same modeling method used by Milliam and Ma (2005) was used in this study: hinged connection used for longitudinal joint and truss elements for steel diaphragms. EDs were present in the models. It was found that the presence of IDs can be beneficial for interior girder based on the results. A plot from the study showing the impact of IDs is presented in Figure 2-2.

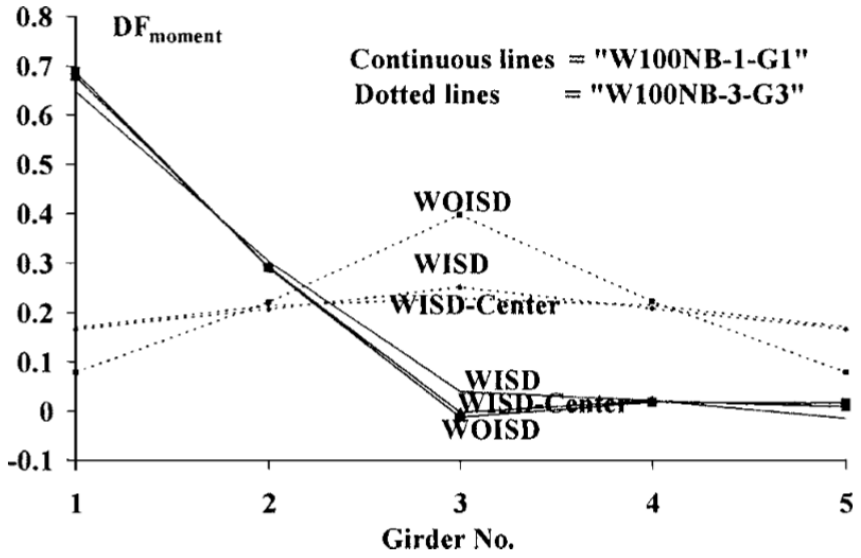

Figure 2-2: Impact of intermediate diaphragms on load distribution (Ma et al. 2007)

The continuous lines in the plot represent load applied over an exterior girder and the dotted lines represents load positioned on the center interior girder (Girder No. 3). WISD is a bridge with five steel diaphragms, WISD-Center denotes one ID present, and WOISD represents no diaphragm. The introduction of steel diaphragms in the bridge reduced the moment LLDFs for interior girder 3 and increased the distribution factor for the exterior girders. The distribution factors for girders 2 and 4 remained approximately the same with and without the presence of IDs. A small difference was noticed between the WISD and WISD-Center bridge models. WISD consisted of five IDs uniformly distributed along the bridge span while WISD-Center had one ID located at midspan. The one lane loaded model gave smaller LLDFs when compared to the model with two loaded lanes.

Li and Ma (2010) conducted a parametric study to determine the effect of IDs on the behavior of DPPC girders with EDs. The study was performed using three-dimensional finite-element models calibrated through the field tests from Milliam and Ma (2005). The main components in the model were the IDs, concrete girders, and longitudinal connection. Although the group considered modeling the longitudinal joint as a hinged connection, they decided to proceed with using shell elements. The shell elements restrained all three displacement and rotation degrees of freedom. Steel diaphragms were modeled using truss elements and the concrete girders along with the diaphragms were modeled using solid elements. The bridge was assumed to be simply supported at both ends.

Five bridge models were developed in the study. One of the models had no IDs, another had one layout of concrete IDs, and the other three had different steel diaphragm

configurations. The model with concrete IDs considered a rigid moment connection between the diaphragm and the girder. Truck loads were placed at five different locations in the transverse direction of the bridge. Results indicated that the effect of the diaphragms is dependent on the load position in the transverse direction of the bridge. An example plot showing how IDs affect deflection differently when load is placed at three different locations is presented in Figure 2-3.

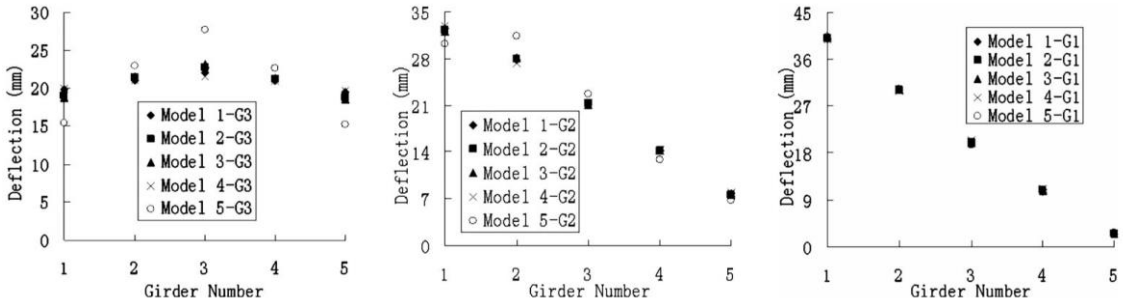

Figure 2-3: Comparison of deflection between models (Li and Ma 2010)

In Figure 2-3, model 1 has five steel IDs, Models 2 has one steel diaphragm at mid-span, model 4 has one concrete diaphragm at mid-span, and model 5 has no IDs. The labels G1, G2, and G3 represent the position of loads over girders 1, 2, and 3, respectively. When load is positioned at the middle in the transverse direction, the effect is significant. IDs reduced deflection for interior girders and increased deflection for exterior girders when load was placed over girder 3. IDs had less influence on deflection when the load was located close to the edge of the bridge as shown in the results for loading positions G1 and G2. It was also found that the additions of five diaphragms produced similar results to having one diaphragm at mid-span. By looking at the moment in the joints, the group concluded that IDs reduced the maximum bending moment in the

longitudinal joint. They recommended that one intermediate diaphragm located at mid-span should be used for Decked Bulb Tee girders in accelerated bridge construction.

Although the grouted shear keys used in these studies have shown to be effective in helping with load distribution, concerns were raised about their durability. The spacing of the welded steel connectors of 4 ft. limits their ability to help control flexural cracks along the longitudinal joints. Cracking and joint leakage seemed to be an issue limiting a wider use of Decked Bulb Tees with grouted shear keys in some states. The problems in these joints, led Li et al. (2010) to investigate alternate joint details for DPPC girder bridges. They studied three types of alternative connection details: hooked bar (U-bar), headed bar, and spiral bar.

It was found that using the U-bar connections posed concerns in achieving the desired bend radius within the 6 in. depth of the top flange while still satisfying the cover requirements. Using spiral bar connection seemed to be difficult and time consuming in field assembly. Headed bar connection details was perceived to not provide a good load path with reliance on welded wire reinforcement for load transfer and field placement could be difficult. After analyzing more advantages and disadvantages of each connection detail, headed bar was selected for further investigation. An experimental program was carried out using the model specimen and test set up shown in Figure 2-4.

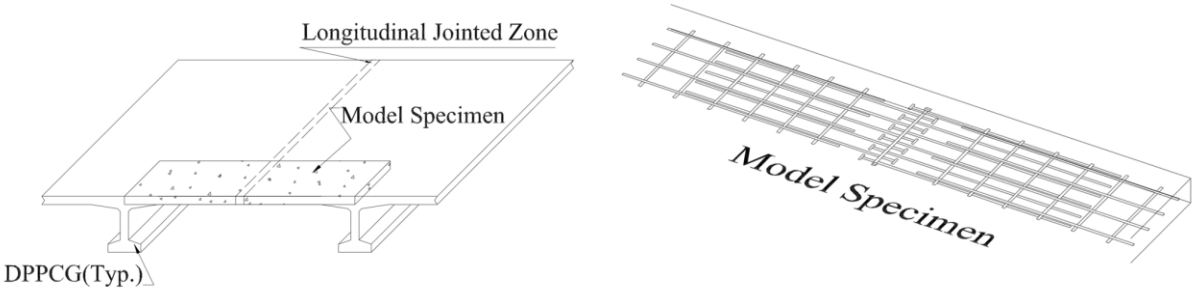

(a)

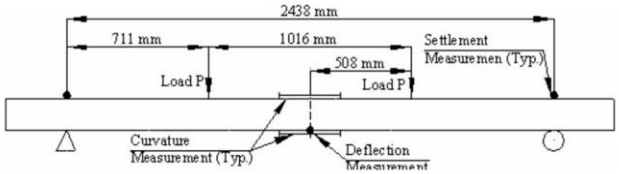

(b)

Figure 2-4: (a) specimen to evaluate joint behavior (b) Testing setup (Li et al. 2010)

Laboratory testing was conducted on seven reinforced concrete beam specimens connected with lapped headed reinforcement or lapped welded wire reinforcement. The results obtained from the experiment were evaluated according to moment capacity, curvature, cracking, deflection, and steel strains. Based on the evaluation, a headed bar detail with a 6 in. lap length was recommended for replacing the welded steel connector detail. The headed bar detail would provide continuous force transfer between the girder while minimizing the width of the joint.

2.4 Summary of Literature Review

According to several studies, AASHTO LRFD formulas produce more accurate live load distribution factors than the AASHTO LFD simple S/D equation in general. However, in some cases AASHTO LRFD formulas can also be conservative for some bridges when compared to a refined method of analysis such as FEA. The formulas can sometimes significantly overestimate LLDFs when using the lever rule to determine distribution factors for exterior girders. The models used to validate these formulas did not include the effects of certain factors like end and intermediate diaphragms. Including the contribution of diaphragms in modeling or a simple formula can be challenging due to several parameters that must be accounted for in analyzing effects of diaphragms. Some of the parameters include type, layout, and stiffness of diaphragms which varies depending on the bridge system.

End diaphragms are recommended in bridges since most of the research on effects of diaphragms has proven that it is beneficial for providing stability and improving load distribution. However, there is no clear consensus on the role of intermediate diaphragms on girder moments and deflections as found from the various studies reviewed here. Some research reports have indicated that intermediate diaphragms are beneficial in distributing load and reducing the maximum moment and deflection in the girders. Other research studies have shown that intermediate diaphragms make girders more vulnerable and increases the chances of overloading exterior girders. In terms of cost, certain reports say that IDs brings unnecessary cost to bridge construction.

Although the simplified formulas provide reasonable LLDFs for most bridges, the formulas loose accuracy for decked precast/prestressed girder bridges which are

connected by longitudinal joints and diaphragms. Studies focusing on Decked Bulb Tee girder bridges containing grouted shear keys located in Alaska have shown that this type of bridge system can experience different moments than those given by code. The presence of intermediate diaphragms in these bridges also influences the distribution factors. The grouted shear keys in the bridges used to calibrate the FEA models in those studies pose certain design and construction issues that has pushed designers to seek alternative joint details.

Given the large differences in results as summarized here from the literature review conducted for this research, the effect of longitudinal joints in combination with models that include diaphragms placed at various locations for precast/prestressed decked girders were studied for this thesis. The following chapters describe the details of the results of the study based on a selected prototype bridge and laboratory testing of the longitudinal connection used between precast/prestressed girders.

CHAPTER 3

PROTOTYPE BRIDGE & FINITE ELEMENT MODEL

3.1 Prototype Bridge

The Manhan Bridge, located in Easthampton, MA was selected as the prototype bridge to be used in this thesis. This bridge was rebuilt with precast concrete girders in 2013 to replace a steel girder-floorbeam-stringer system that was found to be structurally deficient as part of the MassDOT Accelerated Bridge Program. The superstructure of the bridge is made of precast prestressed Decked Bulb Tee girders. This was the first time MassDOT implements this type of superstructure to build or enhance their bridges (DTC 2013). Fabricating the girders offsite and connecting them with the closure pour connections accelerated construction time for this bridge project. The project was completed about five weeks ahead of schedule (DCT 2017). Figure 3-1 shows the girders during the construction of the bridge.

Figure 3-1: Manhan Bridge under construction (PCIMidwest-Project)

The cross section of the bridge is presented in Figure 3-2. The bridge is designed for two 11 ft. wide travel lanes. There are a total of eight 95 ft. long and 4 ft. deep girders spaced at 5.5 ft. in the structure. The bridge is single-span with a span length of 93 ft. The top flange of the girders is considered as the deck of the bridge and it is integral with the web. End and intermediate reinforced concrete diaphragms are present in the bridge as shown in the frame plan in Figure 3-3. The end diaphragms are located at the two ends of the bridge and intermediate diaphragms are located at mid-span. Sidewalks (8 in. thick by 5.5 ft. wide) were placed on both sides of the roadway; S3-TL4 steel railings were placed at the each edge of the bridge for crash protection. The nominal compressive strength of the girders and diaphragms are 8000 psi and 4000 psi, respectively. The girders rest on elastomeric bearing pads placed on top of the two abutments. To carry design loads given the local geology, the north abutment is supported on 16 micro piles that were installed and the south abutment was constructed directly on bedrock.

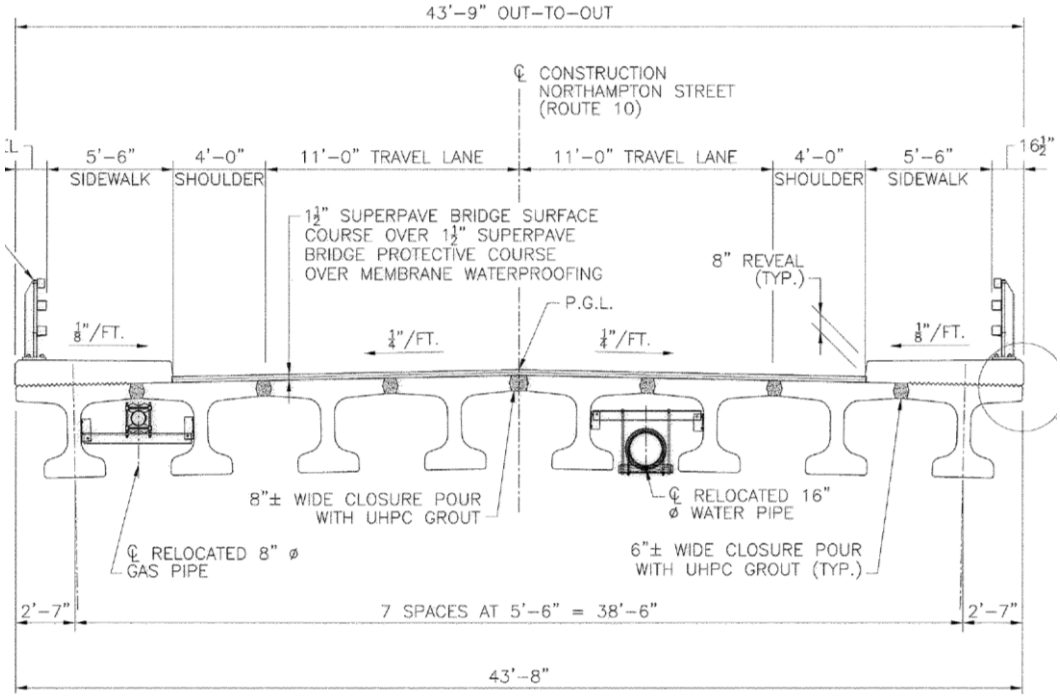

Figure 3-2: Bridge Section

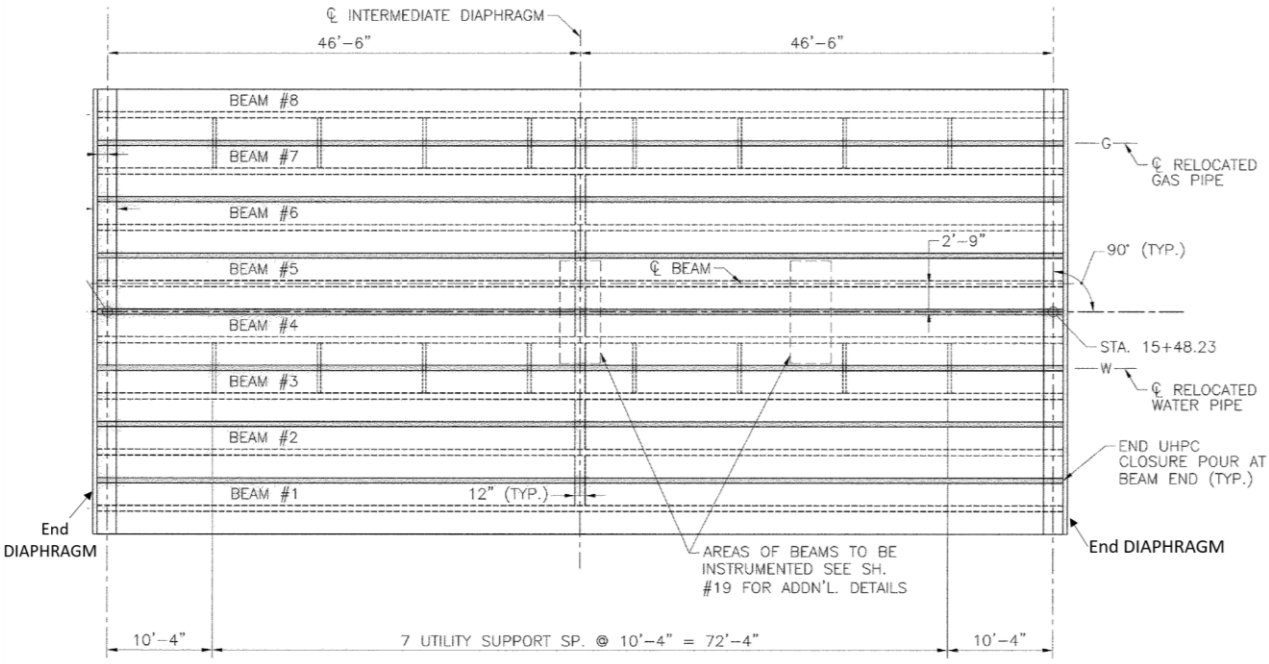

Figure 3-3: Bridge frame plan

A cross-sectional view of the interior and exterior girders at mid-span is shown in Figure 3-4. Both girders have the same dimensions for the web and bottom flange. The top flange edges contain shear keys as required for closure pour connections to adjacent girders (edge girders contain shear keys on the interior edge of the top flange only). Number 4 reinforcing bars placed horizontally in the top flange (deck) project out of the top flange on both ends of the interior girders and one end of the exterior girders. These bars overlap within the longitudinal joint. The two center girders are connected using an 8 in. wide closure pour while the others are connected with a 6 in. joint. Photographs of the closure pour and typical joint detailing are presented in Figure 3-5. Ultra High Performance Concrete (UHPC) was used in the closure pour joints. UHPC is a cementitous, concrete material with steel fibers that is capable of reaching a 28-day compressive strength in excess of 20,000 psi.

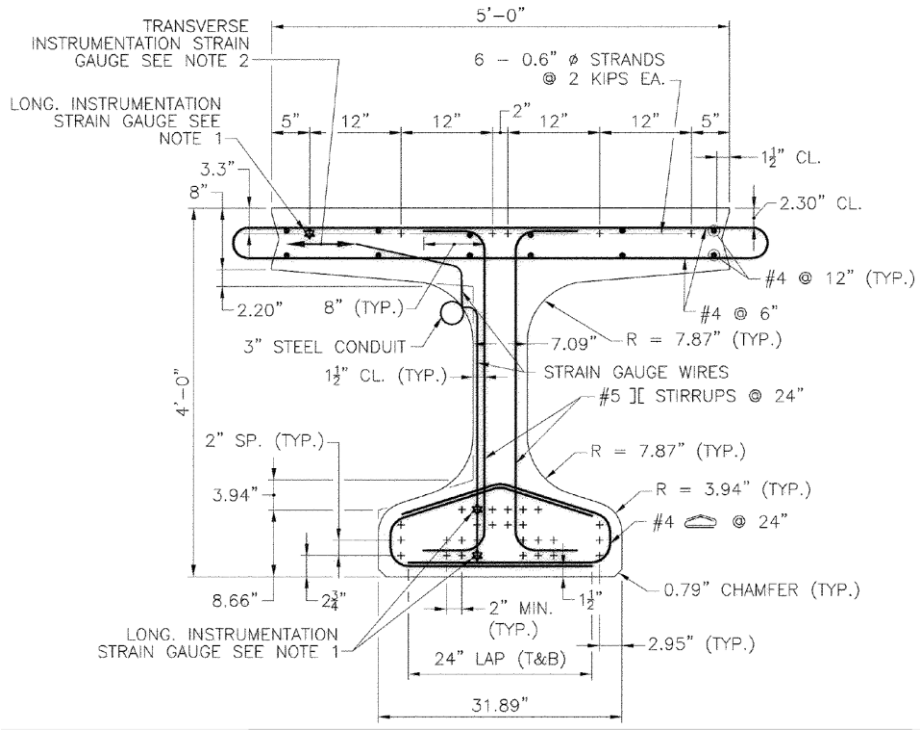

(a)

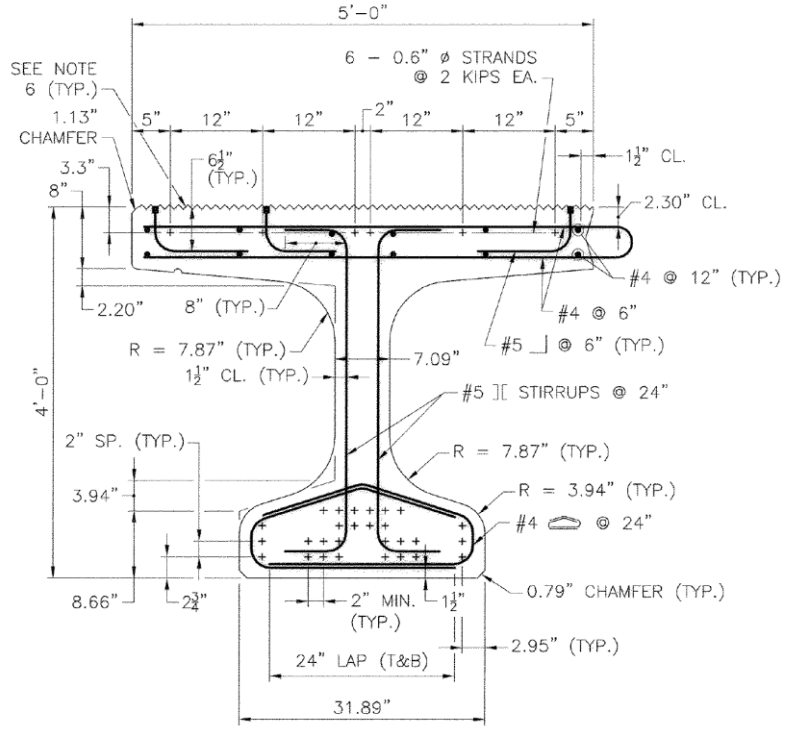

(b)

Figure 3-4: Typical girder section (a) interior girder (b) exterior girder

(a)

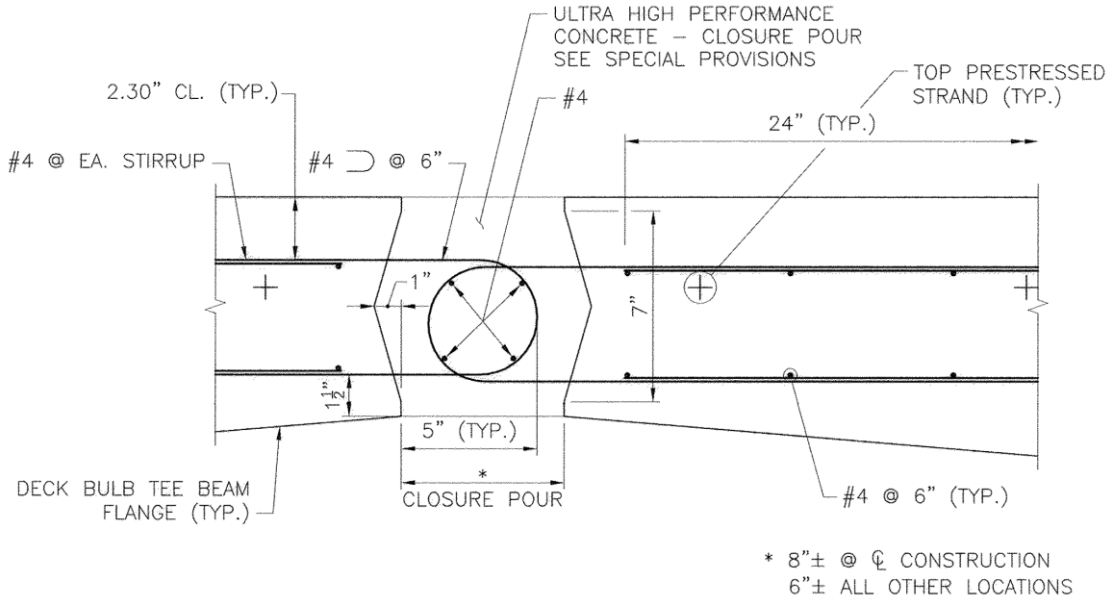

(b)

Figure 3-5: (a) Closure Pour (Pictures courtesy of S. Brena) (b) Joint detailing

3.2 Finite Element Model of Prototype Bridge

The finite element models discussed in this section were created by using characteristics of the Manhan Bridge provided in the construction drawings. The modeling and the analyses were done in CSiBridge v20.2.0. This section describes the modeling aspects of the superstructure, substructure, and foundation. Bridge deck, beams, closure pours, and diaphragms are the components of the superstructure while the bearing pads and the abutments are categorized in the substructure.

3.2.1 Bridge Girder Modeling

In modeling the bridge, the Decked Bulb Tee girders were divided into two components. Taking into consideration that the top flange of the girder is intended to be the structural deck, the deck and the beam were treated as two different structural elements for modeling purposes, but were rigidly connected in the model. The division and the assumed cross section of the beam are presented in Figure 3-6. The total depth of the girders is 48 in. The top 8 in. of the top flange was used as the thickness of the deck and the bottom 40 in. was considered as the height of the beam.

The deck was modeled using four-node quadrilateral shell elements. The assumed beam was modeled using frame elements. The cross section for the beam was created in the section designer panel of CSiBridge as shown in Figure 3-6(b). Frame Insertion tool was used to ensure the two elements were fully connected to simulate behavior as a single unit. In this approach, shells and frames are initially defined in the same plane, at the elevation of deck centroid sharing the same joints. The girder is then placed below the deck using frame joint offsets and the top center insertion point command in CSiBridge. The analytical model can be seen in Figure 3-7.

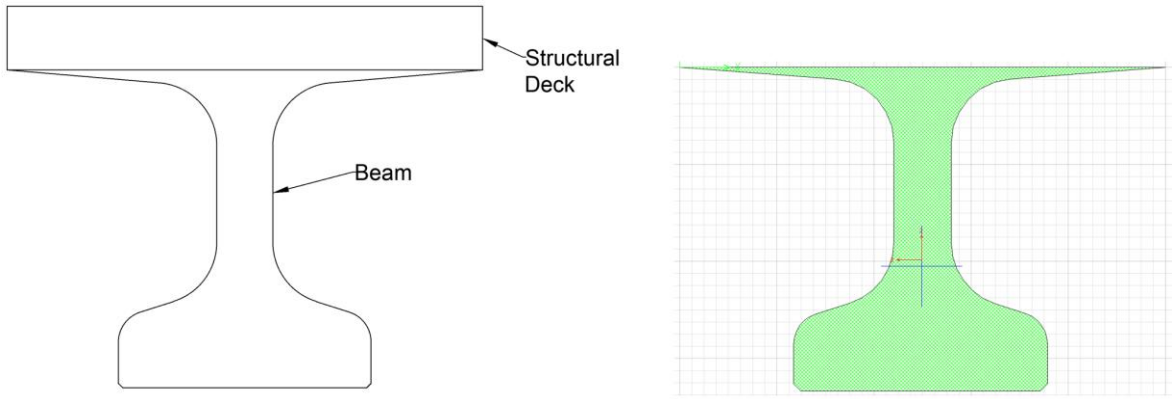

(a) (b)

Figure 3-6: (a) Bridge structural deck and beam (b) beam cross-section in CSiBridge

The section and material properties of the girders are presented in Table 3-1. The area and moment of inertia of the interior and exterior girders from the actual bridge vary slightly due to the modifications in the top flange. As discussed earlier, the exterior girders contain shear keys on the interior edge of the top flange only while the interior girders contain shear keys on both edges. Despite the discrepancy in the top flange, the overall properties of the interior and exterior girders are similar as shown in the table. Therefore, only one beam section was created in CSiBridge and applied to both interior and exterior girders. The difference in section properties of the girders included for the finite element model and the actual bridge girders is small, with a percent difference less than one. Each girder was assigned a compressive strength of 8000 psi. The model considers the full length of the girder (95 ft.) as the span length instead of the original 93 ft. bridge span length.

Table 3-1: Material and section properties

Properties	Interior	Exterior	Model	Percent difference (interior to model)	Percent difference (exterior to model)
Depth (in)	48	48	48	0	0
Area (in^2)	1109	1112	1107	0.18	0.45
I_{33} (in^4)	326850	327540	325562	0.39	0.61
Weight (lb/ft)	1155	1158	1154	0.09	0.35
Compressive strength (psi)	8000	8000	8000	0	0

3.2.2 Closure Pour Modeling

The closure pour connection was modeled using a series of nonlinear zero-length link elements. The connection was simulated by connecting the nodes of adjacent shell elements used to model the deck with a two-joint link element. Adjacent nodes of the deck elements of each girder were joined together with the link element along the length of the bridge as depicted in Figure 3-7. The mesh in the deck was sufficiently refined to ensure an accurate behavior of the closure pour and increase confidence in the modeling results.

The nonlinear properties for the links connecting adjacent shell elements were defined using data from the experiments presented in Chapter 4. Load-deflection and moment-rotation relationships were used as input in the link properties to describe the nonlinear behavior of the element. The load and moment from the experiment were adjusted for the model. The adjustment was done by dividing the load by the width of the specimen (3 ft.–8 in.) and then multiplying by the tributary length of deck that each link element connects. These plots are provided in Figures A-2 to A-4 under Appendix A.

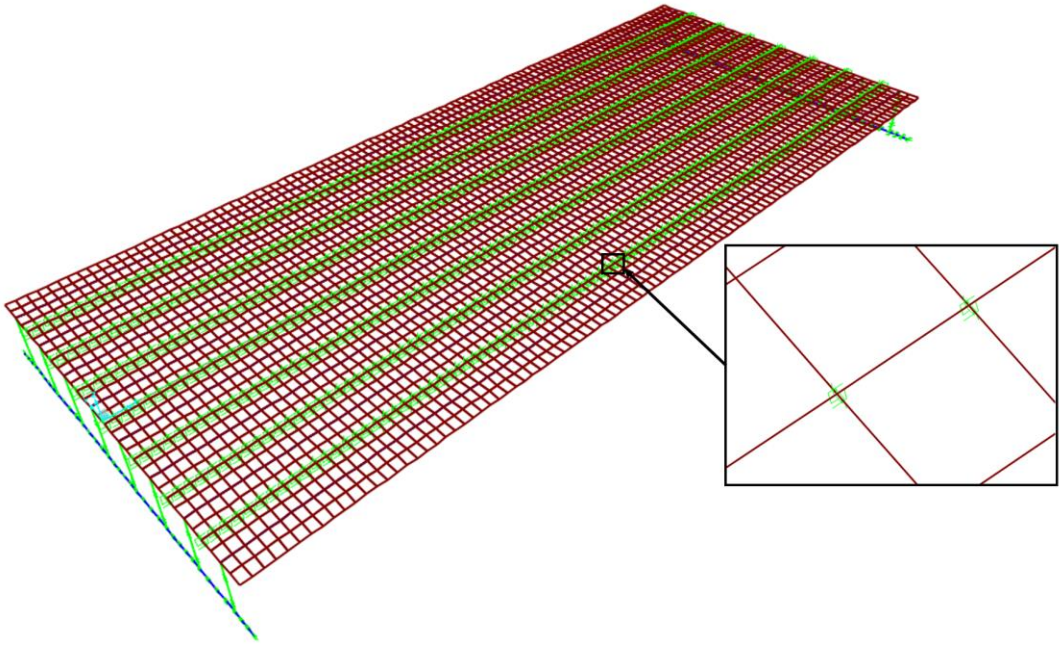

Figure 3-7: Finite element model

3.2.3 Substructure and Foundation Modeling

The substructure of the bridge consists of elastomeric bearing pads that are supported on abutments. The bearings were represented in the model using link elements with appropriate vertical and horizontal restraints to represent a simply supported bridge. The abutments were modeled using frame elements as shown in Figure 3-8. Foundation spring support was used to connect the substructure to the ground. The spring property was defined as a link element with all six degree of freedoms being specified as fixed to represent rigid support condition at the bottom of the abutments.

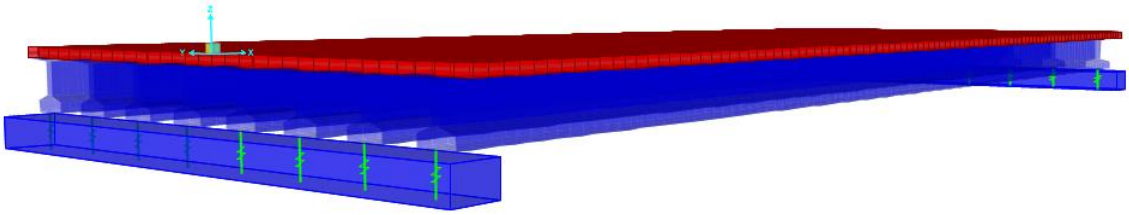

Figure 3-8: Model showing girders, abutments, and bearings

3.2.4 End and Intermediate Diaphragms Modeling

A total of four finite element models were considered for this study. Each model included all the details described above in the development of the model. The only difference in each of the four models was on presence and location of diaphragms connecting girders. The first model incorporated the same diaphragm layout as in the Manhan Bridge, presented in the frame plan (Figure 3-3). In this model, end and intermediate diaphragms were included as part of the bridge. Details of the diaphragms from the drawings shown in Figure 3-9 were used to create the diaphragms in the model. The details in the figure include elevation view of end and intermediate diaphragms along with typical diaphragm cross sections.

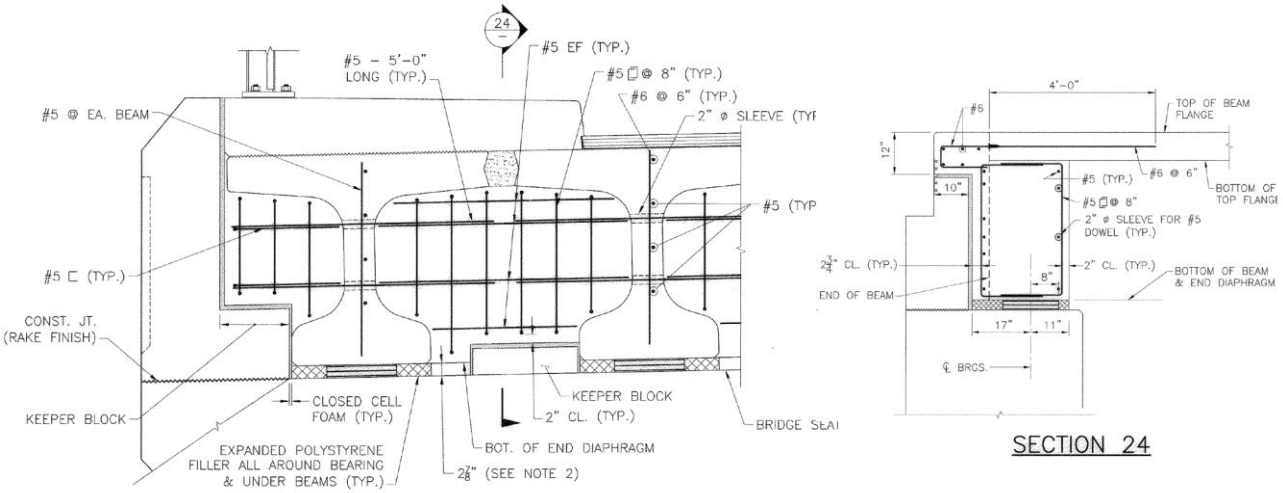

(a)

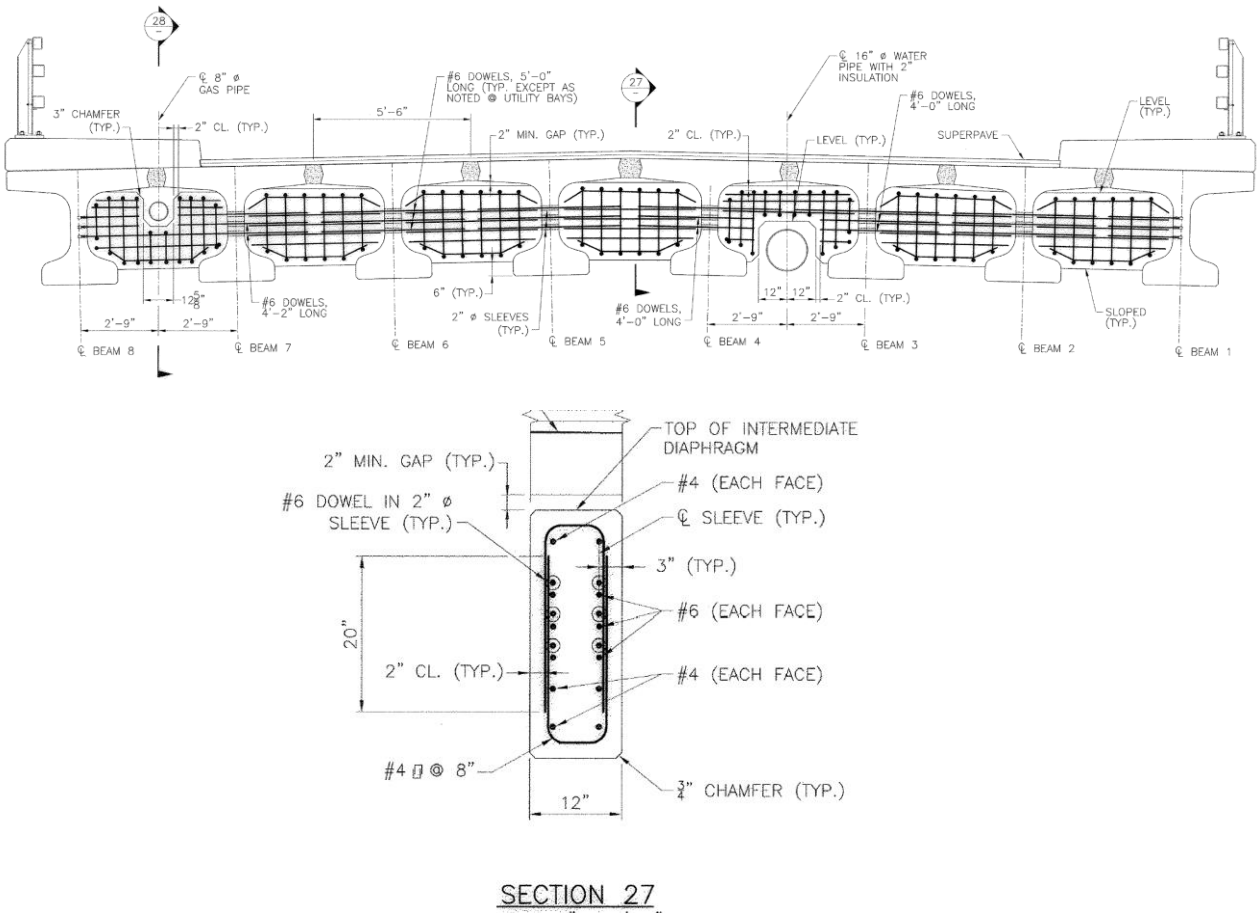

(b)

Figure 3-9: (a) End diaphragm details (b) Intermediate diaphragm details

The diaphragms were modeled using frame elements with the properties provided in the drawings. A rigid diaphragm-girder connection was assumed given the fact that reinforcing bars pass continuously through girder webs and are fully anchored into the diaphragms. The diaphragms were modeled as non-composite with the deck slab. The stiffness of the diaphragms was assumed to vary between uncracked conditions to cracked conditions by assuming a two-thirds reduction in moment of inertia from the gross value in the uncracked diaphragm. The variation in diaphragm moment of inertia was included in the models to investigate effects of reduced stiffness in the load transfer

characteristics between girders. The actual stiffness of the Manhan Bridge diaphragms is unknown.

In the second model, intermediate diaphragms were removed. End diaphragms are recommended by code, so the second model was chosen to analyze how end diaphragms influence live-load distribution factors in comparison with simplified AASHTO LRFD equations. The third model was constructed including only intermediate diaphragms. In practice, it is unlikely that a bridge would be designed containing intermediate diaphragms only without end diaphragms. Therefore, the purpose of this third model was to gain a better understanding of how the presence of intermediate diaphragms affects the transverse distribution of live loads. The fourth model was built with no diaphragms. AASHTO LRFD live-load distribution factor equations were developed using models without considering the effects of diaphragms, so this model reflects the original assumptions used for the AASHTO simplified equations.

In the next chapter, Chapter 4, testing procedure and results are presented for laboratory tests performed on concrete closure pours. The tests were conducted on specimens connected with closure pour connections comprised of steel and concrete that simulated the connections of typical deck portions of decked prestressed girders. The data obtained from the experiment was applied to the closure pour modeling discussed in Section 3.2.2 of this chapter.

CHAPTER 4

CLOSURE POUR EXPERIMENT

4.1 Overview

Results from two large-scale laboratory tests conducted at UMass Amherst on concrete closure pour connections were used to calibrate models intended to capture the response of longitudinal joints in a general bridge model. The tests were performed using a high early-strength concrete mixture that was designed to satisfy performance requirements of ABC closure pours in New England. The mixture was used to fabricate the longitudinal closure pour cast between two panels to simulate the connection between two bridge deck panels. The specimens were tested one day after casting.

Specimen design, fabrication, design strength, testing procedure, and test results are presented in this chapter. These tests were not intended to characterize the long-term cyclic performance of the connection; the objectives were only to evaluate whether the connection develops the required short-term strength (one day), and to document any distress that may occur because of loading at early ages. A second goal of these tests was to investigate whether narrow closure pours could be used in combination with the developed mixture without negative effects on transverse strength between the panels.

4.2 Specimen Design

The test specimens were designed to represent typical deck portion of two adjacent Decked Bulb Tee girders connected together through a longitudinal joint. The represented portion of the deck is highlighted in red in Figure 4-1. The design was done following PCI Northeast Deck Bulb Tee Guidelines (NEDBT) in coordination with AASHTO

LRFD Bridge Design Specifications. Drawing details for hooked bar connection from the guide provided guidance on the selection of closure pour width, dimensions for the deck panels, and steel reinforcement used in this experiment. The guide indicated that the closure pour width generally varies from 12 in. to 24 in. and requires that the concrete closure pour material in the longitudinal section must be a mix with a minimum compressive strength of 4000 psi. Higher strength mixes may be used which could result in a narrow closure pour connection. Following this recommendation, the specimens in this experiment uses joint widths of 8 in. and 6 in. with the high early-strength concrete to determine the behavior of the specimens with a smaller joint.

Figure 4-1: Deck portion of Decked Bulb Tee girders simulated in the experiment

Two specimens with similar dimensions were fabricated for testing. Each specimen consisted of two conventional concrete precast panels connected using a narrow closure pour that contains a triangular shear key filled with the closure pour material. Elevation view, joint section view, plan view, and reinforcement details of the specimens can be seen in Figures 4-2 through 4-5. Each panel was 44 in. long and 8 in. deep. Panels for specimen 1 were 34 in. wide connected together with the 8 in. wide longitudinal connection. Panels for specimen 2 were 35 in. wide connected together with

the 6 in. joint. The total length of the specimens after connecting the panels together was 76 in. long, 44 in. wide, and 8 in. deep. Spacing and size of the deck longitudinal bars were designed using AASHTO provisions. The resulting longitudinal reinforcement was as follows: No. 5 bars spaced at 9 in. top and bottom for specimen 1; No. 5 bars spaced at 9.5 in. top and bottom for specimen 2. Two longitudinal No. 5 bars run through the hooked bars in the closure pour connection as shown in the drawings.

The transverse reinforcement details were established by replicating the detailing for hooked bars connection from section *NEDBT – 05 Beam Deck Details* found in the guideline. Specification for the connection reinforcement (transverse bars) requires No. 4 bars to be placed along the entire width of the panels with 6 in. spacing. The transverse bars of two deck panels are staggered at a distance of 3 in. in the closure pour connection as seen in Figures 4-4b and 4-5b to avoid interference of bars between adjacent panels and to facilitate construction. These bars project 7 in. and 5 in. into the joint with an overlap length of 6 in. and 4 in. for specimen 1 and specimen 2, respectively, as depicted in Figures 4-2b and 4-3b. The inside bend diameter for No. 4 hooked bar is 3 in. ($6d_b$). Clear cover for the reinforcing bars was designed to be 2.5 in. on the top and 1.5 in. on the bottom for both specimens. All reinforcement used in the specimens satisfied ASTM 615 grade 60 reinforcement and contained epoxy coating.

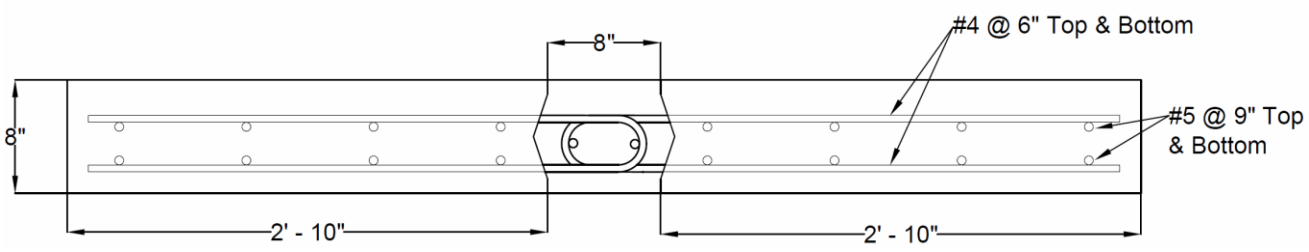

(a)

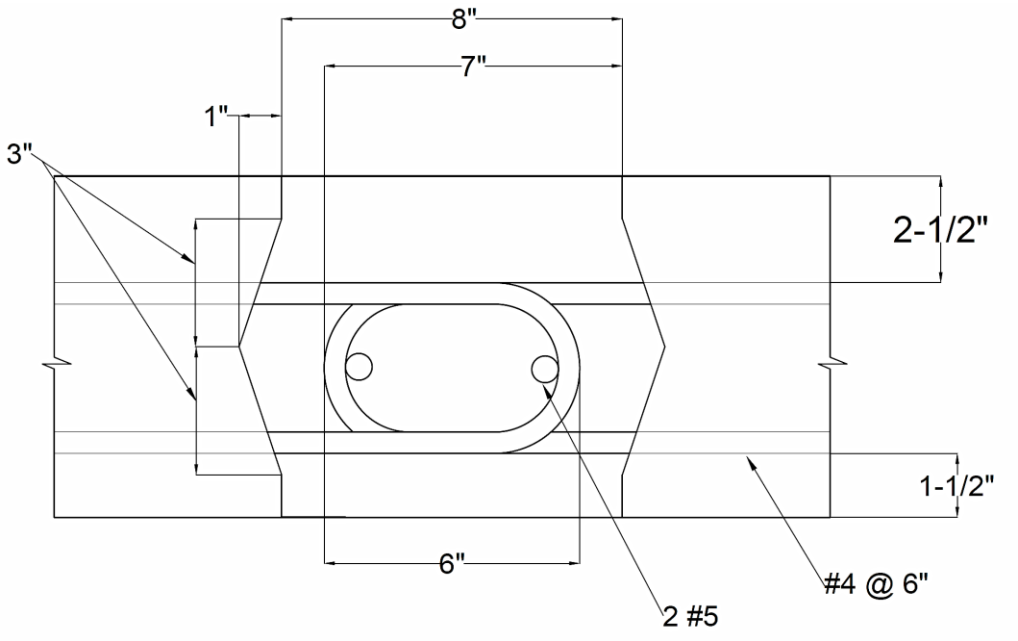

(b)

Figure 4-2: Detailing for specimen 1: (a) Elevation view of test specimen; (b) section view of joint detail

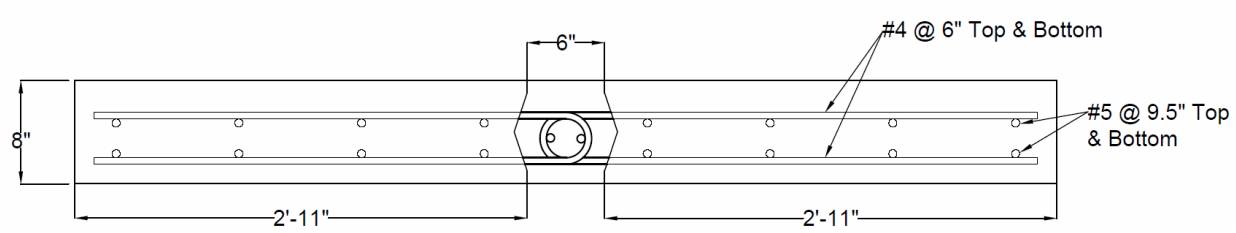

(a)

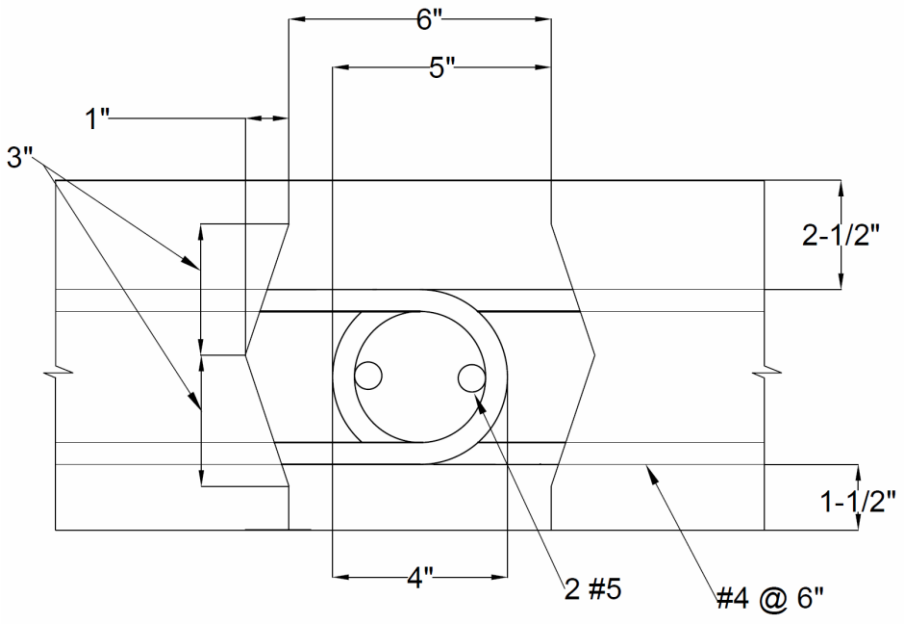

(b)

Figure 4-3: Detailing for specimen 2: (a) Elevation view of test specimen; (b) section view of joint detail

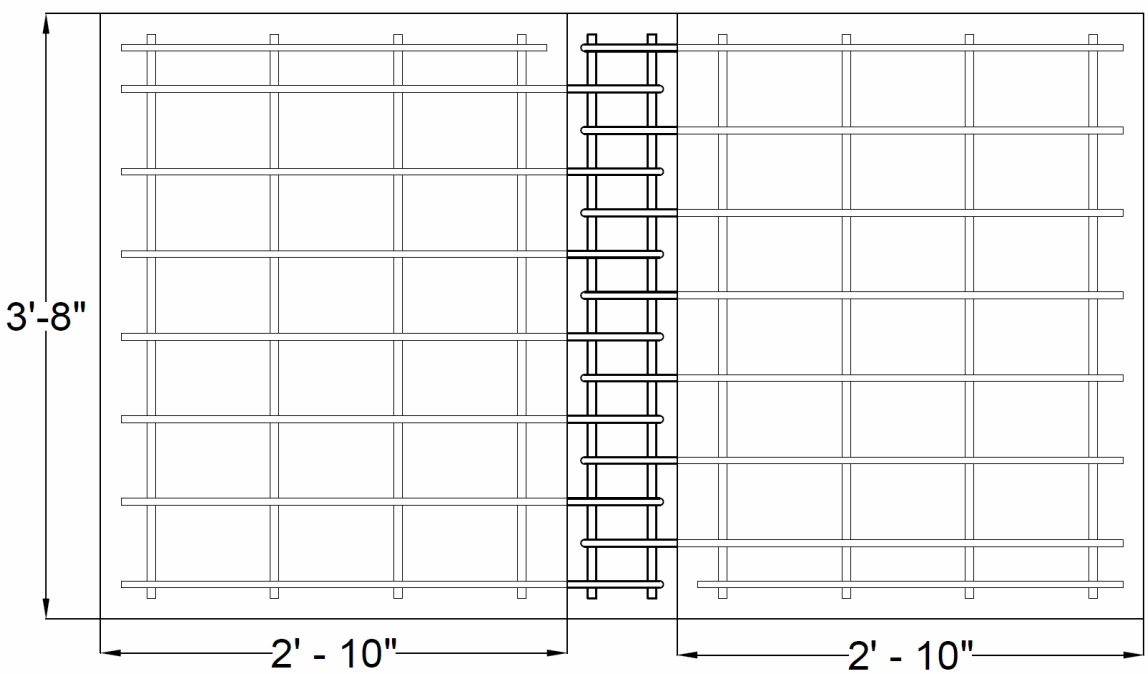

(a)

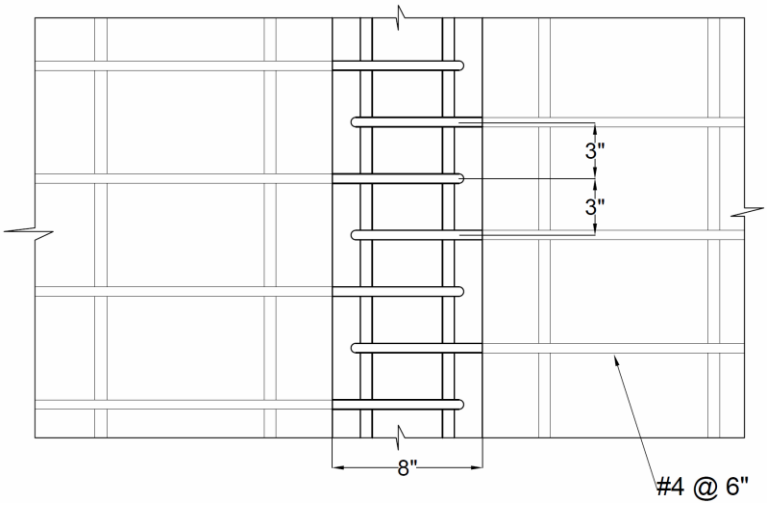

(b)

Figure 4-4: Detailing for specimen 1: (a) Plan view of test specimen; (b) Plan view of joint detail

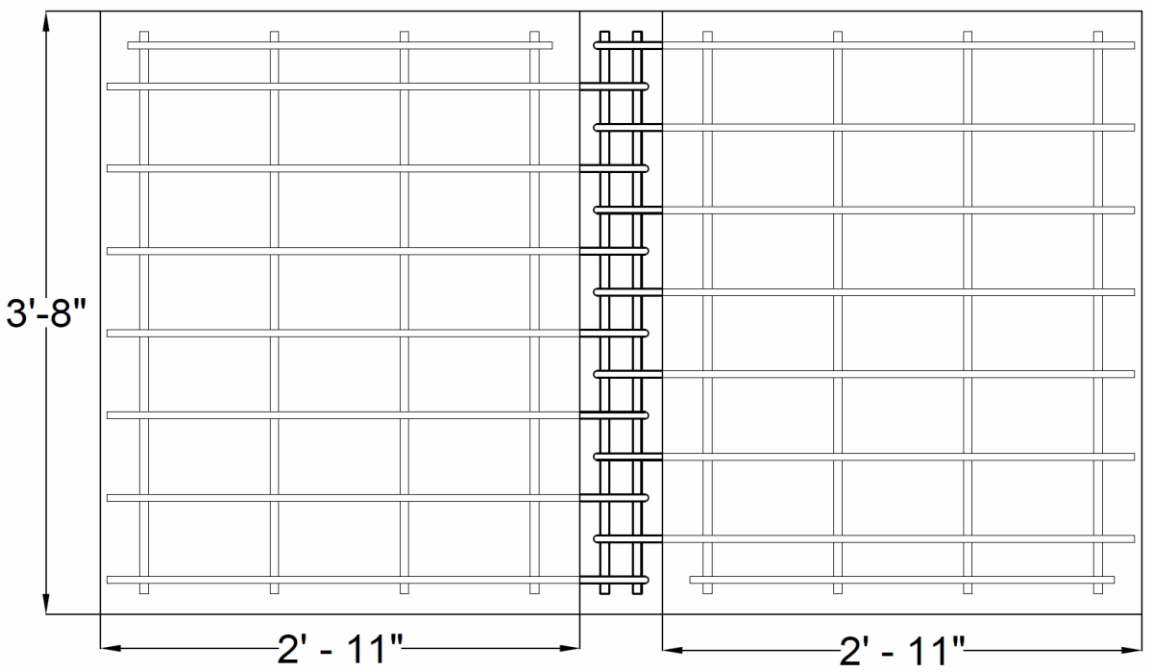

(a)

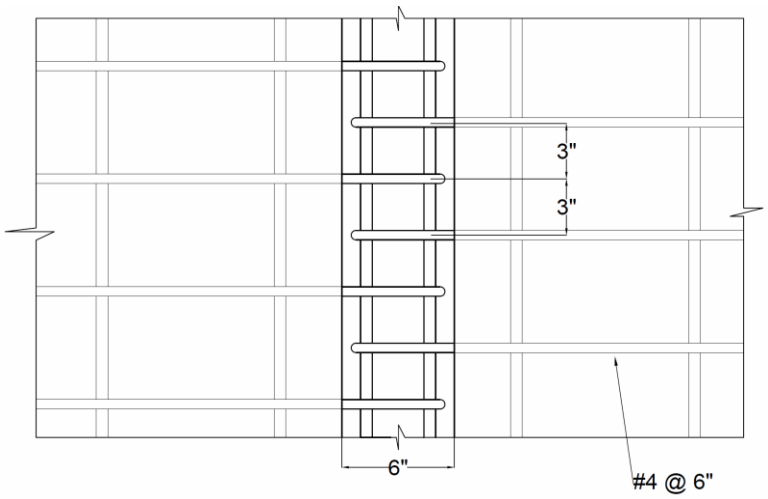

(b)

Figure 4-5: Detailing for specimen 2: (a) Plan view of test specimen; (b) Plan view of joint detail

4.3 Specimen Fabrication

Once the design was finalized, construction process for the specimens began. The specimens were constructed in two stages, with stage I involving building formwork and casting of the deck panels, followed by stage II which involved casting the closure pour connection. Test specimens were fabricated and tested in the Gunness Structural Engineering Laboratory at University of Massachusetts Amherst.

4.3.1 Panel Fabrication

In stage I, a total of four deck slabs were fabricated. The formwork for these slabs was built using standard lumber and plywood sheets. Lifting hooks were placed in the formwork prior to pouring for specimen handling. During casting, a ready-mix concrete truck was ordered to perform the pour using normal-weight concrete with maximum aggregate size of ¾ in. A target 28-day compressive strength of 4000 psi was specified and a slump of 4 in. to 6 in. was requested before concrete placement. As concrete was being poured in the panels, concrete cylinders were made for compressive strength. Once all the panels were poured, the concrete was allowed to cure in a controlled curing environment; specimens and concrete cylinders were cured under the same laboratory environment conditions. Burlap and plastic were used to cover exposed concrete surfaces during the curing process. Concrete was allowed to cure for 28 days. Photographs in Figures 4-6(a)-(c) show the panels before and after casting.


(a)


(b)


(c)

Figure 4-6: Panel fabrication: (a) formwork and installed rebars; (b) casting; (c) cured specimens

4.3.2 Joint Construction

In stage II, two panels of each specimen were positioned and properly oriented to satisfy the overlap lap length and spacing of the hooked bars in the closure pour connection. Plywood sheets were used to form the two free edges of the closure pour region and the joint was prepared for casting the high early-strength concrete mixture. The mix for the pour was done in accordance with ASTM Standard C192: *Standard Practice for Making and Curing Concrete Test Specimens in the Laboratory*. A STOW Model CM6 concrete mixer with a capacity of 6 cu ft. was used to perform the mix for the closure pour concrete. Prior to each mix, the recommended steps were taken to dampen the barrel of the mixer to reduce the amount of water absorbed by the residue adhered to the walls of the barrel.

During the mix, the aggregates were added first and mixed together until a homogeneous mixture was formed. The remaining constituents were added to the mixer in the order specified: cement, fly ash, pure mixing water, and mixing water containing the high-range water reducer chemical admixture. The constituents were mixed for 3 minutes, followed by a 3-minute rest period with the barrel opening covered with a layer of plastic, then a 2-minute final mixing period. After completing the mix, the concrete was poured into a wheelbarrow and cast into the joint between the two respective panels. Concrete cylinders were cast using the same mixture and cured under the same conditions as the closure pour. The mix produced a viscous concrete mixture without segregation. As concrete was being cast into the joint, a vibrator was not needed as the concrete did not require any vibrating to be consolidated within the joint. Photographs illustrating steps for the joint construction are shown in Figures 4-7(a)-(c).

(a)

(b)

(c)

Figure 4-7: Joint Construction: (a) panels positioned (b) concrete casting (c) finished surface

4.4 Test Set Up

All the specimens were tested under the loading and boundary condition shown in the schematic of the specimen test set up in Figure 4-8. The specimens were tested in a rigid loading frame composed of steel beams and columns. A 110 kip hydraulic actuator fitted with a load cell was used to apply the load. The actuator load was transferred to the specimens via two transverse rigid steel spreader beams. The load from the spreader beams was transferred to the concrete surface through two steel plates intended to act as point loads.

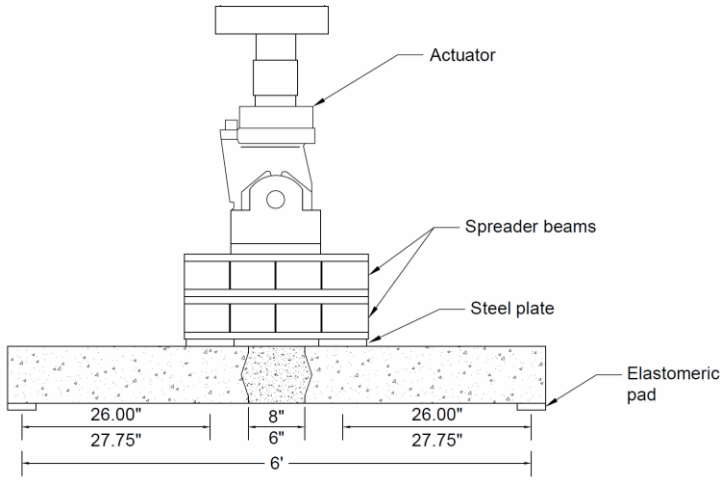

Figure 4-8: schematic of the specimen test set up

The specimens were simply supported with a 6 ft. span. A 4 in. by 36 in. elastomeric bearing pad having a 1 in. thickness was placed between the slabs and the support steel beams to ensure boundary condition was achieved. The shear span for specimen 1 and specimen 2 was 26 in. and 27.75 in., respectively, as shown in the schematic drawing where the top and bottom dimensions are those corresponding to specimen 1 and 2, respectively. These dimensions for the shear span considers the distance from the center of the bearing pad to the center of the steel plate. The joint zone

was located in the center of the span and experienced a maximum constant moment and zero shear. A 4 in. linear potentiometer was positioned and centered on the top surface of the specimens to record deflection. A photograph of the final test set up including loading frame, specimen, actuator, and potentiometer is shown in Figure 4-9.

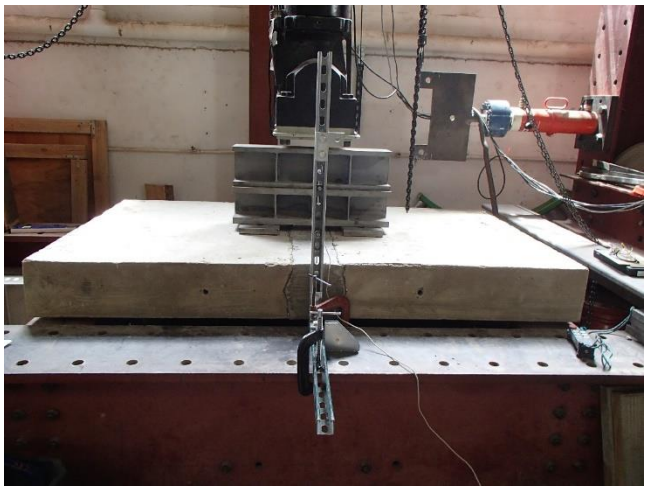

Figure 4-9: Test set up

4.5 Design Strength

Capacity of each specimen was determined two ways using nominal and measured material properties. Calculation for nominal material strength considers a compressive strength of 4000 psi and a yield strength of 60 ksi. In the calculation for measured material strength, the reinforcing steel was assumed to have an over strength of 20%, reaching a yield strength of 72 ksi; the average concrete compressive strength of the panels was 4570 psi. All the calculations were done using the force illustration shown in Figure 4-10. The shear and moment diagrams are also shown in the figure. The load from the actuator plus the self-weight of the spreader beams and steel plates was taken as two equal point loads positioned at the distance shown in the drawing with respective to each joint width. The shear (V) is equal to the load divided by two (P/2). The maximum

moment (M_{max}) is determined by multiplying the point load (P/2) by the shear span. Rotation point of the slab was assumed toward the inner face of the bearing pad, thus decreasing the shear span from 26 in. to 24.75 in. and 27.75 in. to 26.50 in. for specimen 1 and specimen 2, respectively. This behavior was verified during the test.

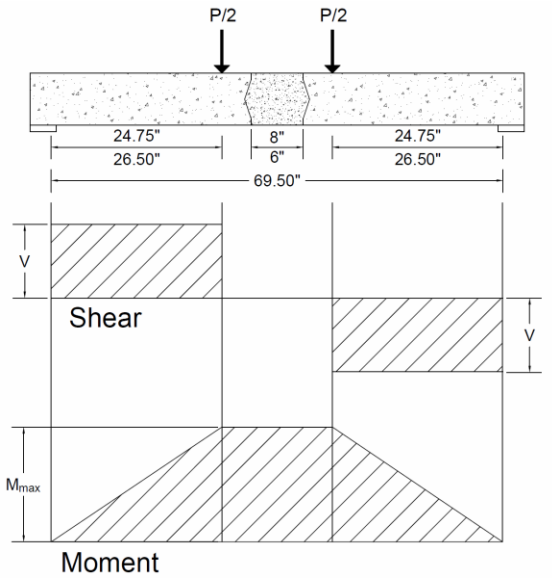

Figure 4-10: Test specimen force diagram

Calculation results for specimen capacity are shown in Table 4-1. The calculated capacity using nominal and measured material strength for specimen 1 was 52.0 kips and 62.2 kips, respectively. The calculated capacity using nominal and measured material strength for specimen 2 was 48.5 kips and 58.1 kips, respectively. The strength calculated using nominal material strength resulted in a more conservative load while the strength using measured material properties gave a higher load which is consistent with the load obtained from the experimental tests presented in the test results section.

Table 4-1: Summary of specimen Capacity

Specimen	Nominal material strength		Measured material strength	
	M_n (kip-ft)	P (kips)	M_n (kip-ft)	P (kips)
1	53.6	52.0	64.2	62.2
2	53.6	48.5	64.2	58.1

4.6 Testing

Each specimen was tested a day after casting of the high early strength concrete in the closure pour connection. Concrete cylinders were tested the day of testing to obtain the compressive strength of the closure pour mixture. The strength of the closure pour concrete obtained from the 4 in. by 8in. cylinder tests are presented in Table 4-2. Specimen 1 and specimen 2 were tested at approximately 26 hours after casting. The mixture in specimen 1 reached an average compressive strength of approximately 8400 psi in about 22 hours and 8640 psi in about 28 hours. The average 12-hour and 24-hour compressive strength for the mixture in specimen 2 was approximately 7395 psi and 8985 psi, respectively. The normal-strength concrete used in the deck panels had a measured compressive strength of about 4570 psi the day of testing.

Table 4-2: Compressive strength from the cylinder tests

Cylinder	**High early-strength concrete Specimen 1**			**High early-strength concrete Specimen 2**		
	Compressive Strength (psi)	Force (lbs)	Time	Compressive Strength (psi)	Force (lbs)	Time
C1	8640	108610	9:50am	7280	91495	9:28pm
C2	8375	105250	10:10am	7510	94385	9:49pm
C3	8190	102900	10:30am	-	-	-
Average	**8402**	**105587**	**22 hrs**	**7395**	**92940**	**12 hrs**
C4	8550	107440	4:16pm	8755	110055	9:25am
C5	8520	107100	4:47pm	9090	114245	9:56am
C6	8860	111365	5:01pm	9110	114500	10:14am
Average	**8643**	**108635**	**28 hrs**	**8985**	**112933**	**24 hrs**

During the test, the specimens were loaded continuously at a load rate of approximately 4 kips/minute until failure. Failure was identified as the formation of large wide cracks and crushing of concrete. Each specimen was visually observed multiple times throughout the test to document any distress on the slabs. The specimens were inspected using visual crack techniques to monitor crack formation.

4.7 Test Results

Top view and front view of the specimens throughout the test are shown in Figures 4-11 through 4-17. In specimen 1, cracking was observed in the upper zone of the interface connection and within the top layer of the joint. Cracking in specimen 2 developed within the joint as depicted in Figure 4-11. Hairline flexural cracks formed in the deck panels at a distance of approximately 10.5 in. and 11.5 in. from the interface for specimen 1 and specimen 2, respectively. As loading progressed, the crack that developed within the joint of specimen 1 widened and extended into the panel as seen Figure 4-13. In specimen 2, another crack formed in the bottom layer of the joint and progressed towards the top layer of the joint. Near the peak load, concrete crushing occurred in the top surface, as expected of a flexure controlled failure mode. Concrete crushing was more pronounced in the concrete within the deck panels which were fabricated using normal-strength concrete. The joint concrete containing the high early-strength concrete did not suffer crushing as is evident in Figures 4-14 and 4-15.

Photographs of the specimens after failure can be seen in Figures 4-15 and 4-16. Crack formation in the connection interface in specimen 1 led to separation of the high early-strength concrete from the normal-strength concrete of the panels in the shear key connection as shown in Figure 4-16. The cracks that were initially observed only in the surface of the concrete in specimen 2, continued to propagate deeper into the joint until reaching one the transverse reinforcing bar as loading progressed. These cracks intersected and caused a portion of the concrete to fall out. The end of the hooked bar can be seen in Figure 4-16. A similar crack pattern noticed in the front view of the specimens was observed in the rear view of the specimens as shown in Figure 4-17.

The failure mode of the two specimens is a typical flexural failure with concrete crushing at the top surface of the panels and cracks forming and widening from the bottom surface of the panels that are subjected to tension forces. Specimen 1 reached a maximum load of approximately 63.2 kips at a deflection of about 1.35 in. Specimen 2 registered a maximum load of approximately 58.3 kips corresponding to a deflection of about 1.26 in. Globally, specimen 1 and specimen 2 showed same general behavior as the deformation was concentrated in the closure pour connection. Locally, failure was different in terms of crack formation in the joint.

Figure 4-11: Crack in the joint: Specimen 1 (left); Specimen 2 (right)

Figure 4-12: Flexure cracks in the panels: Specimen 1 (left); Specimen 2 (right)

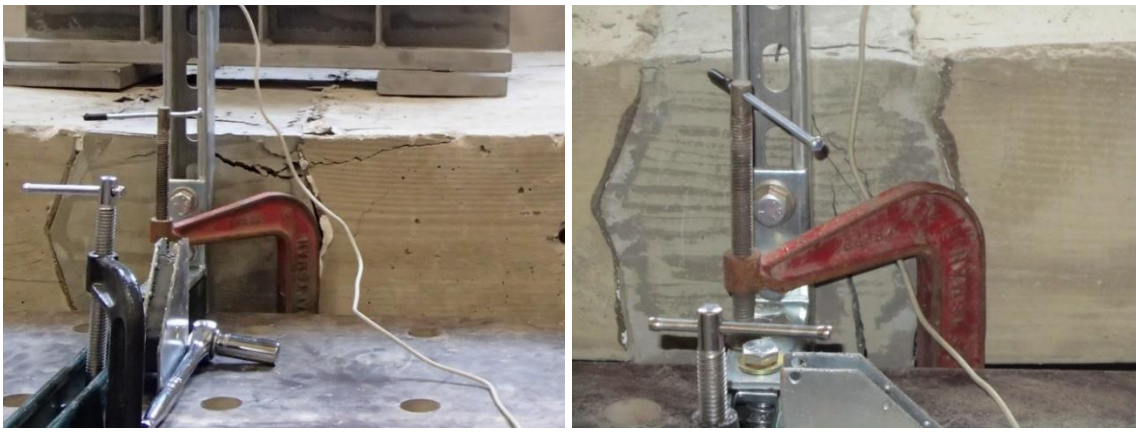

Figure 4-13: Crack propagation: Specimen 1 (left); Specimen 2 (right)

Figure 4-14: Concrete crushing: Specimen 1 (left); Specimen 2 (right)

Figure 4-15: Top view after specimen reached failure: Specimen 1 (left); Specimen 2 (right)

Figure 4-16: Front view of the joint after specimen reached failure: Specimen 1 (left); Specimen 2 (right)

Figure 4-17: Rear view of the joint after specimen reached failure: Specimen 1 (left); Specimen 2 (right)

The load-deflection relationship for each specimen is shown in Figures 4-18 and 4-19. It can be noticed that at a load of approximately 44 kips specimen 1 was unloaded. At this load, the test was halted for quick adjustments in the elements used to transfer load. At this time there was not any major sign of distress noticed in the specimen. After the adjustment, loading was continued until failure of the specimen. There is a linear load deflection relationship in both plots from initial loading to a load of approximately 33 kips at a deflection of about 0.3 in. After this point, a change in stiffness can be observed from the curve. The change in stiffness was assumed to be the result of cracks that

formed in the joints. After unloading and reloading specimen 1, a linear relationship is once again noticed up to a load of about 45 kips. Specimen 2 was loaded continuously without any interference of unloading and reloading as seen in Figure 4-19. Design load using nominal and measured material strength are displayed with dashed lines in the plots to be compared with the peak load measured in the tests.

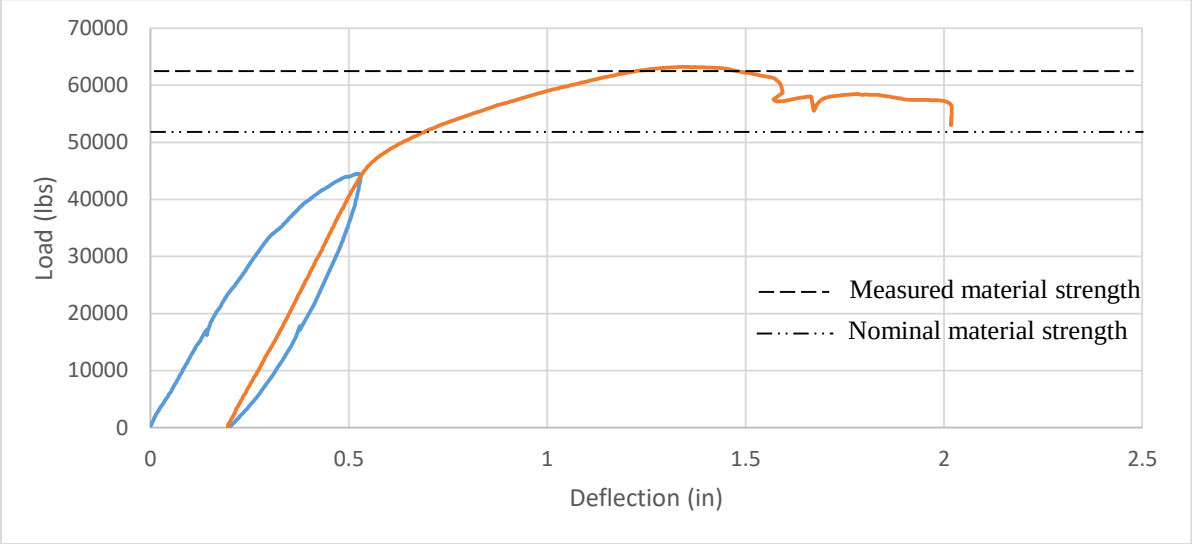

Figure 4-18: Load-Deflection Plot from Specimen 1 test

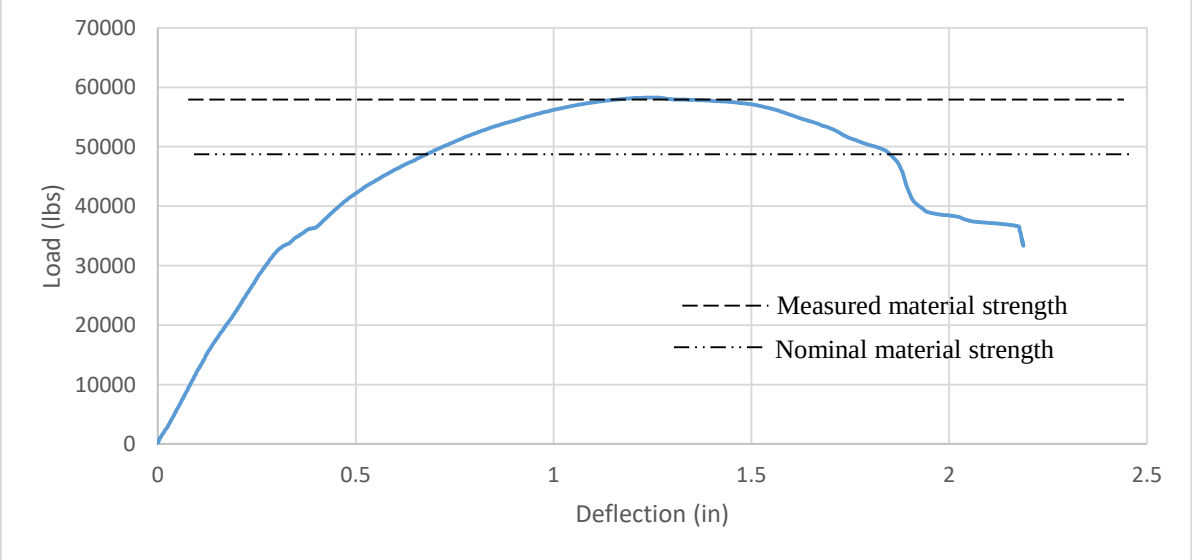

Figure 4-19: Load-Deflection Plot from Specimen 2 test

Calculated capacity using nominal and measured material properties along with the failure load obtained from the experiment are presented in Table 4-3. For purposes of comparison, percent difference for calculated capacities and experimental failure load is also presented in the table. It can be seen that the design capacity using nominal material properties results in a lower capacity when compared with experimental results, underestimating the failure load by almost 19%. The design load using measured material properties is close to the failure load from the experiment, with a percent difference less than 2% for both specimens.

Table 4-3: Calculated capacity and experimental failure load comparison

Specimen	Nominal material strength	Measured material strength	Experiment failure load	Nominal & Experiment % Diff	Measured & Experiment % Diff
1	52.0 kip	62.2 kip	63.2 kip	19.4 %	1.6 %
2	48.5 kip	58.1 kip	58.3 kip	18.4 %	0.3 %

4.8 Summary of Laboratory Experiments

Two large-scale tests were conducted to investigate the performance of longitudinal closure pour connections between two panels representing typical decks of Decked Bulb Tee girders. The concrete used for the closure pour was developed as part of a larger project intended to develop a high early-strength concrete mixture for use in New England. The primary objectives of the tests were to evaluate whether the connection performed adequately to develop the required short-term strength and document any distress that may occur because of loading at early ages. Another goal was to investigate whether narrow closure pours could be used in combination with the high early-strength concrete mix without negative effects on transverse strength between the

panels. The two specimens were designed, fabricated, and tested under four-point bending in the structural laboratory. During the tests, flexural cracks and crushing of concrete were observed on the precast slabs, outside of the closure pour region. The specimens were loaded continuously until experiencing flexural failure characterized by concrete crushing at the top surface and cracks forming and widening from the bottom surface.

Based on the results of the tests, the concrete closure pour connection comprised of hooked bars detailing according to recommended practice obtained from PCI Northeast for decks of Decked Bulb Tee girders in combination with the developed mixture performed well in the experiment. The connections were capable of reaching the required high early-strength and provide adequate transfer of forces between the structural components in one day. Using measured material properties, commonly used design equations adequately predicted the strength of the connections measured in the laboratory. The load-deflection plots from the experiment will be used to define the load-deformation properties of the closure pours in the finite element models presented in subsequent chapters. Results from specimen 1 (8 in. joint) will be applied to the 8 in. closure pour and results from specimen 2 (6 in. joint) will be applied to the 6 in. closure pours.

CHAPTER 5

SIMPLIFIED BRIDGE MODEL ANALYSIS

5.1 Simplified Model Description

When performing finite element analysis for bridges, decks are typically assumed to be continuous and are modeled using shell elements. In this study, nonlinear link elements were introduced to the bridge deck to connect adjacent shell elements and simulate closure pour connections between girders. The function of closure pours is to make the deck continuous and provide adequate load transfer between the adjacent girders. In order to validate that the link elements served this function, a simplified model was developed to investigate load transfer between the girders via link elements. The simplified model can be seen in Figure 5-1.

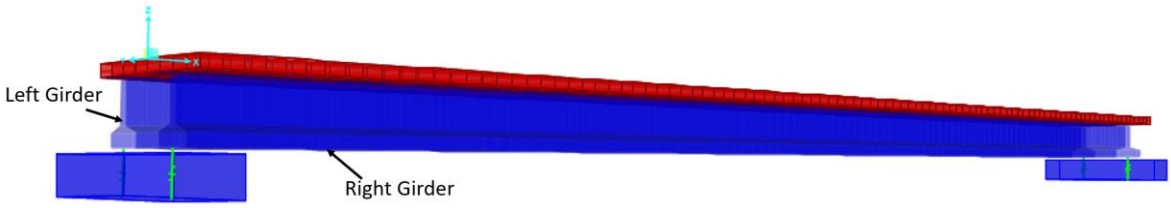

Figure 5-1: Simplified finite element model

The model was built with only two of the eight girders from the full-scale model described in Chapter 3. The two girders were joined together through deck elements connected using nonlinear link elements. The girders are referred to as left girder and right girder in this chapter as shown in Figure 5-1. The analysis on the model was initiated with a mesh convergence study performed to refine the mesh in the deck to ensure accurate results, including the nonlinear response of the closure pour. Afterwards, moment values at three different locations along the length of the simplified model were

determined to verify that the links were properly distributing loads between the two girders. The model was subjected to uniformly distributed dead loads and concentrated live loads calculated based on the AASHTO LRFD specification. Details on each analysis are presented and discussed in the sections below.

5.2 Deck Mesh Refinement

The mesh in the deck of the model was refined in order to obtain accurate and practical results from the analysis. The deflection calculated by using the elastic formula presented below was set as the criteria in fine-tuning the mesh. After different meshing trials, the model was able to produce results close to the desired solution. For example, applying a load of 0.2 ksf (1 kip/ft.) to each girder gives a maximum deflection of 1.56 in. using the deflection formula for a simply supported beam subjected to uniform loading (Equation 5-1). For the purpose of this assessment, a compressive strength of 4000 psi was used to define girder material property. The maximum deflection from the model was 1.59 in., which is about 1.9% difference from the value obtained from hand calculation. Proximity of the maximum deflection obtained from the model and hand calculation using equations based on linear-elastic material properties reassured the adequacy of the mesh and the chosen modeling method in reproducing realistic results.

$$\Delta = \frac{5wL^4}{384EI} \qquad \text{(Equation 5-1)}$$

L = 1140 in. (span length = 95 ft.), E = 3605 ksi, I = 325562 in^4

5.3 Trial Load Tests

Trial loads were applied to the girders in the simplified model in order to investigate if the link elements were adequate in transferring forces between the two girders. The loads that were applied to the models were applied to deck elements as area loads. Moments calculated at quarter-span, mid-span, and three-quarter-span for each trial are listed in Table 5-1. An initial load of 0.2 ksf (1 kip/ft for the entire width of the model) was applied to the left girder over the entire 95 ft. span-length. This load produced a maximum moment of 1128.13 kip-ft. in the entire model. The maximum moment from the model at mid-span was equal to the expected moment calculated using statics (M= $WL^2/8$). The maximum moment in the left and right girders were 645.58 kip-ft. and 482.55 kip-ft., respectively. The left girder experienced a higher moment than the right girder as expected since the area load was applied directly over the left girder. The same load of 0.2 ksf was applied to the right girder and the results were the same as when the load was applied over the left girder. That is, the girder under the applied load was subjected to a higher moment than the girder away from the load.

Table 5-1: Moments from the Simplified Model

Load		0.2 ksf		32, 32, 8 kips	0.2 ksf	32, 32, 8 kips	
Load Location		Left Girder		Left Girder	Right Girder	Right Girder	
1/4 dist. Moment (kip-ft)	Entire Bridge	846.09	--	939.84	846.09	939.84	--
	Left Girder	553.39	65%	616.92	292.68	322.9	34%
	Right Girder	292.70	35%	322.92	553.41	616.94	66%
1/2 dist. Moment (kip-ft)	Entire Bridge	1128.13	--	1428.16	1128.13	1428.16	--
	Left Girder	645.58	57%	884.49	482.50	543.61	38%
	Right Girder	482.55	43%	543.67	645.63	884.56	62%
3/4 dist. Moment (kip-ft)	Entire Bridge	846.09	--	772.16	846.09	772.16	--
	Left Girder	553.39	65%	488.52	292.68	283.63	37%
	Right Girder	292.70	35%	283.64	553.41	488.53	63%

In the second part of the test, point loads representing vehicle tire loads were applied to the model. The point loads were distributed over a rectangular (10in. x 20in.) area on the deck elements (patch loading). Three point loads with a magnitude of 32 kips, 32 kips, and 8 kips spaced at 14 ft. were first applied to the left girder. These load magnitudes and spacing correspond to a nominal HS20 truck that is part of the live-load model in the AASHTO LRFD Specification. The maximum moment in the entire model was found to be 1428.2 kip-ft. The maximum moment in the left and right girders were 884.5 kip-ft. and 543.7 kip-ft., respectively. The left girder took 62% of the load while the right girder received 38% of the load. Again, the left girder experienced a higher moment as expected from the results. The same analysis was repeated for the right girder and it produced similar results. The moment at both ends of the bridge was zero for all the load tests. The results from these trial load tests showed that the links were successful in transferring loads between the adjacent girders.

5.4 Bridge Loads

Live and dead loads from AASHTO LRFD (2012) were applied to the simplified model. The purpose of this analysis was to apply the specified loads to the model and confirm the results from the analysis with hand calculations. Doing this comparison was especially beneficial for confirming placement of the design truck load to generate the maximum moment in the bridge. Using the actual AASHTO LRFD load model was also useful to determine whether links would be expected to go into the nonlinear range for realistic loading scenarios.

5.4.1 Dead Load

Dead loads defined in the LRFD specification considered in this study were the self-weight of the girders, utilities, wearing surface, railings, and curbs. All structure dead loads with the exception of wearing surface and utilities are classified as component dead load DC. Dead load of wearing surface and utilities are categorized as DW. CSiBridge calculates moment from self-weight based on the structural material and section properties defined in the model. Hand calculation was performed to validate the moment obtained from the analysis. The calculations can be found in Appendix B. The values used for each dead load are presented in Table 5-2. It was assumed that the two girders would experience approximately a quarter of the total dead loads from the full-scale bridge. These loads were applied to the model as area loads over the entire length of the bridge.

Table 5-2: Summary of dead loads in the Simplified Model

Component	Load (lb/ft)
Girders	2307
Railing	125
Curb	138
Wearing surface	188
Utilities	100

5.4.2 Live Load Description

Live loads specified in the LRFD specification that apply to this bridge are HL-93 vehicular live load and pedestrian load. The pedestrian load is provided as an area load of 75 psf that is placed over the sidewalk region. HL-93 vehicular live load is a combination of the design truck or design tandem with a design lane load. Analysis must be performed

using both trucks to determine the one that governs for design. Design truck had the most significant effect on the bridge used in this study, so live load analysis was performed based on the design truck. The design lane load is given as a uniform load of 640 lb/ft. distributed in the longitudinal direction. It is applied to a 10 ft. wide design lane.

Multiple presence factor was not considered in the simplified model analysis for the purpose of the study. The dynamic load allowance (33%) was applied to the truck load. Illustration of the design truck is shown Figure 5-2. The truck has three axles in the longitudinal direction. The front axle has a loading of 8 kips, and the middle has a loading of 32 kips and is located 14 ft. behind the first axle. The rear axle also has a loading of 32 kips and is positioned at a variable distance ranging between 14 and 30 ft. The axle spacing selected between the middle and real axles should cause critical load effects. For a short-to-medium simply supported bridge, the minimum axle spacing of 14 ft. controls for design.

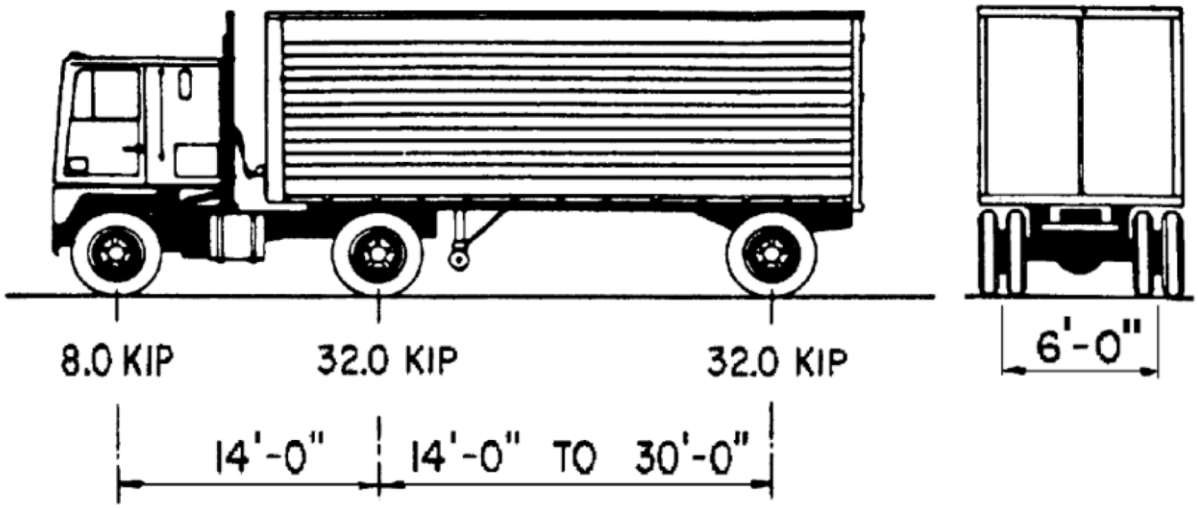

Figure 5-2: HL-93 Design Truck [AASHTO LRFD (2012)]

5.4.3 Design Truck Placement

The simplified model was defined with one 10 ft. wide design lane, which covered the total width of the model. Truck load was centered on the bridge in the transverse direction. Centering the truck load positioned the tires two feet from the edge of the bridge. In the longitudinal direction, the load was positioned for maximum load effect using results from influence line analysis. Influence line ordinates and truck load placement can be seen in Figure 5-3. In the model, the middle axle was placed at mid-span (47.5 ft.) while the front and rear axles were placed at a distance of 14 ft. from the middle one. The load position in Figure 5-3 shows one traffic direction. If the truck was traveling in the other direction, the moment at mid-span would be the same, but the moment in the other locations would be different. Therefore, a load combination envelope was used to consider the two cases and determine the controlling moments at each point along the length of the bridge.

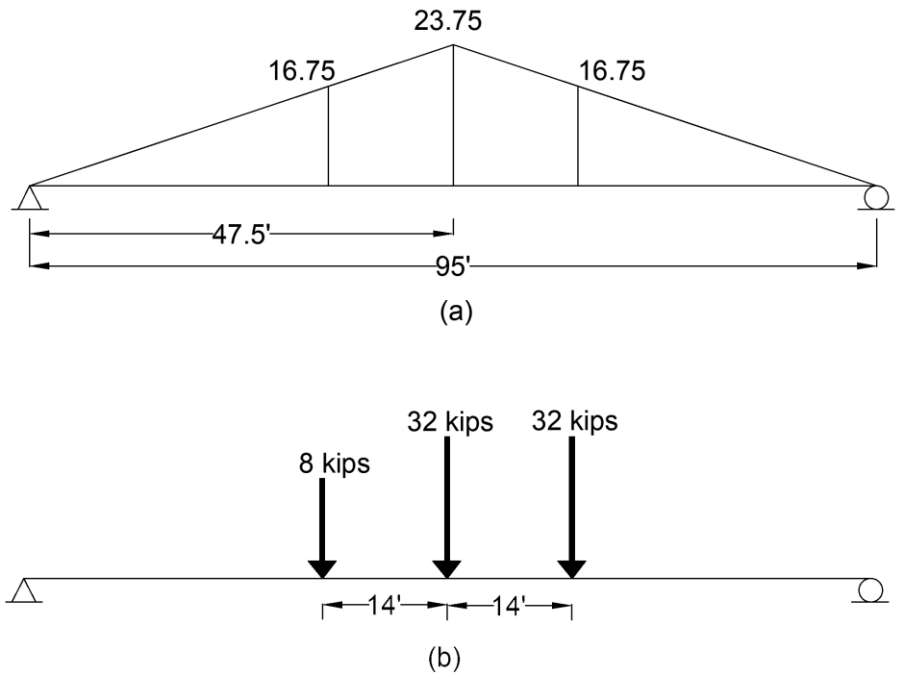

Figure 5-3: (a) Influence line (b) Longitudinal placement of truck axle load

Although the truck loads are depicted in terms of axle point loads, the real point of contact between the truck and the surface of the bridge is the individual tires. AASHTO LRFD suggests that designers use a rectangular tire contact area measuring 20 in. wide and 10 in. long for a wheel consisting of one or two tires. The tire pressure is assumed to be uniformly distributed over the contact area. Using this recommendation, the truck load was applied to the model in the form of rectangular area loads as shown in Figure 5-4. The 32 kips and 8 kips axle loads were divided into two 16 kips and 4 kips tire loads, respectively.

Figure 5-4: Truck tire load applied to the model

5.5 Load Combination

After performing the analysis with the typical bridge dead and live loads, the maximum moment was calculated based on Strength I load combination. Strength limit states from the LRFD specification ensures that the bridge satisfies the strength and stability requirements to resist significant load combinations that the bridge may experience during its design life. The specified dead and live load factors for Strength I are presented in Equation 5-2. In this equation, DC represents the load from self-weight

of the girders, curb, and railing. DW is the load of wearing surface and utilities. LL and PL are HL-93 and pedestrian loads, respectively.

$$1.25DC + 1.5DW + 1.75(LL+PL) \quad \text{(Equation 5-2)}$$

The maximum moment based on Strength I load combination from the model was 9071.16 kip-ft., which was about the same as the moment calculated from hand calculation of 9071.98 kip-ft. The maximum moment in the left and right girders were 4534.84 kip-ft. and 4536.32 kip-ft., respectively. The results verified that load positioning using the influence line technique and the recommended tire area load was successful. The model was adequate in approximating the maximum moment in the girders.

Overall, the results from each analysis on the simplified model confirmed that the chosen modeling technique was capable of providing accurate results that satisfied the objectives set for this study. The analysis assumptions and load placement method used in the simplified model were implemented in the full-scale models to determine live load distribution factors in each girder, study the effects of diaphragms, and investigate strength of concrete closure pours. The analyses on the full-scale models are presented in Chapters 6 and 7.

CHAPTER 6

FULL-SCALE BRIDGE MODEL ANALYSIS

6.1 Model 1 Analysis

The purpose of developing Model 1 was to investigate live-load distribution characteristics in a precast/prestressed concrete bridge with longitudinal closure pour connections containing end and intermediate diaphragms. The investigation was conducted by calculating moment live-load distribution factors for each girder using a finite element model representing the selected prototype bridge. The distribution factors were compared to those from AASHTO LRFD (2012) to determine if the presence of longitudinal joints and diaphragms affected load distribution characteristics. After this comparison, an investigation was also conducted on the moment-rotation behavior of closure pours to determine if these joints provided the strength and deformation required to adequately transfer loads across precast/prestressed concrete bridges.

6.2 Live-Load Distribution Factors

This section presents moment live-load distribution factors (LLDF) calculated from Model 1 and the corresponding AASHTO LRFD LLDF formulas.

6.2.1 Live-Load Distribution Factors from Model 1

In the analysis of the simplified model presented in Chapter 5, the HL-93 live-load model was centered on the bridge in the transverse direction considering that the width of the bridge was only 10 ft. In the full-scale model presented and discussed in this chapter, the load model was positioned at different locations in the transverse direction to determine the critical moment in each girder. This was done by moving the truck

transversely across the width of the bridge and computing moment at each location for one-lane, two-lane, and three-lane design loads. The number of design lanes was calculated as the clear roadway width between the railings divided by twelve as specified in AASHTO LRFD Specification (2012). Following this procedure, a total of three design lanes was calculated for the prototype bridge. The width of the design lanes was 10 ft. as stipulated in the AASHTO LRFD Specification.

In the longitudinal direction, the load was applied using the method described in Chapter 5 to produce the critical load effect. The suggested tire contact area loading shown in Figure 5-4 was incorporated in the analysis on Model 1. The different truck positions in the transverse direction and the moment obtained for each case can be found in Appendix C in Figures C-1 to C-3 and Tables C-1 to C-5, respectively. The initial and final load position for each lane loaded is shown in Figure 6-1. There were a total of 12, 8, and 4 load position cases for one-lane, two-lane, and three-lane loads, respectively. The maximum moments each girder will experience after considering all the different HL-93 load positions are summarized in Table 6-1.

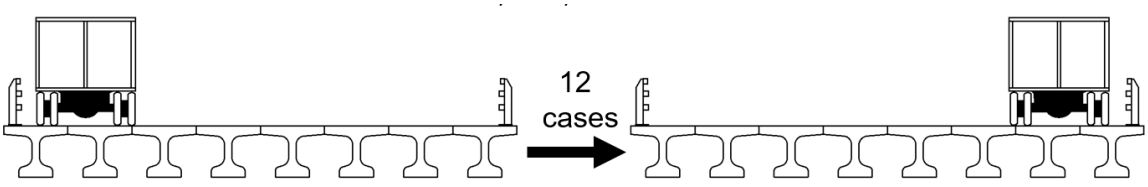

(a)

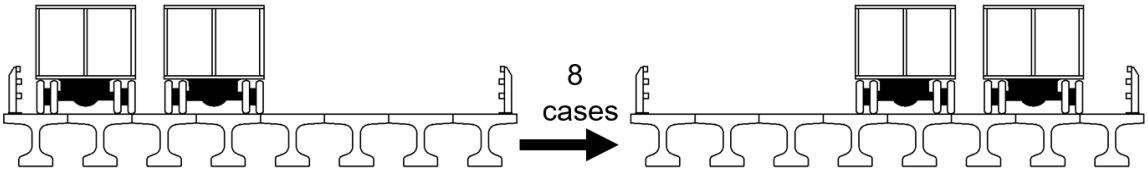

(b)

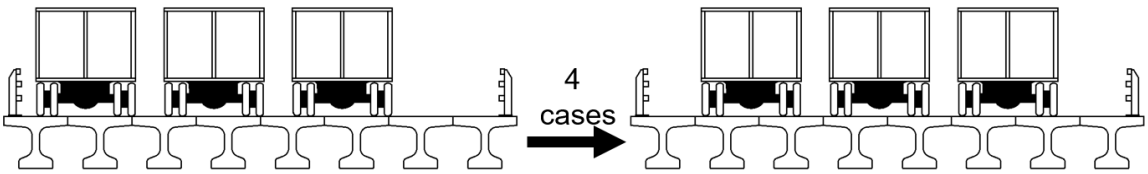

(c)

Figure 6-1: Initial and final load positions (a) one lane (b) two lanes (c) three lanes

Table 6-1: Maximum moment in each girder for each load case

Girder	Moment (kip-ft.)				
	1 Lane	2 Lanes	2 Lanes-R*	3 Lanes	3 Lanes-R*
1	878.00	1086.00	1063.25	1009.25	984.56
2	692.00	996.10	1014.76	1001.75	996.93
3	570.00	855.75	905.34	959.53	979.09
4	490.00	775.95	817.89	949.81	968.50
5	490.00	775.95	817.89	949.81	968.50
6	570.00	855.75	905.34	959.53	979.09
7	692.00	996.10	1014.76	1001.75	996.93
8	878.00	1086.00	1063.25	1009.25	984.56

*R indicates the models that used a reduced stiffness for diaphragms

In Table 6-1, the girders are numbered from 1 to 8, starting from the left exterior girder to the right exterior girder as shown in the cross-section of the bridge in Figure 6-2. The girders numbered 2 to 7 are considered the interior girders while 1 and 8 are considered the exterior girders. The labels *1 Lane, 2 Lanes, and 3 Lanes* represent the results from the model that used uncracked conditions of the diaphragms. The other labels, *2 Lanes-R* and *3 Lanes-R,* are from the model that considered cracked conditions by reducing the stiffness of the diaphragms. Cracked conditions were incorporated in the models by assuming a two-thirds reduction in moment of inertia from the gross value in the uncracked diaphragms.

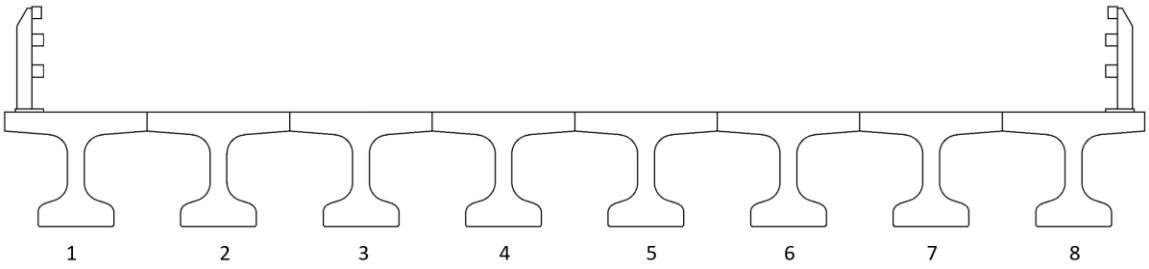

Figure 6-2: Cross-section showing numbers assigned to each girder

The reductions in stiffness was not used for one lane loaded because the moments calculated from this load case were smaller than the other two cases and would not govern design. The moment values listed in Table 6-1 considered the adjustment for multiple presence provided in AASHTO LRFD Specification. The multiple presence factor for one, two, and three design lanes are 1.2, 1.0, and 0.85, respectively. In order to determine LLDF from finite element analysis, the following ration is calculated:

$$g = \frac{M_{girder}}{M_{bridge}} \qquad \text{(Equation 6-1)}$$

Where: g = Live-load distribution factor (LLDF)

M_{girder} = Maximum moment in one girder

M_{bridge} = Maximum moment in the bridge under one lane of HL-93 loading

AASHTO LRFD treats LLDFs for interior and exterior girders differently. One distribution factor is used for design of all interior girders while exterior girders are designed determining a different distribution factor. To calculate the distribution factor for interior girders in Model 1 for comparison with AASHTO LRFD equations, the maximum moment out of the critical moments in girders 2 to 7 was selected as M_{girder}. For exterior girders, M_{girder} was the maximum moment determined in girder 1 or girder 8. For one lane of HL-93 loading, M_{bridge} was determined to be 2621.46 kip-ft. The distribution factors calculated from each load case are presented in Table 6-2. Based on

the results, the two-lane load considering diaphragms with reduced stiffness controlled the design for interior girders and two-lane load with full and reduced diaphragm stiffness governed design of exterior girders.

Table 6-2: Live load distribution factors from Model 1

Girder	1 Lane	2 Lanes	2 Lanes-R	3 Lanes	3 Lanes-R
Interior	0.26	0.38	0.39	0.38	0.38
Exterior	0.33	0.41	0.41	0.38	0.38

According to bridge design standards, the interior and exterior girders from Model 1 would be assigned a distribution factor of 0.39 and 0.41, respectively. Although the two-lane loading condition governed design of all interior girders according to AASHTO, a review of the moments in Table 6-1 indicates that the higher moments were found in interior girders 3 to 6 for three lanes loaded than those determined in these girders for two lanes loaded. This can be seen more clearly in Figure 6-3. Based on the results shown in the figure, two-lane load condition governed moments for the exterior girders and interior girders 2 and 7, while three-lane load controlled the design for the rest of the interior girders. Designing interior girders 3 to 6 using a distribution factor of 0.39 would be conservative as these girders will not experience the same moment experienced by interior girders 2 and 7. Girders 3 to 6 would be designed using a moment value about 5% higher than the actual moment these girders will experience.

Figure 6-3: Maximum moment on each girder from one, two, and three design lanes

The observation that three lanes loaded, instead of two lanes loaded, controlled the design moment for some of the interior girders is in agreement with the conclusions of Ypisof and Hindi (2007). They recommended using FEA for certain bridge types in order to obtain more accurate moment values in each girder. The results found from the analysis on Model 1 confirmed that using FEA is more accurate in obtaining moments for multiple lanes loaded when compared to AASHTO LRFD.

The influence of uncracked and cracked conditions of the diaphragms on load distribution is evident in Figure 6-3. It can be seen that the reduction in stiffness caused a moderate decrease in the moment for exterior girders and an increase in the moment for interior girders. In general, the load was distributed more uniformly in the bridge under three lanes loaded. One-lane loading produced a higher difference in moments among interior girders and resulted in much lower moment values when compared to the other

two cases. This result is consistent with the findings of Ma et al. (2007) who also conducted a study on load distribution using Decked Bulb Tee girders.

6.2.2 Distribution Factors from AASHTO LRFD

In the calculations of live load distribution factors using AASHTO LRFD procedures, the deck superstructure (J) was selected and the bridge was assumed to be sufficiently connected to act as a unit. The LRFD formulas applicable to this bridge type for each loading case are presented in Table 6-3. The same equations are used for two and three loaded lanes.

Table 6-3: LLDF formulas from AASHTO LRFD (2012)

Design Lane Loaded	Interior	Exterior
One lane	$0.06+\left(\frac{S}{14}\right)^{0.4}\left(\frac{S}{L}\right)^{0.3}\left(\frac{K_g}{12.0Lt_s^3}\right)^{0.1}$	Lever Rule
Two or more lanes	$0.075+\left(\frac{S}{9.5}\right)^{0.6}\left(\frac{S}{L}\right)^{0.2}\left(\frac{K_g}{12.0\,Lt_s^3}\right)^{0.1}$	$g = e\,g_{interior}$ $e = 0.77 + \frac{d_e}{9.1}$

In the Table 6-3:
S is the girder spacing (ft.)

L is the span length (ft.)

t_s is the slab thickness (in.)

d_e is the distance from the center of the exterior girder and the inside edge of the barrier

K_g is the longitudinal stiffness parameter (in^4)

$K_g = n(I_g + e_g^2 A)$, where

n is the modular ratio, (E_{beam}/E_{deck})

I_g is the moment of inertia of the beam (in^4)

e_g is the distance between centers of gravity of the beam and deck (in.)

A is the area of the beam (in^2)

The values used for the variables presented above to calculate LLDFs are listed in Table 6-4. Two cross sections, shown in Figure 6-4, were used to calculate the distribution factors. The first cross-section was the beam section assumed during the modeling process described in Chapter 3. In this assumed cross-section, the deck was considered as the 8 in. portion of the top flange and the beam was the smaller portion of the top flange along with the web and bottom flange. The height of the beam was 40 in.

Table 6-4: Variables used to calculate LLDFs

Section	n	I (in^4)	A (in^2)	e_g (in.)	K_g (in^4)	S (ft.)	L (ft.)	t_s (in)
Assumed	1	112685	628	28.6	625205	5	95	8
NEDBT	1	76254	567	32.4	671349	5	95	8.53

The second cross-section is from PCI Northeast Deck Bulb Tee Guidelines (NEDBT). In the guide, the following assumptions are made for the recommended cross-section: The stem is treated as an individual stringer; the web/bottom flange portion of the beam is the stringer (up to the top of the top radius); the top flange portion of the beam is the composite deck (top of top radius to the top of the beam).

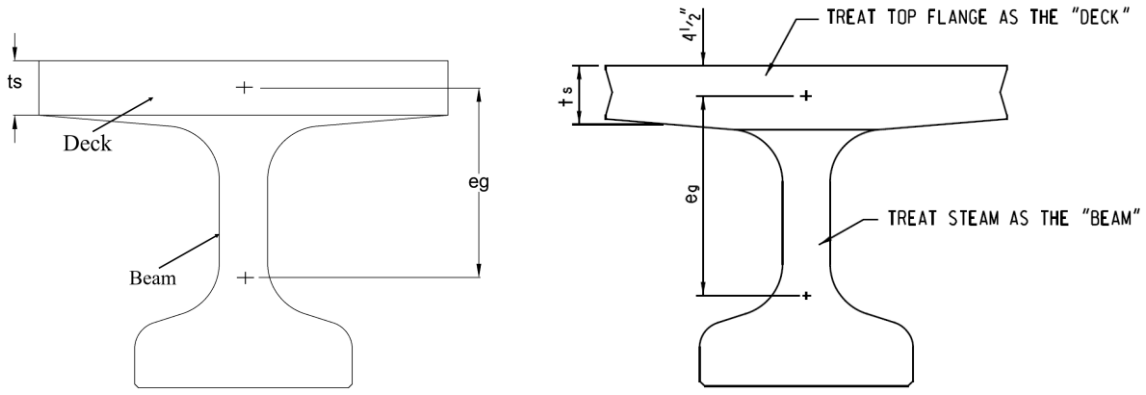

(a) (b)

Figure 6-4: (a) Assumed cross-section (b) NEDBT cross-section

The values obtained for LLDFs based on the assumed and NEDBT cross sections for interior and exterior girders using AASHTO LRFD formulas can be seen in Table 6-5. The distribution factors calculated by using the two cross sections were generally similar. The factors determined using the NEDBT cross-section for interior girders under both loading cases were slightly lower than those from the assumed cross-section. The values for exterior girders under two or more lanes loaded were also a little lower. The distribution factors for exterior girders for one-lane loaded were the same since the lever rule was used for both cross sections.

Table 6-5: Distribution factors based on AASHTO LRFD formulas

Design lane loaded	Assumed cross-section		NEDBT cross-section	
	Interior	Exterior	Interior	Exterior
One lane	0.34	0.49	0.33	0.49
Two or more lanes	0.46	0.41	0.45	0.40

6.2.3 Comparison of LLDFs from Model 1 and AASHTO LRFD

The LLDFs obtained from the analysis on Model 1 were compared to those from AASHTO LRFD Specification calculated based on the assumed cross-section. Comparison of the results are graphically presented in Figure 6-5. For interior girders, the factors from AASHTO LRFD formulas were conservative for each load condition. The formulas overestimated the factors by approximately 27%, 7%, and 19% for one, two, and three lanes loaded, respectively. Calculating LLDFs using the lever rule overestimated the distribution factors for exterior girders by almost 39% as seen in the comparison for one-lane loaded. These findings are consistent with the conclusion of

Ypisof and Hindi (2007) that AASHTO LRFD equations can be conservative, especially when the lever rule method is implemented to calculate distribution factors.

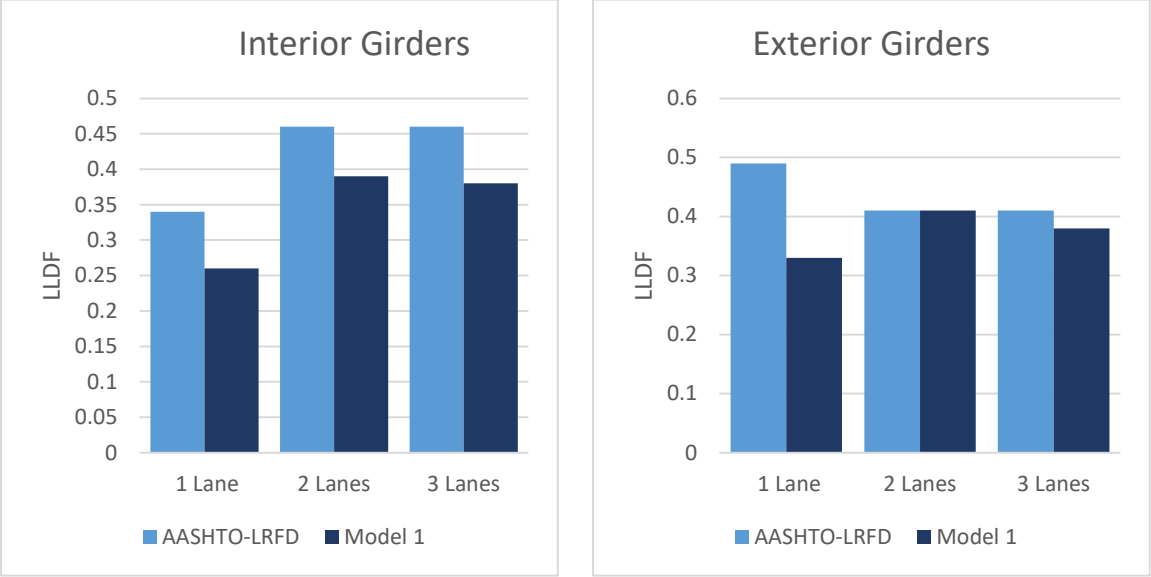

Figure 6-5: Comparison of LLDFs from AASHTO LRFD & Model 1

Despite the large differences in LLDFs for interior girders and one-lane loaded for exterior girders, the formula did provide reasonable estimates for two or more lanes loaded in exterior girders. For the two-lane load, the formula was accurate and for three lanes loaded the formula was within about 8% of the value from FEA. Overall, the results indicated that AASHTO LRFD formulas can be conservative in approximating LLDFs as observed by other studies [Ypisof and Hindi (2007), Barr et al. (2001), and Cai (2005)].

Model 1 was constructed with end and intermediate diaphragms, which could be the reason for the large difference in most of the distribution factors as the AASHTO LRFD formulas do not account for effects of diaphragms. In order to gain a better understanding on the contribution of diaphragms, further investigation on load distribution was conducted on other models built with only end diaphragms and without diaphragms. The results from these analyses showed the direct effect of diaphragms by

comparing the bridges with and without diaphragms. Distribution factors from the models with end diaphragms and without diaphragms were also compared to those from the AASHTO LRFD Specification. The analyses and results from these models are presented in Chapter 7.

Based on the examination of the results from the analysis on Model 1 and the comparison of moments in Chapter 5, it can be concluded that the longitudinal closure pour joints provided adequate transfer of moments induced by the design vehicular live-load. Although the closure pours were successful in transferring moments between the adjacent girders, there are some concerns pertaining to the design of these joints. A particularly important concern is the development length of the reinforcing bars in narrow closure pours. Reinforcing bars are required to reach certain design strength to enhance performance of closure pours. However, using narrow joints might not allow the bars to meet this requirement which in turn can compromise the safety of the structure. Therefore, an additional investigation was conducted to study the strength of the closure pours. The investigation is presented in the sections below.

6.3 Strength of Concrete Closure Pours

This section describes the analysis performed to validate performance of closure pours in developing the required strength.

6.3.1 Development Length of Reinforcing Bars

Closure pour connections comprised of steel and concrete has been commonly used to connect prefabricated components in Accelerated Bridge Construction. A typical detailing of the closure pour that has been found to perform well consists of a

combination of some type of high strength concrete material and reinforcing hooked steel bars, also known as U-bars. The hooked bars are preferred for closure pours because these bars have much smaller development length than straight bars and can be well suited for narrow closure pours.

When used with certain type of concrete materials such as UHPC, the U-bars are capable of developing the yield strength within narrow joints. Because this thesis used the combination of these bars with a recently developed high early-strength concrete mixture, the development length of the bars must be addressed. The equation for development length (L_d) for hooked bars from ACI 318-14 is given below:

$$L_d = \frac{0.02\,\psi_c \psi_e f_y}{\lambda \sqrt{f_c^{'}}} d_b \qquad \text{(Equation 6-2)}$$

Where ψ_c is a cover factor, ψ_e is a coating factor; f_y is the specified yield strength of reinforcement; λ is a lightweight concrete factor; f_c' is the specified compressive strength of concrete (28-day strength); and d_b is the nominal diameter of the reinforcing bar. The results for compressive strength from Table 4-2 in Chapter 4 were used to calculate the development length. The average compressive strength of 8400 psi and 8600 psi from 22 and 28 hours, respectively, were applied to the calculation for the 8 in. joint. The average 12-hour and 24-hour compressive strength of 7400 psi and 9000 psi, respectively, were used for the 6 in. closure pour.

In the research to develop the high early-strength concrete, the mixture was designed to reach the required strength in 12 hours (Castine 2017). The compressive strength of 7400 psi was used to calculate the development length of the bars at the target

12-hour strength of the concrete. In the laboratory experiments presented in Chapter 4, the mixture was tested 24 hours after casting. The compressive strength of 9000 psi was used to calculate the development length of the bars during the tests. Number 4 epoxy coated bar with a yielding stress of 60,000 psi was used in the calculations.

The development lengths for the reinforcing bars in the 8 in. joint at 22 hours and 28 hours were 5.50 in. and 5.43 in., respectively. The 12-hour and 24-hour development lengths for the reinforcing bars in the 6 in. joint were 5.86 in. and 5.31 in., respectively. The dimensions provided for the 8 in. closure pour allowed the bars to develop yield as seen in the elevation view of the longitudinal joints in Figure 6-6. However, the bars in the 6 in. closure pour were not capable of developing yield within the provided width of the joint.

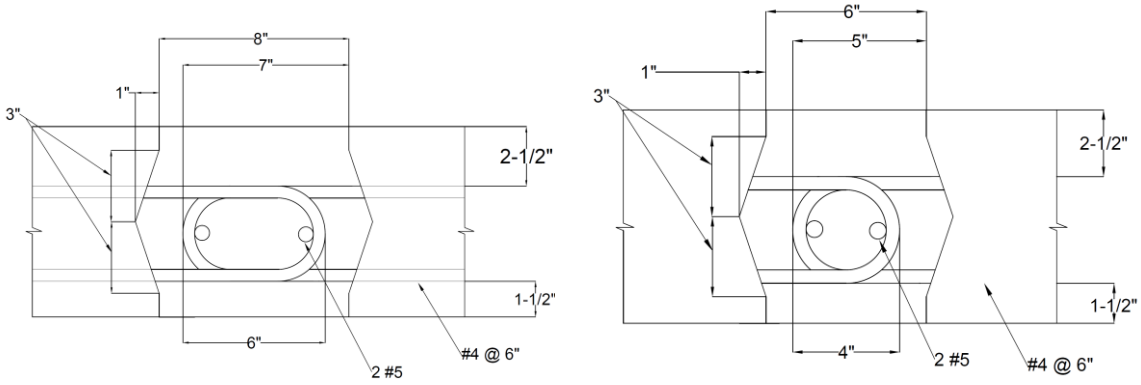

(a) (b)

Figure 6-6: Elevation view (a) 8 in. longitudinal joint (b) 6 in. longitudinal joint

Using a width of 6 in. resulted in insufficient length for the reinforcing bars to reach a yield strength of 60,000 psi within the joint. It was assumed that these bars reached a yield stress of approximately 51,200 and 56,500 psi in 12 and 24 hours, respectively, based on the assumption of linearly varying stress along the calculated

development lengths. Because the bars were not able to fully develop, an analysis was performed on Model 1 to determine the maximum moment in the longitudinal joints when the structure is subjected to the typical design bridge loads. The maximum moment from the model was compared to the reduced capacity of the closure pour as result of insufficient length for the bars to develop. The analysis and results are discussed in Section 6.3.2.

6.3.2 Maximum Moment in the Longitudinal Joints

Dead and live loads described in Chapter 5 were applied to Model 1 to obtain moment in the longitudinal joints under the applicable bridge loads. Dead loads were applied as area loads at their respective location in the prototype bridge. HL-93 load was moved transversely across the width of the bridge to determine the maximum moment in the closure pour. After running all three design lane loads, two lanes loaded governed for the maximum moment in the joint. The critical load position can be seen in Figure 6-7. The connection circled in red in the figure was the closure pour that experienced the highest moment. It can be noticed that one of the truck's tire is over the joint.

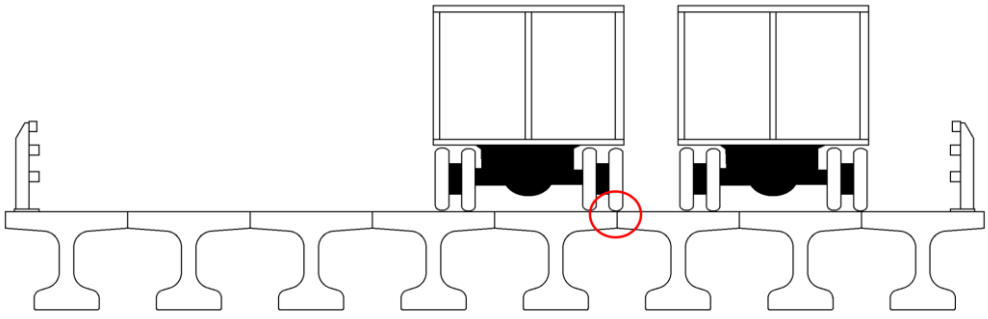

Figure 6-7: Critical load position for maximum moment in the joint

The link element used to model the closure pour at the location of maximum moment was defined using the data for the 6 in. joint. The element that experienced the maximum moment was located at mid-span of the bridge. The maximum moment calculated based on factored dead and live loads (Strength I) in the closure pour was approximately 1,600 lb-ft/ft. The capacity (ΦM_n) of the closure pour was determined to be approximately 12,600 lb-ft/ft and 13,700 lb-ft/ft using the 12 and 24 hours compressive strength. Despite the shortage in development length of the U-bars, the narrow closure pour was still capable of developing a strength that greatly exceeded the maximum moment the joints experienced from factored bridge loads.

Removing the diaphragms from the model increased the maximum moment by 75% to approximately 2,800 lb-ft/ft. Although the moment increased, it was still well below the capacity of the closure pour. The results of Li and Ma (2010) also showed that the introduction of diaphragms to decked precast, prestressed concrete girder bridges leads to a reduction of the maximum moment in the longitudinal joints.

6.3.3 Push-Down Analysis

A push-down analysis was performed on Model 1 by using the HL-93 load positioned at the location depicted in Figure 6-7. The intention for this analysis was to determine the load that would generate the nonlinear moment-rotation behavior in the link elements used to model the joint in Model 1. It was found that applying a load of approximately 15 times greater than the HL-93 load initiated the nonlinear behavior of the link element as shown in Figure 6-8, so it is unlikely that joints would ever experience nonlinear action during the service life of the bridge.

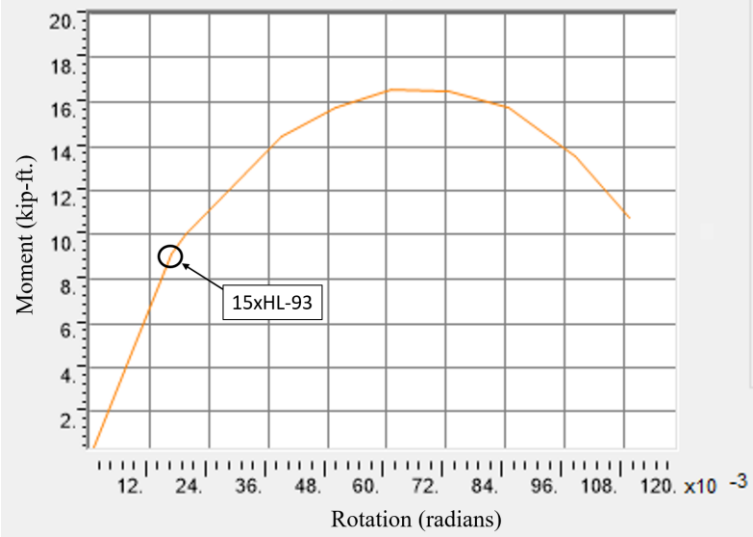

Figure 6-8: Moment-Rotation plot of the link element in the location of maximum moment

The nonlinear curve can be seen as load increased. The push-down analysis was halted after the model became unstable. The model became unstable at a load exceeding 20xHL-93 load. These results show that the joints were capable of handling additional loads beyond the typical factored loads the bridge will experience during its design life. It also indicates that the joints have the ability of handling design permit load which are generally based on oversize or overweight vehicular loads.

The analyses on Model 1 discussed in this chapter provided an understanding of how load is distributed between girders in a precast/prestressed concrete bridge with closure pour connections and diaphragms. The analyses also revealed the contributions of reinforcing hooked bars and a recently developed high early-strength concrete mixture to the strength of concrete closure pours. In the next chapter, effects of diaphragms on precast/prestressed concrete bridges is analyzed based on additional finite element models created with different configuration of diaphragms.

CHAPTER 7

EFFECT OF DIAPHRAGMS ON LIVE-LOAD MOMENT DISTRIBUTION

7.1 Effect of Diaphragms on Live-Load Distribution

The analyses discussed in Chapter 6 were performed on a bridge model containing diaphragms at three locations: at the two ends of the bridge and at mid-span. Results from the analyses revealed that girders in a precast/prestressed concrete bridge with end and intermediate diaphragms experience different moments than those calculated by code equations. In order to gain a better understanding on the direct effects of diaphragms, additional analyses were performed on bridge models constructed with different number and location of diaphragms. Live-load distribution factors from these models were compared to those from AASHTO LRFD Specifications (2012). Moment experienced by the interior and exterior girders in models with diaphragms were compared to moments from a model built without diaphragms. The analyses and results are discussed in this chapter.

7.2 Comparison of LLDFs from Models 2 to 4 with Code

The second model, referred to as Model 2, was built with diaphragms only at the ends of the bridge. The third model (Model 3) was constructed with only intermediate diaphragms located at mid-span. The fourth model (Model 4) was built without diaphragms. Live load distribution factors for the three models were calculated using the same method used for Model 1 discussed in Chapter 6. These distribution factors are compared to those from AASHTO LRFD formulas in Figures 7-1 to 7-3. Cracked and uncracked conditions of the diaphragms were considered in Models 2 and 4. The cracked

conditions were captured by using one-third of the gross moment of inertia of diaphragms. Cracking was not incorporated to Model 3 because the objective of this model was to investigate how load was shared transversely between girders on a hypothetical bridge with only intermediate diaphragms.

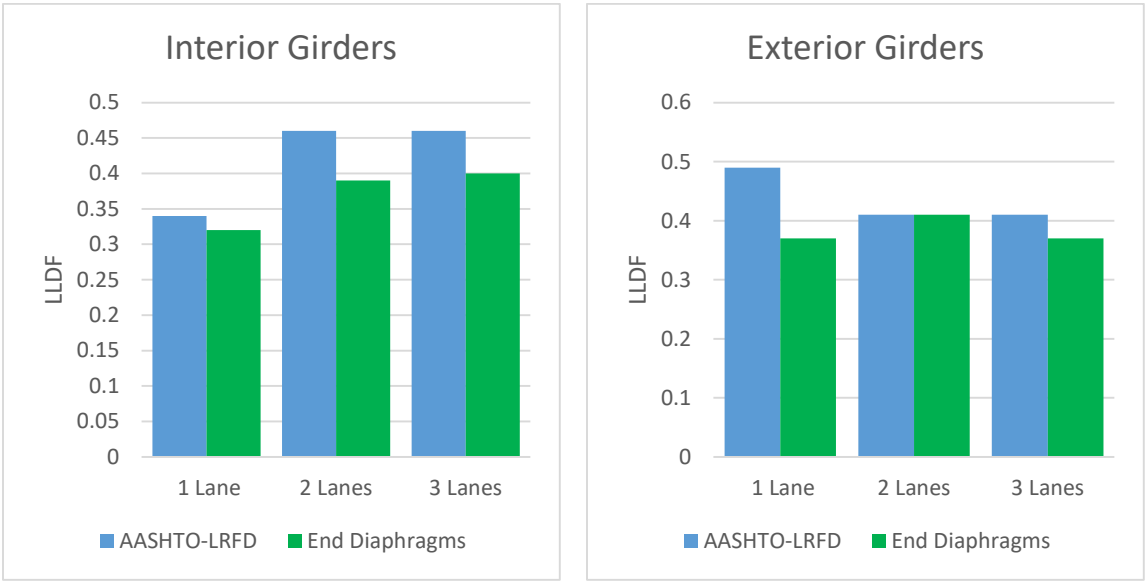

Figure 7-1: Distribution factors from Model 2 and AASHTO LRFD

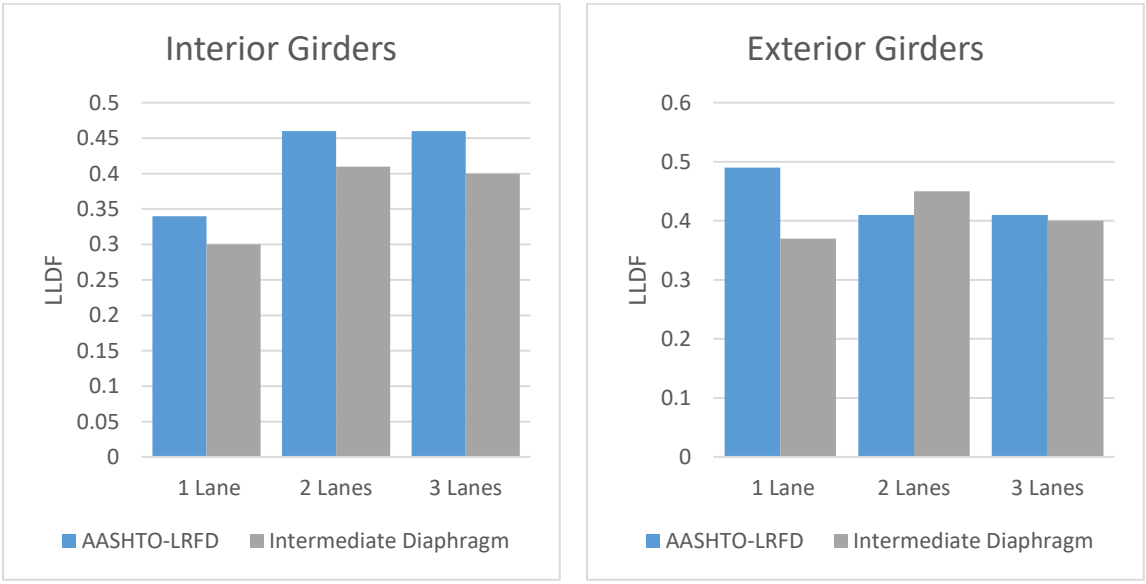

Figure 7-2: Distribution factors from Model 3 and AASHTO LRFD

Figure 7-3: Distribution factors from Model 4 and AASHTO LRFD

Based on the comparison of LLDFs presented in the plots, the factors from the bridge model without diaphragms were generally the closest to the LRFD factors when compared to the values from the other two models. This result is expected because the LRFD formulas were developed using finite element models that didn't consider the effects of diaphragms. Therefore, Model 4 reflects the original assumptions used for the simplified formulas. Although the formulas provided better estimates for this model, AASHTO LRFD was still conservative for the most part.

The formulas overestimated the LLDFs by almost 10% for multiple lanes loaded in the interior girders when compared to the factors from the model without diaphragms. Using the lever rule to determine the distribution factor for one-lane load in exterior girders overestimated the value by approximately 15%. There were also some cases in which the LRFD specification underestimated the distribution factors. For one-lane load

in interior girders and two-lane load in exterior girders, the formulas underestimated the factors by about 3% and 5%, respectively.

The influence of diaphragms on live load distribution factors for interior and exterior girders can be seen in Figures 7-4 and 7-5, respectively. Comparison of LLDFs from code with the models with diaphragms reveals that the LRFD formulas overestimated the factors for interior girders for all three design lane loads. For exterior girders, the formulas provided reasonable estimates for the model with end diaphragms under two lanes loaded and the model with intermediate diaphragms for three lanes loaded. The lever rule overestimated the distribution factor for one lane loaded in exterior girders by approximately 28% for both models. When comparing the results from the two models, it can be observed that the distribution factors from the models are the same for three-lane load in interior girders and one-lane load in exterior girders.

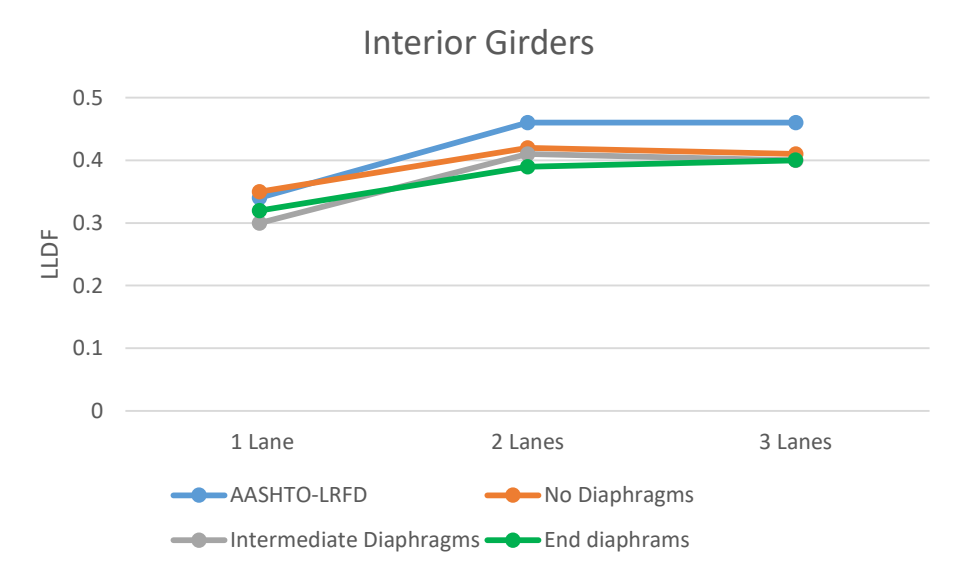

Figure 7-4: Effect of diaphragms on LLDFs for interior girders

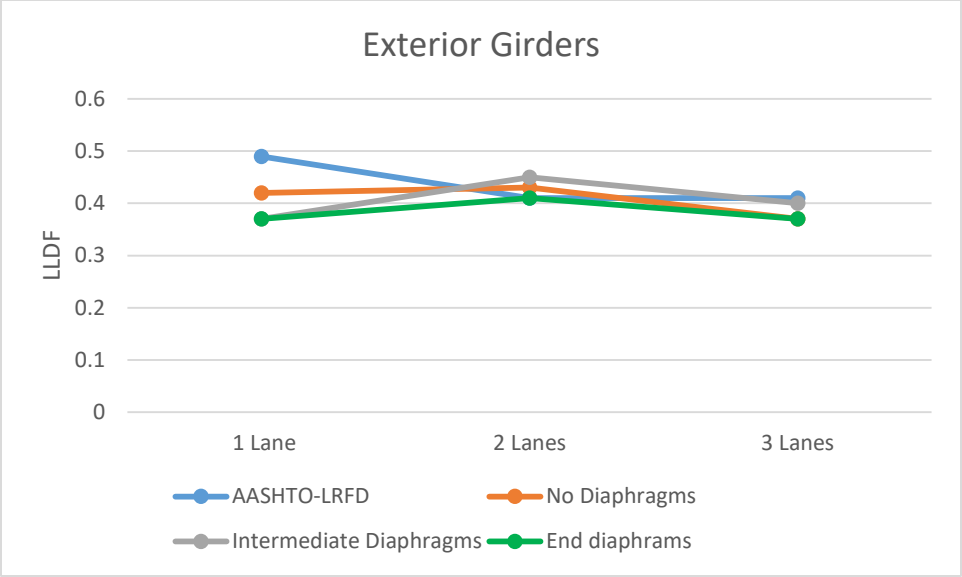

Figure 7-5: Effect of diaphragms on LLDFs for exterior girders

The model with only intermediate diaphragms produced higher values of distribution factors than the other models for multiple lanes loaded in exterior girders. This finding indicates that intermediate diaphragms tend to transfer more loads to exterior girders as observed by other research studies [Barr et. al (2001), Wong and Gamble (1973), Chandolu (2005), Ma et al. (2007)]. In fact, the distribution factor is even higher than the one from AASHTO LRFD Specification for two lanes loaded. This result was also observed in the comparison of the model without diaphragms to the formula. It is rare for live load distribution factors calculated from finite element analysis to be more conservative than those from code. However, this case does occur for certain bridge systems as presented in the results of Ypisof and Hindi (2007).

7.3 Influence of Diaphragms on Number of Lanes Loaded

Comparisons of moments in each girder from Models 1, 2, and 4 are presented in this section to determine how diaphragms affect live-load distribution for different lanes loaded. This comparison is done graphically to visualize the maximum moment each

girder experiences under one-lane, two-lane, and three-lane design loads. The moment in the graphs represent moment envelopes resulting from all the different positions of load shown in Figures C-1 to C-3 in Appendix C. Therefore, these moments do not occur simultaneously in all girders for a single loading position. The results for each load position can be found in Tables C-1 to C-16 under Appendix C.

7.3.1 Influence of Diaphragms on Girder Moments: One-Lane Loaded

The plot in Figure 7-6 compares the moment at mid-span in each girder from the different models under one lane loaded. By comparing the results for bridge models with and without diaphragms, it can be noticed that the presence of diaphragms have an effect on moment in the individual girders. The models with three diaphragms and end diaphragms reduced the moment in all the girders when compared to the model without diaphragms. The reduction is more pronounced in the model with three diaphragms.

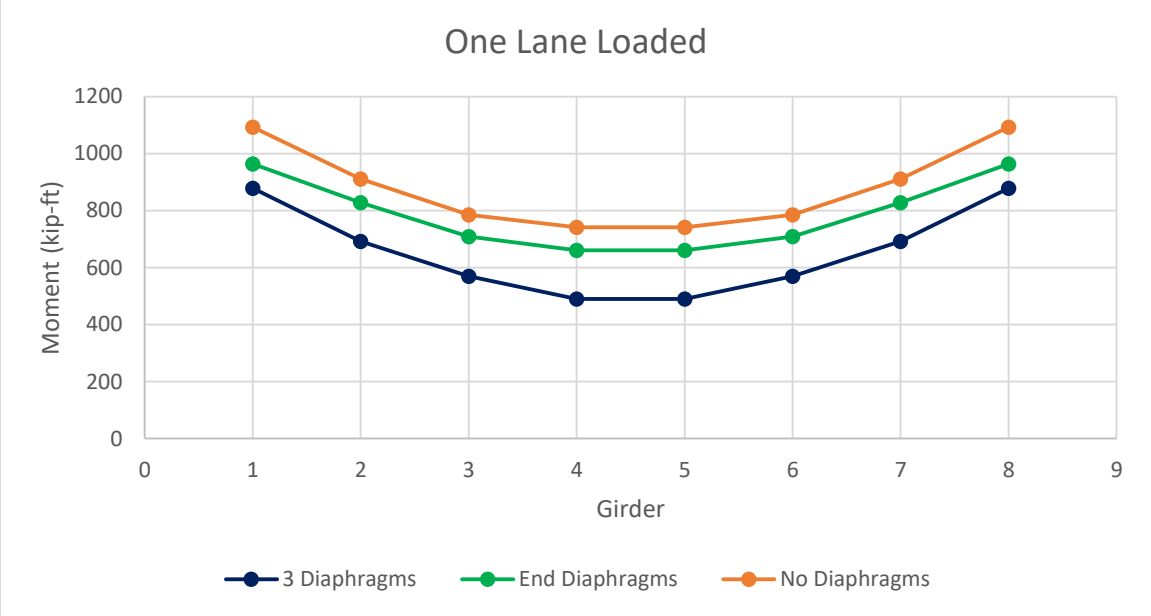

Figure 7-6: Comparison of moments for one lane loaded

Under one lane loaded, the exterior girders experienced the largest moment in all the three models. The highest moment for interior girders was found in girders 2 and 7. These moment values were used in calculating the distribution factors for one lane loaded in the plots presented in Figures 7-1 and 7-3. As discussed in Chapter 6, most of the interior girders do not experience the design moment that would be assigned to them using the distribution factors presented in the previous section. Interior girders 4 and 5 have moment values that are much lower than the girders with the maximum interior moment, especially the ones in the model with three diaphragms. More investigation on the moments in Figure 7-6 reveals that the shape of load distribution are the same for all three models. Moment decreases from the exterior girders to the girders closest to the center of gravity of the pattern of girders.

7.3.2 Influence of Diaphragms on Girder Moments: Two-Lanes Loaded

Moments obtained from two lanes loaded for each model can be seen in Figure 7-7. A review of the figure reveals that the addition of diaphragms also reduced moments in each girder for two lanes loaded when compared to the bridge without diaphragms. The moments from the model with end diaphragms followed a similar trend as the model without diaphragms but with reduced values. The exterior girders in both models experienced the largest moment; slightly higher than the moments found in interior girders 3 and 6. Changing the number of the diaphragms from two diaphragms at the ends of the bridge to three diaphragms significantly reduced the moment for interior girders 3 to 6 when the two lane load was applied to the model.

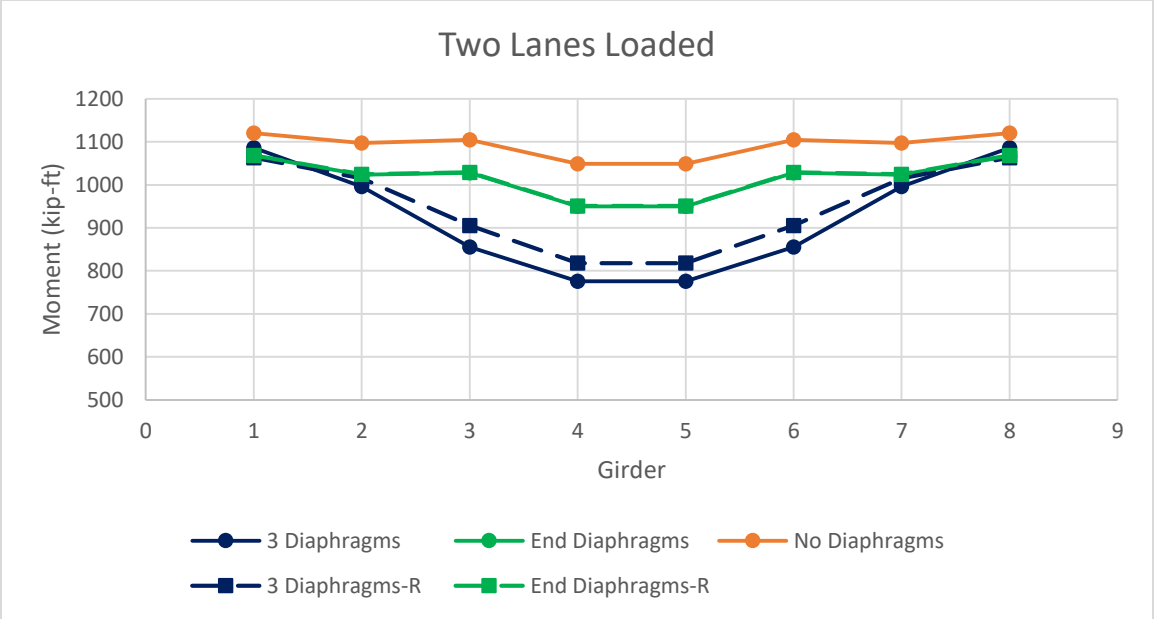

Figure 7-7: Comparison of moments for two lanes loaded

Applying the cracked conditions of diaphragms to the model with end diaphragms yielded the same results from the model that used uncracked conditions as the values overlap in the graph. This result is expected since those diaphragms are located at the ends of the bridge where the structure is restrained. Considering full stiffness of the diaphragms in the model with three diaphragms produced slightly higher moments in exterior girders when compared to the moments in the model with end diaphragms. This result is in contrast to the observation made for one lane loaded, where the exterior girders in the model with three diaphragms experienced a load approximately 9% lower than those in the exterior girders from the model with end diaphragms.

Reducing the stiffness of the diaphragms in the model with three diaphragms resulted in a decrease of the moments in exterior girders when compared to the uncracked stiffness case. The moments decreased to a value close to the moments from the model with end diaphragms. However, the decrease of the moments in the exterior girders led to

an increase of the moments in the interior girders. This increase in moment was more significant for interior girders 3 to 6 in which the moment increased by almost 6%. Interior girders 2 and 7 experienced an increase in moment by about 2%.

The observations made on the change in moment caused by alternating the stiffness of diaphragms when the bridge was subjected to two loaded lanes are in agreement with conclusions from other research studies [Wong and Gamble (1973) and Cai et al. (2002)]. These studies on the effects of diaphragms in concrete bridges observed similar behavior after assuming the stiffness varies between uncracked conditions to cracked conditions. Wong and Gamble (1973) stated that when the stiffness of the diaphragms exceeds an optimum stiffness, the moment in interior girders will decrease while the moment in exterior girders will increase; which implies that stiffer diaphragms are generally more effective in reducing moments for interior girders than exterior girders.

7.3.3 Influence of Diaphragms on Girder Moments: Three-Lanes Loaded

The plot comparing the effects of diaphragms on three lanes loaded is presented in Figure 7-8. Examining the plot reveals that the end diaphragms were effective in reducing moments only in interior girders. It caused a moderate increase in the moment on the exterior girders. In the results from one-lane and two-lane loads presented above, the end diaphragms reduced moments in every girder, including the exterior girders. Reduction in stiffness in the end diaphragms produced the same results as assuming uncracked stiffness as it was also observed in the results from two lanes loaded.

The shape of the load distribution of the model with end diaphragms follows the same pattern as the model with no diaphragms in general. This behavior was also noticed in the case for two lanes loaded. The addition of three diaphragms produced a greater reduction in the moments for interior girders 3 to 6. There was almost no change in moment for interior girders 2 and 7 when the model with three diaphragms is compared to the model without diaphragms. Moments in the exterior girders from the model with three diaphragms were greater than the moments from the other two models. This result was not noticed for one and two lanes loaded.

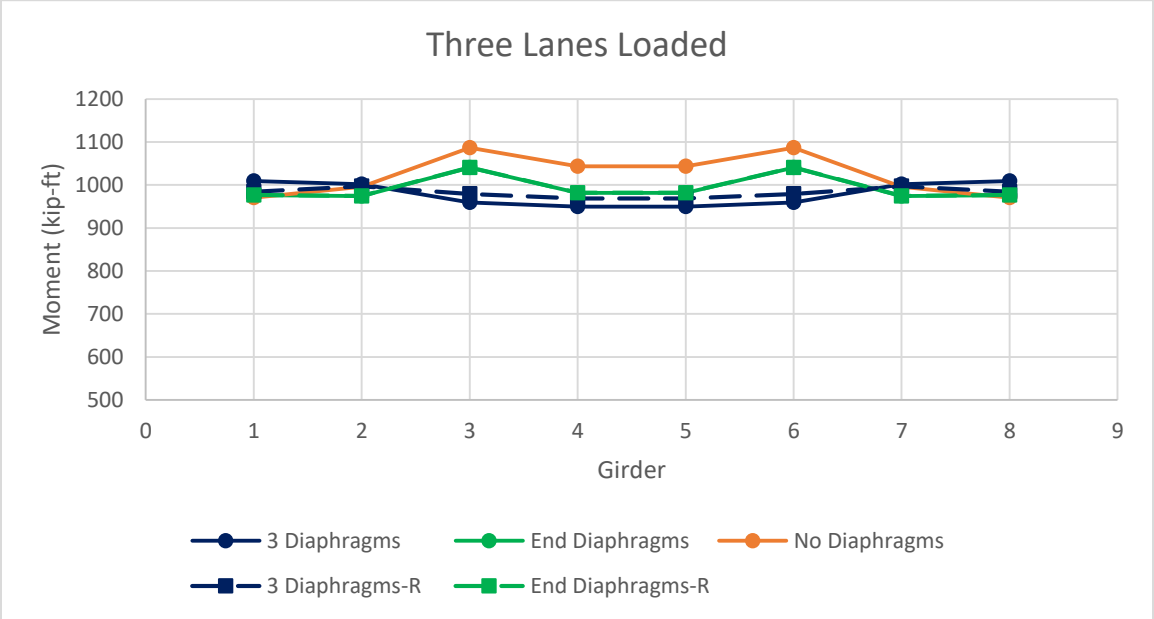

Figure 7-8: Comparison of moments for three lanes loaded

Changing the diaphragm stiffness to one-third of the gross stiffness in the model with three diaphragms increased the moment in most of the interior girders and decreased the moment in the exterior girders. As it was observed for two lanes loaded, the increase was more prominent for interior girders 3 to 6. The change in moment for interior girders 2 and 7 was negligible under three lanes loaded. When the bridge model was subjected to

one and two lanes loaded, the exterior girders experienced a higher moment than the interior girders in the models with end diaphragms and without diaphragms. However, in the case for three lanes loaded, interior girders 3 and 6 experienced the highest moment. This moment was about 8% higher than those of the exterior girders. In the model with three diaphragms, the exterior girders had the highest moment as observed in the results for one and two lanes loaded.

The results obtained from three loaded lanes are consistent with the conclusions of Chandolu (2005), Sithichaikasem and Gamble (1972), and Ma et al. (2007). The addition of an intermediate diaphragms can be beneficial for most of the interior girders in reducing the moment. However, an increase in the moment in the girders close to the edge of the bridge can be observed. The increase will depend on the stiffness assigned to the diaphragms. Sithichaikasem and Gamble (1972) recommends that designers must be careful in selecting an appropriate flexural stiffness in order for diaphragms to be effective in improving bridge performance.

7.4 Design Moments

After analyzing the effects of diaphragms on each load case, design moments for the bridges constructed with end diaphragms and no diaphragms were determined using the method applied to the bridge with three diaphragms presented in Chapter 6. Comparison of moments caused by one-lane, two-lane, and three-lane loads in each model is graphically presented in Figures 7-9 and 7-10. In the model with no diaphragms, the design moment in every girder was governed by two lanes loaded.

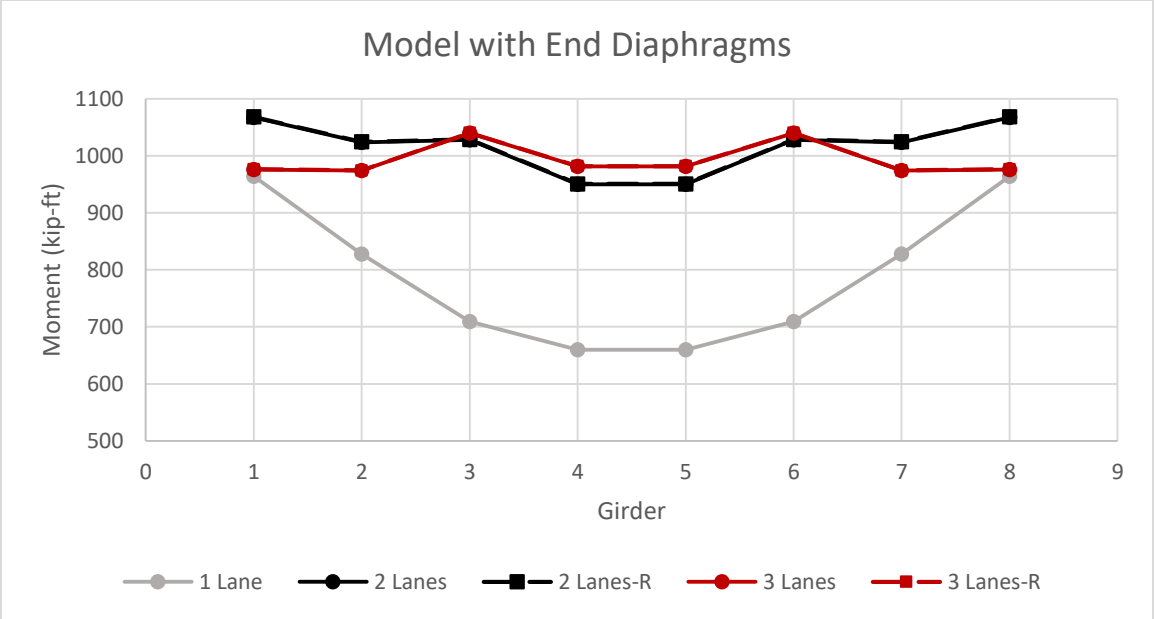

Figure 7-9: Controlling moment in the model with end diaphragms

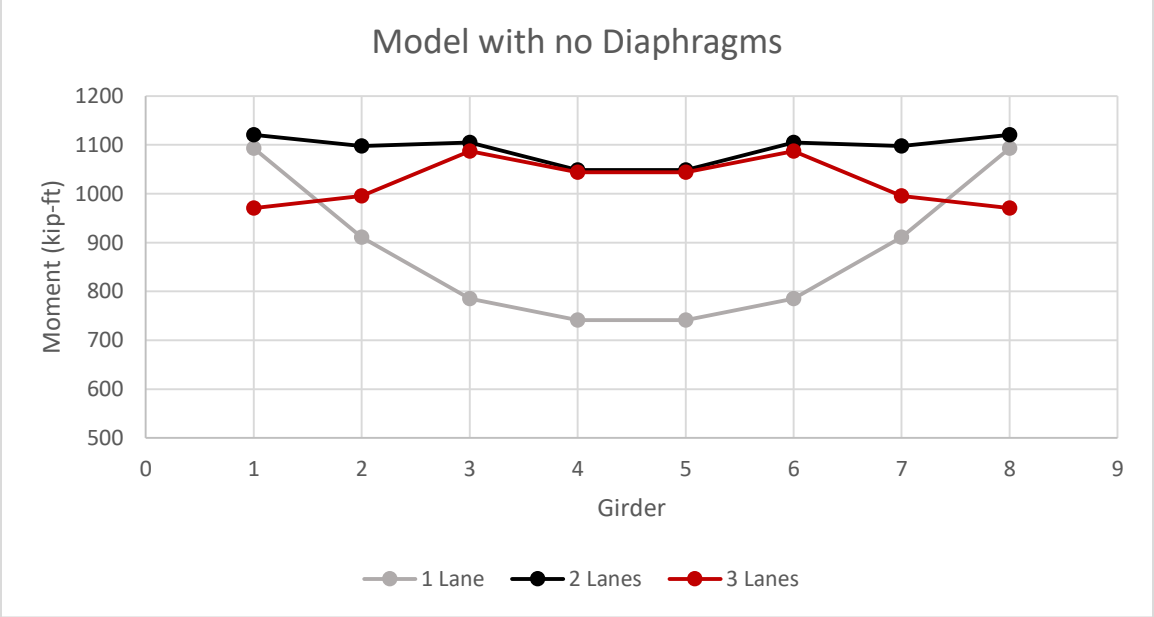

Figure 7-10: Controlling moment in the model with no diaphragms

In the model with end diaphragms, the design moment for interior girders 3 to 6 was governed by three lanes loaded. The design moment for exterior girders along with interior girders 2 and 7 was controlled by two lanes loaded. The same load cases that controlled the design moment for the girders in the model with end diaphragms governed

the design moment in the model with three diaphragms. The design moments for each model are compared to those suggested by AASHTO LRFD in Figure 7-11. The LRFD specification assigns a higher moment value to the exterior girders. One moment value is assigned for all the interior girders. It can be observed that the moments calculated using AASHTO LRFD Specification is conservative.

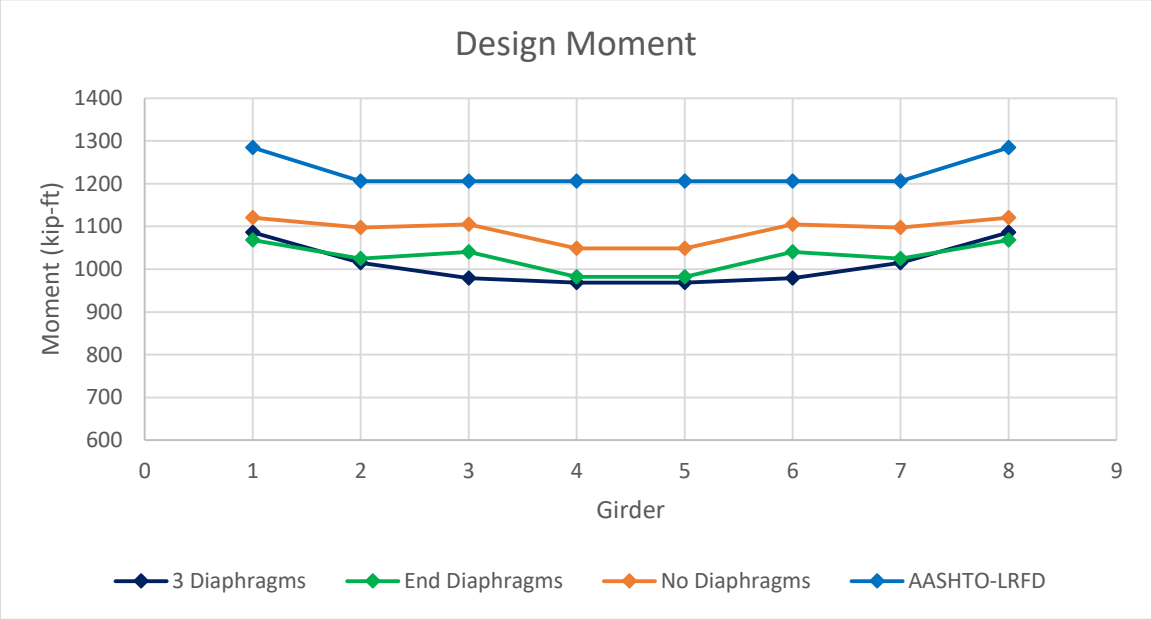

Figure 7-11: Design moment for individual girders

As discussed earlier, the moments from the bridge model with no diaphragms are the closest to the values from AASHTO LRFD Specification since it does not consider the effects of diaphragms. There is a difference of about 11% and 14% in the moment values for interior and exterior girders, respectively, when comparing the results from AASHTO LRFD to those from the bridge without diaphragms. AASHTO LRFD formulas overestimated the moments for interior and exterior girders in the bridge models with diaphragms by approximately 21% and 18%, respectively. By comparing the two models with diaphragms, it can be concluded that the moments for the girders were

generally similar; with the exception of interior girders 3 and 6. This similarity in design moments supports the reports from other research stating that intermediate diaphragms might not be needed in precast/prestressed concrete bridges.

It appears that if the intermediate diaphragms were added only between the three girders close to the edge of the prototype bridge, it would reduce the moment in interior girders 3 and 6. The proposed location of the diaphragms can be seen in Figure 7-12. If the moment in those two interior girders decreased, it would reduce the number of diaphragms required at mid-span of the bridge. Based on the results from the analyses in this chapter, it is predicted that this attempt to decrease the moment in interior girders 3 and 6 would increase the moment in the exterior girders. From Figure 7-11, it can be noticed that the design moment in the exterior girders from the model with end diaphragms is lower than those from the model with three diaphragms. This comparison indicates that the increase in moment in the exterior girders would still be within permissible values.

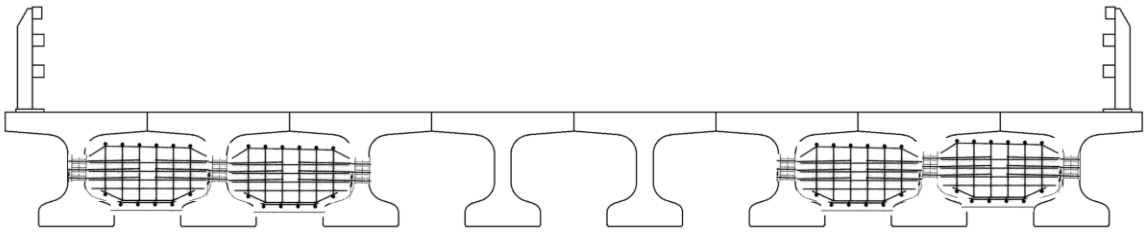

Figure 7-12: Proposed location for intermediate diaphragms

Further finite element analysis using this configuration of diaphragms is required to confirm that this proposed method would actually reduce the moment of the two interior girders. If this method is able to improve the performance of the bridge, then interior girders 3 to 6 can be designed using a lower moment value than those of interior

girders 2 and 7. The interior girders experience a different moment as shown in Figure 7-11. If this method does not reduce the moment in interior girders 3 and 6, then connecting all the girders with diaphragms at mid-span would still allow girders 3 to 6 to be designed with a different moment. This type of connection was used in the bridge model with three diaphragms.

Another solution is to increase prestressing strands in the prestressed concrete girders to resist the load rather than adding the intermediate diaphragms. In order to determine which solution is more effective, a cost analysis is recommended. More details on the proposed investigations are presented in Chapter 8 under future work.

7.5 Live-Load Distribution Factors from Millian and Ma (2005)

Milliam and Ma (2005) developed a new set of distribution factor equations to describe the behavior of decked, precast/prestressed concrete (DPPC) girder bridge system under a single-lane loading condition as part of a study funded by Alaska DOT. The equations were developed based on parametric study conducted using grillage models that were calibrated with field tests. In the grillage models, transverse beam elements were used to approximate the behavior of the longitudinal joints. The group estimated that the joints behaved somewhere between two extreme conditions: a rigid and hinged connection. The rigid condition assumed the connection is fully fixed and has full transverse continuity. In the hinged connection the joint was released in flexure in the transverse direction. After conducting the parametric study, the following equations were recommended for calculating the live load distribution factors:

Moment over interior girder

$$DF = \frac{S}{12.5} + \frac{I}{300} - \frac{L}{10}\left(\frac{S-3}{200}\right)$$

Moment over exterior girder

$$DF = \frac{S}{10} + \frac{I}{300} - \frac{L}{10}\left(\frac{S-1}{300}\right)$$

Where *S* is girder spacing, that is, the distance between the centerlines of two consecutive girders, (unit: ft.); *L* is the span length of the bridge measured from the center of each support, (unit: ft.); *I* is the moment of inertia about the horizontal axis of one girder in the bridge system. Unlike in the LRFD equations, the moment of inertia is calculated based on the whole girder, including the whole width of the top flange deck portion. The equations are accurate only when the bridge being modeled is within the following parameters:

- The girders are typical decked, precast/prestressed concrete girders with the deck poured together with the girder as a single unit.
- The girder height is between 36 and 66 in.
- The deck thickness is between 4 and 8 in.
- The number of girders of the bridge is greater than or equal to four
- The span length of the bridge is between 40 and 180 ft.
- The girder spacing is between 4 and 9 ft.
- The bridge is loaded by only a single lane of traffic

The prototype bridge used in this study falls within the parameters required to use the equations. The live load distribution factors for interior and exterior girders on the

prototype bridge using the proposed equations are 0.36 and 0.43, respectively. Milliam and Ma (2005) stated that the grillage models could not approximate the effects of intermediate diaphragms on preventing the girder from rotating about the hinged joint. They realized that the use of intermediate diaphragms on DPPC girder bridges has an impact on single-lane live load distribution factor and recommended further study on its impact.

The live load distribution factors from the finite element model from this thesis that was built without diaphragms were compared to those from the proposed equations of Milliam and Ma (2005). The distribution factors from the model without diaphragms for interior and exterior girders under one lane loaded were 0.35 and 0.42, respectively. These values are very close to the ones from the proposed formulas. The proximity in these results increased confidence in the chosen modeling technique and FEA results presented in this thesis. It also implies that there could be similar behavior in transverse live load distribution via concrete closure pours and grouted shear keys in DPPC girder bridges.

The analyses presented in this chapter gave insights on how diaphragms influences live load distribution factors in DPPC girder bridges. Results from models with different number and location of diaphragms were compared to those from a model without diaphragms and recommendations from code. Conclusions regarding the effect of diaphragms were drawn from these results. A summary along with the conclusions of the study are presented in Chapter 8.

CHAPTER 8

CONCLUSIONS AND RECOMMENDATIONS

8.1 Summary of Work

Live-load distribution characteristics in precast/prestressed concrete bridges with concrete closure pour connections and diaphragms were investigated in this study. The investigation was conducted using finite element bridge models containing closure pour joints and different number and location of diaphragms. The models were developed using characteristics of the Manhan Bridge, located in Easthampton, MA. The Manhan Bridge was built with eight Decked Bulb Tee girders connected with longitudinal concrete closure pours as part of MassDOT Accelerated Bridge Program. The material and section properties of the bridge components provided in the construction drawings were used to define the properties in the finite element models.

The longitudinal joints in the models were calibrated using data from laboratory tests conducted on concrete closure pour panel specimens. The test specimens were designed to represent typical deck portion of two adjacent decked, precast/prestressed girders connected together through a longitudinal joint. The closure pour connections were comprised of hooked steel reinforcing bars and a recently developed high early-strength concrete mixture. The experiment evaluated whether the connection performed adequately to develop the required short-term strength (one day) and the feasibility of using narrow closure pours with the selected steel and concrete materials. Two specimens were designed, fabricated, and tested in a structural laboratory at UMass Amherst.

Moment-rotation curves were developed using results from the two tests to define the element properties for the closure pour connections in the finite element models.

A finite element analysis (FEA) model was constructed of a simplified 2-girder model to assess the accuracy of the selected modeling technique for the prototype bridge used in this thesis. A mesh convergence study and trial load tests were performed on the simplified model with the goal of ensuring that the finite element models produced realistic and accurate results. After assessing the selected modeling method, analyses were performed on the full-scale bridge models. The first full-scale analysis was performed to study live-load distribution on a precast/prestressed concrete bridge model containing closure pour joints along with end and intermediate diaphragms. Additional analyses were performed on this model to investigate the strength of the concrete closure pours under typical bridge loads.

Further analyses were then performed on other bridge models constructed with different configuration of diaphragms to gain a better understanding of the direct impact of diaphragms on live-load distribution. The other models included bridges with only end diaphragms and only intermediate diaphragms. The results from these models along with the model constructed with both end and intermediate diaphragms were compared to the results from a bridge model built without diaphragms. The results were also compared to design values determined using the simplified equations in AASHTO LRFD (2012). The conclusions drawn from each analysis are presented in the sections that follow.

8.2 Conclusions

Based on the results of the laboratory experiments and FEA, it was concluded that the concrete closure pour connections provided continuity and adequate transfer of forces between the adjacent bridge girders, allowing transfer of moments induced by the design vehicular live-load. The ability of the closure pours to transfer moments effectively depended on the reinforcing bar detailing and strength of the concrete in the joints. The combination of reinforcing hooked bars and the high early-strength concrete mixture allowed the closure pours to reach the desirable flexural and shear strength to perform well under service and factored loads.

The finite element analysis results indicated that the closure pours allowed bridge moments to be successfully distributed to each girder. When diaphragms were considered in the analysis, the maximum moment in the longitudinal joints decreased, indicating that diaphragms are beneficial in reducing moments locally in individual closure pour connections and engage a larger number of girders. Overall, the effects of diaphragms on live loads distributed to the individual girders depended on the number of lanes loaded. When the bridge models were subjected to one-lane, two-lane, and three lane design loads, distribution of loads were different for each case. Therefore, the following conclusions were drawn from the analyses involving different positions and numbers of lanes loaded. These conclusions are based on moment envelopes resulting from all the different positions of load in the transverse direction of the bridge.

One Lane Loading Condition:

- Diaphragms reduced the moment in every girder based on the comparison of bridges with and without diaphragms.
- The presence of diaphragms at the ends and mid-span of the bridge led to a greater reduction of moment in each girder.
- Exterior girders experienced the highest moment. Moments decreased from the exterior girders to the girders closest to the center of the bridge.

Two Lane Loading Condition:

- Diaphragms reduced the moment in every girder based on the comparison of bridges with and without diaphragms.
- Cracked end diaphragms produced the same effects as uncracked end diaphragms.
- The addition of stiff diaphragms at mid-span in a bridge containing end diaphragms decreased the moment in interior girders and increased the moment in exterior girders.
- Cracked intermediate diaphragms led to a higher moment in interior girders and a smaller moment in exterior girders when compared to uncracked intermediate diaphragms.
- Exterior girders experienced the highest moment. The difference in moment in exterior and interior girders in a bridge with end and intermediate diaphragms was more pronounced than the difference found in the bridges with only end diaphragms and without diaphragms.

Three Lane Loading Condition:

- Diaphragms decreased the moment in interior girders and increased the moment in exterior girders when comparing bridges with and without diaphragms. The effect was more significant when a stiff intermediate diaphragm was added to the bridge.
- Cracked end diaphragms produced the same effects as uncracked end diaphragms.
- Cracked intermediate diaphragms causesd a higher moment in interior girders and a lower moment in exterior girders when compared to uncracked intermediate diaphragms.
- The highest moment was found in some of the interior girders and not the exterior girders.

8.3 Recommendations

Recommendations in terms of design implications and future work in line with this thesis are presented below:

8.3.1 Design Implications

Design implications presented below are based on the results from this research study and are applicable to single-span, straight precast/prestressed concrete bridges, in particularly Decked Bulb Tee girder bridges.

- Refined analyses such as finite element analysis is recommended for determining moments in each girder for these bridges to avoid overestimating the design moment in each girder when using AASHTO LRFD Specifications.

- Moments for some of the interior girders could be designed using lower values because these girders might never experience the moment obtained in the interior girder with the maximum moment.
- Intermediate diaphragms could be completely eliminated or the number of diaphragms at mid-span in the transverse direction could be reduced in these bridges. For Decked Bulb Tee girder bridges similar to the one used in this study, the number of intermediate diaphragms could be reduced based on the findings from further investigations recommended in the future work section below.

8.3.2 Future Work

The findings from this research were used to identify activities that would warrant future study. These activities are described below:

- Perform a cost analysis to determine if it would be more economical to increase the number of prestressing strands in prestressed concrete girders in bridges containing end diaphragms to resist the load or adding intermediate diaphragms.
- Determine live-load distribution characteristics if the number of diaphragms at mid-span is reduced in the transverse direction to improve performance of the bridge. An example of this layout of diaphragms can be found in Section 7.4 under Chapter 7 of this thesis.
- Investigate how diaphragms influence moment at other locations of the bridge apart from the point of maximum moment (mid-span) for detailing purposes.
- As the use of Decked Bulb Tee girders increases in Accelerated Bridge Construction, parametric studies should be conducted to develop more accurate

equations for this bridge system similar to the work of Millian and Ma (2005). The new equations would allow engineers to perform live load analysis on the bridges without using complex 3D analyses.

APPENDIX A

MOMENT-ROTATION AND LOAD-DEFLECTION PLOTS

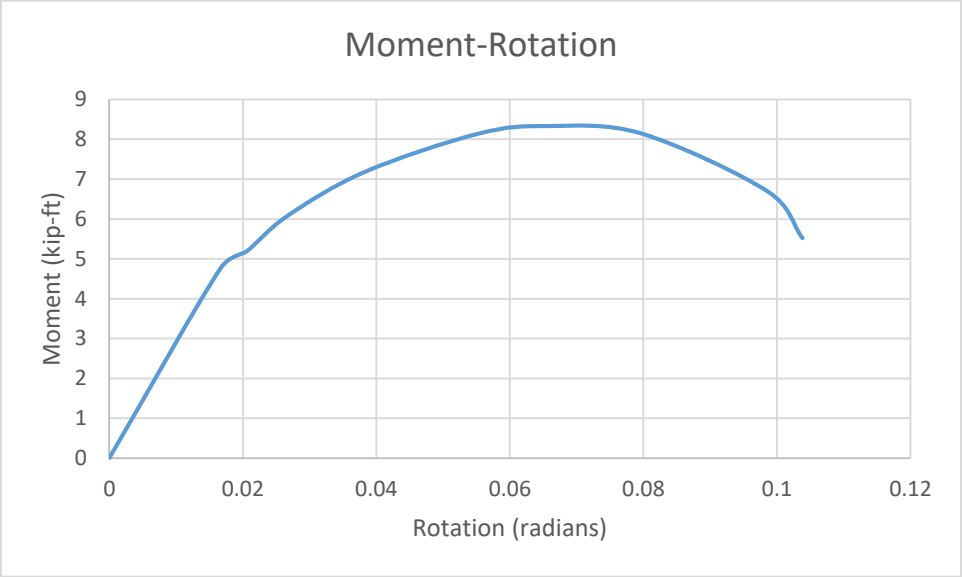

(a)

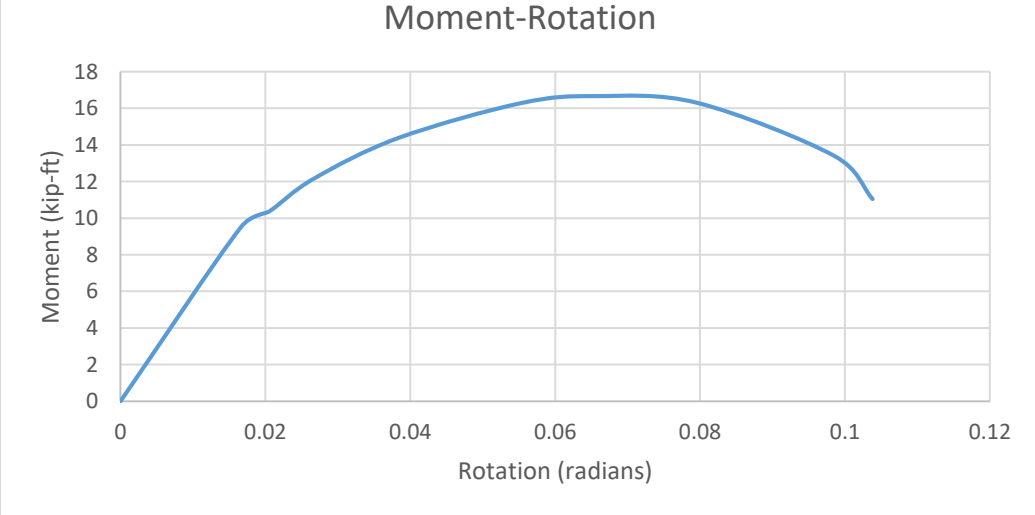

(b)

Figure A-1: Moment-Rotation relationship for 6 in. joint (a) exterior links (b) interior links

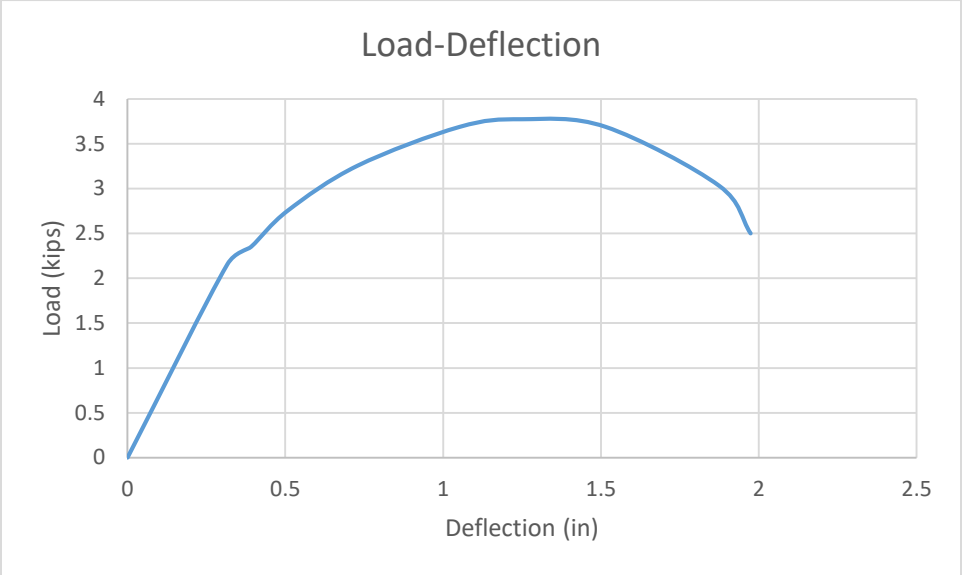

(a)

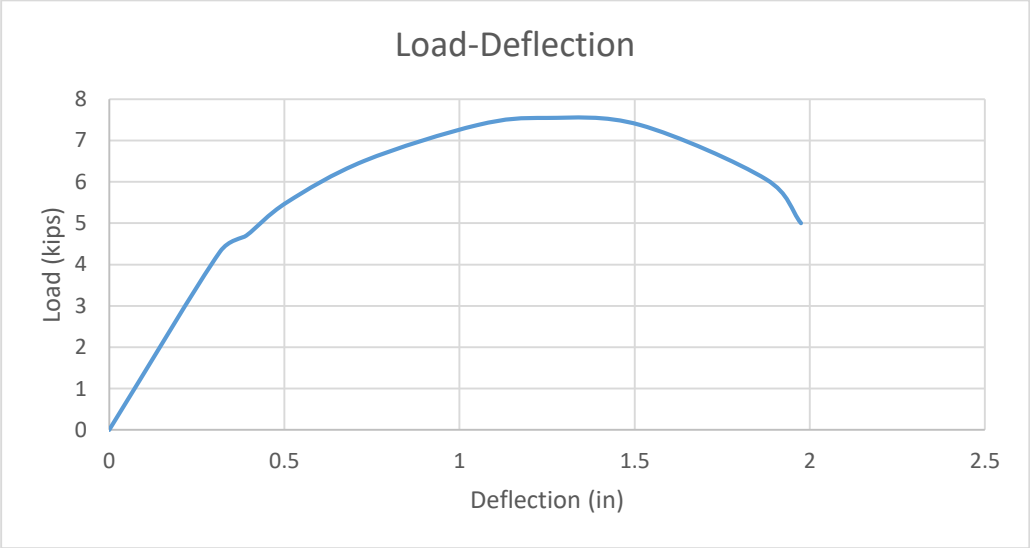

(b)

Figure A-2: (a) Load-Deflection relationship for 6 in. joint (a) exterior links (b) interior links

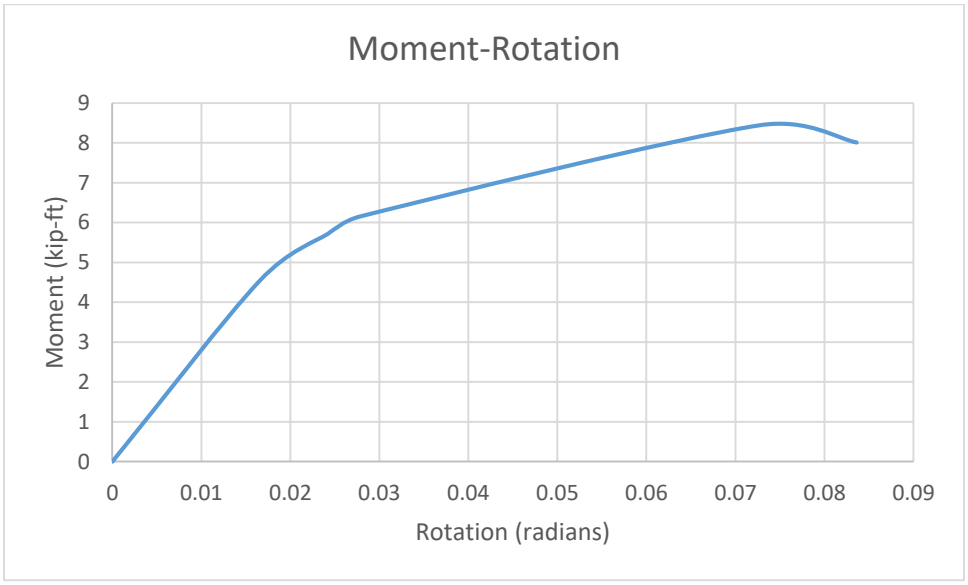

(a)

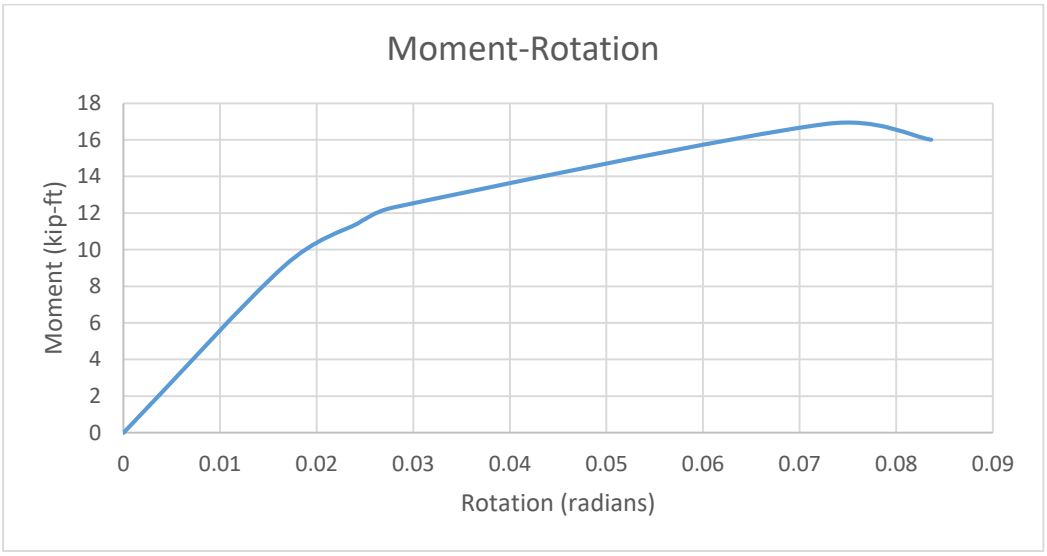

(b)

Figure A-3: Moment-Rotation relationship for 8 in. joint (a) exterior links (b) interior links

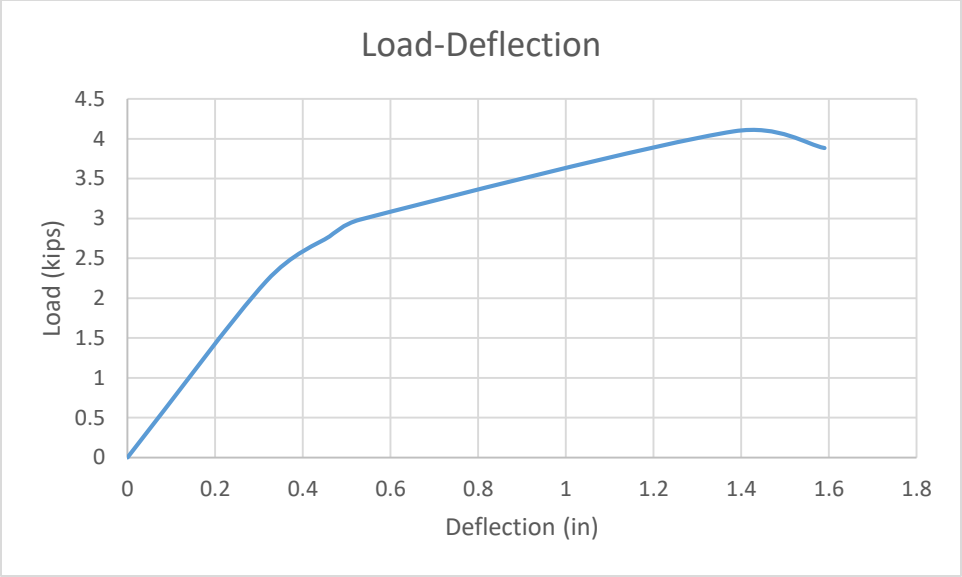

(a)

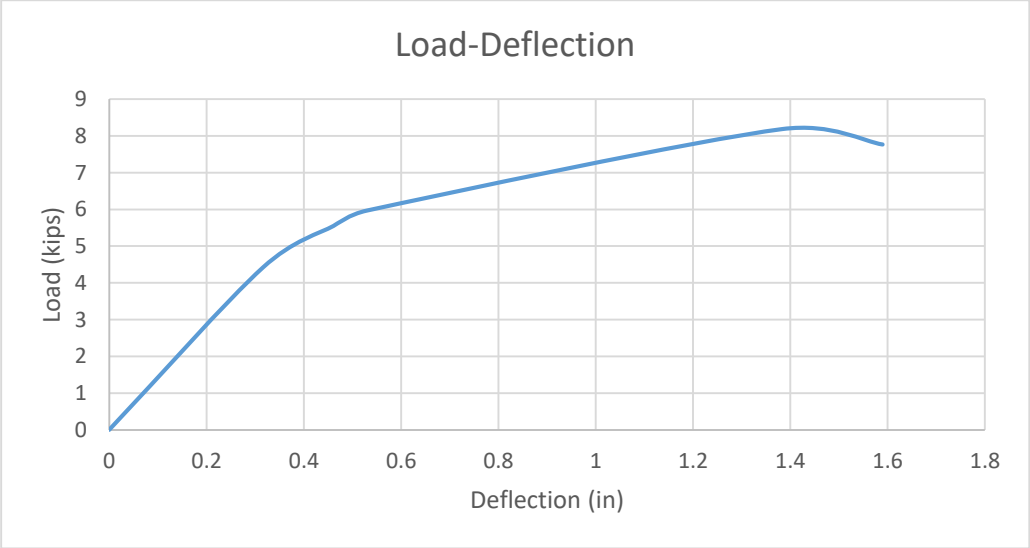

(b)

Figure A-4: (a) Load-Deflection relationship for 8 in. joint (a) exterior links (b) interior links

APPENDIX B

HAND CALCULATIONS FOR THE SIMPLIFIED MODEL BRIDGE LOADS

Dead Load

Self-weight of the girder:

$$\text{Load}_{\text{girder}} = A_{girder} x\ \gamma_{\text{concrete}} x N_{griders} = 7.69\ ft^2\ x\ 0.15\ kcf\ x\ 2 = 2.31\ kip/ft$$

$$M_{girder} = \frac{wl^2}{8} = \frac{2.31x95^2}{8} = 2602.65\ kip - ft$$

Railing

$$\text{Assumed Load} = 0.5\ \text{kip/ft}$$

$$Two\ girders: \frac{0.5}{4} = 0.125\ kip/ft$$

$$M_{railing} = \frac{0.125\ x\ 95^2}{8} = 141.02\ kip - ft$$

Curb

$$w_{curb} = 5.5\ x \frac{8}{12}\ x\ 0.15 = 0.55\ kip/ft$$

$$Two\ girders: \frac{0.55}{4} = 0.138\ kip/ft$$

$$M_{curb} = \frac{0.138\ x\ 95^2}{8} = 155.12\ kip - ft$$

Wearing Surface:

$$0.15t_{ws} = 0.15\ x\ \frac{1.5^2}{12} = 0.0188\ ksf$$

$$0.0188\ ksf\ x\ 10\ ft = 0.188\ kip/ft$$

$$M_{ws} = \frac{0.188\ x\ 95^2}{8} = 212.5\ kip - ft$$

Utilities

Assumed Load: 0.1 kip/ft

$$\mathrm{M_{utilities}} = \frac{0.1\ x\ 95^2}{8} = 112.8\ kip - ft$$

Live Load

HL-93

Truck load

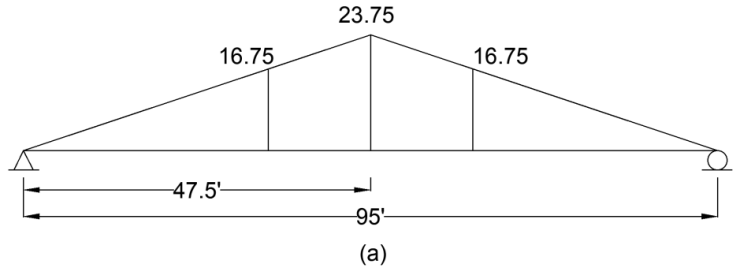

(a)

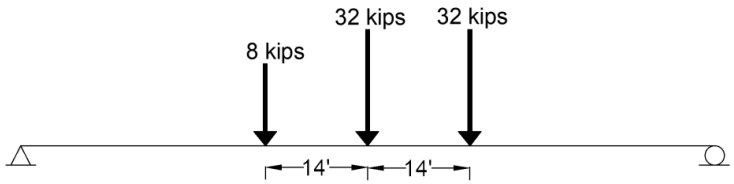

(b)

$$M_{truck} = 32(23.75) + 32(16.76) + 8(16.75) = 1430\ kip - ft$$

$$Truck\ x\ dynamic\ laod\ allowance = 1430\ x\ 1.33 = 1901.9\ kip - ft$$

Lane Load

$$\frac{wl^2}{8} = \frac{0.64\ x\ 95^2}{8} = 722\ kip - ft$$

$$HL - 93\ Moment = 1901.9 + 722 = 2623.9\ kip - ft$$

Pedestrian Live

$$area\ laod: 0.075\ ksf$$

Two girders: $\frac{0.075}{4} = 0.0188\ ksf$

Over 10 ft.: 0.188 kip/ft.

$$M_{pedestrian} = \frac{0.188x95^2}{8} = 211.52\ kip - ft$$

Strength I Load Combination

$$1.25DC + 1.5DW + 1.75(LL + PL)$$

$$1.25(2602.65 + 141.02 + 155.12) + 1.5(211.5 + 112.81) + 1.75(2623.9 + 211.52)$$
$$= \mathbf{9071.98\ kip - ft}$$

APPENDIX C

TRUCK LOAD POSITIONS AND MOMENTS

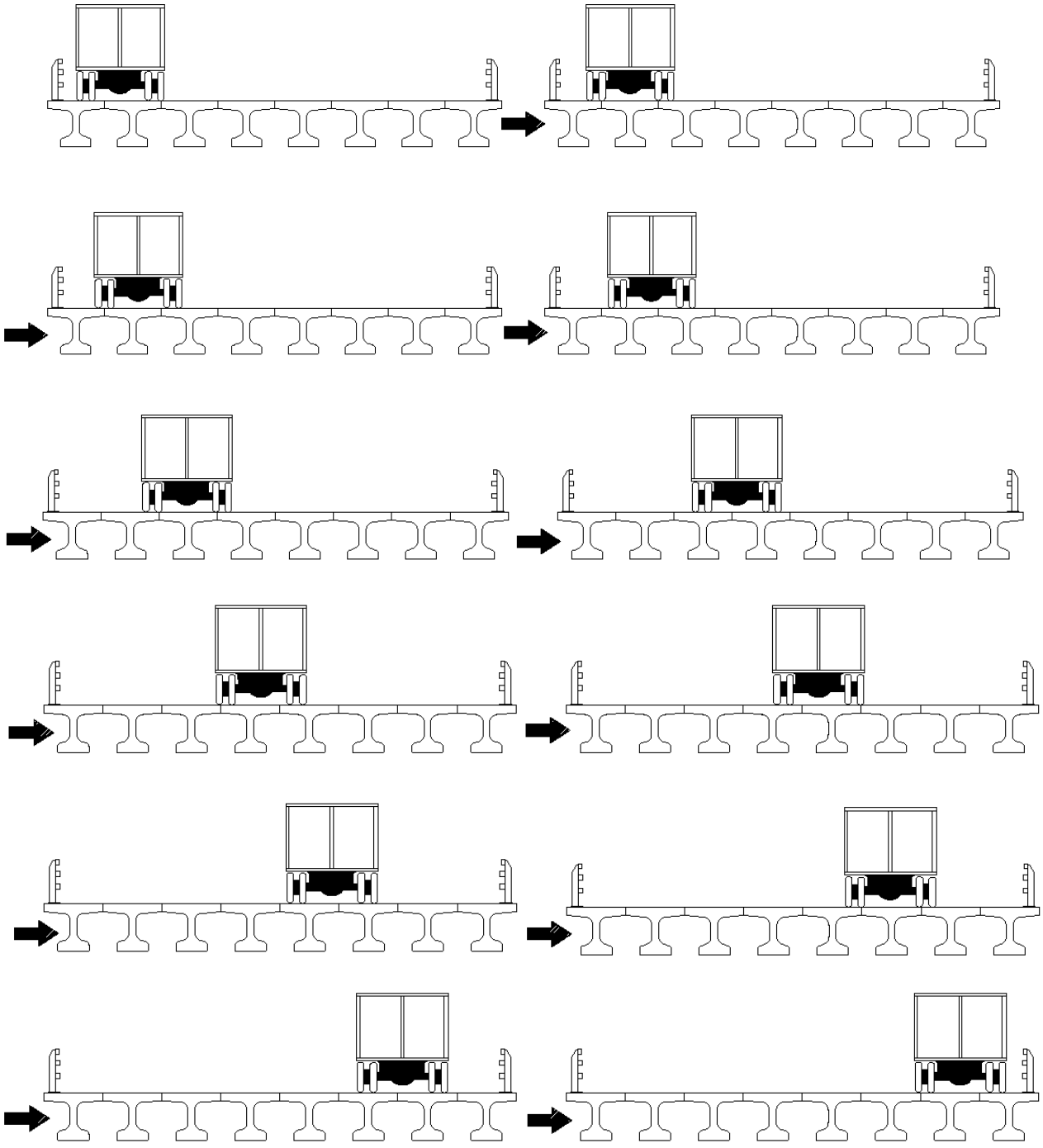

Figure C-1: Transverse position of the HL-93 load for one lane loaded

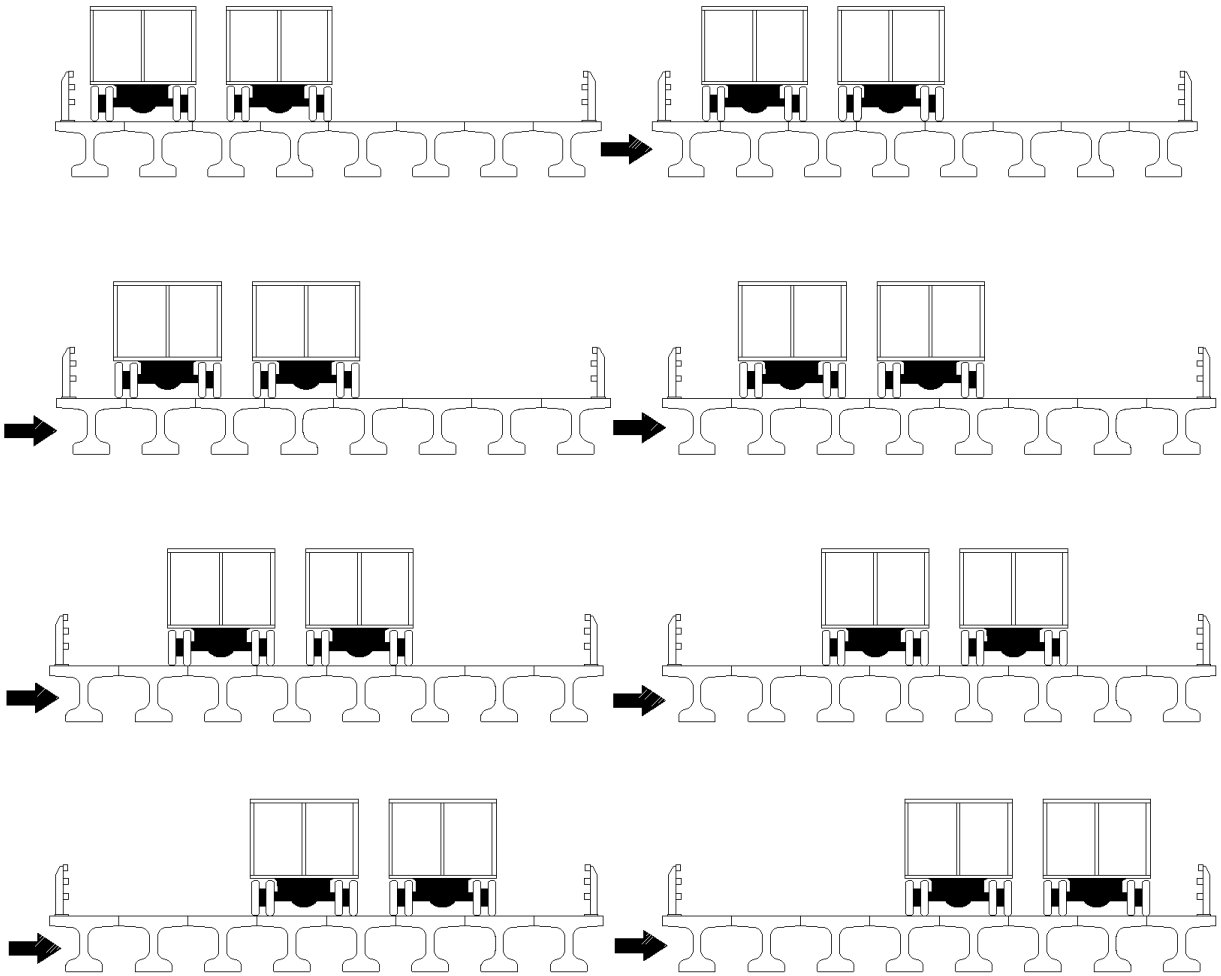

Figure C-2: Transverse position of the HL-93 load for two lanes loaded

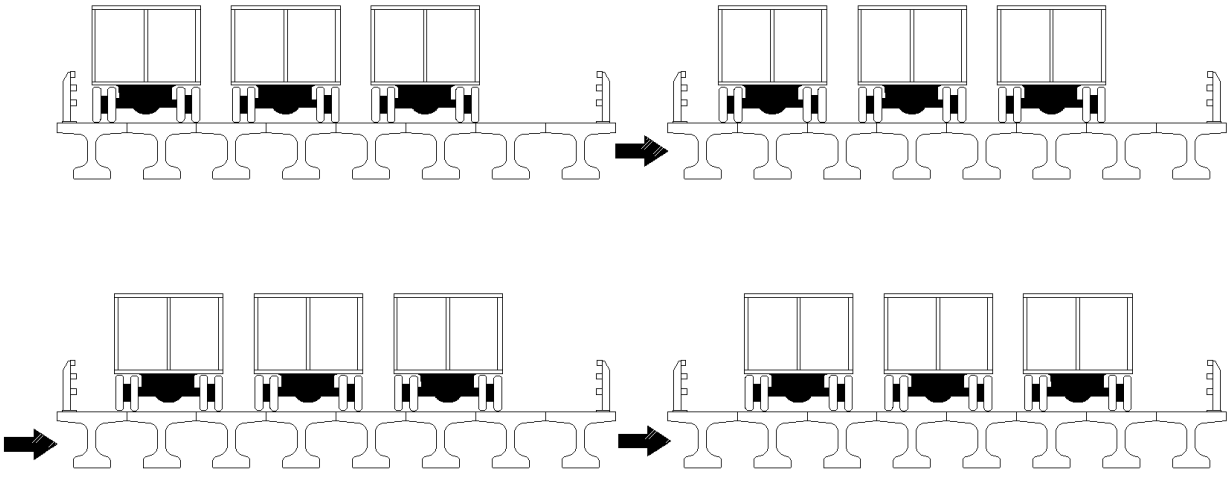

Figure C-3: Transverse position of the HL-93 load for three lanes loaded

Table C-1: Moment (kip-ft.) for load cases 1 to 6 from Model 1 for one lane

Girder	Case 1	Case 2	Case 3	Case 4	Case 5	Case 6
1	878	842	810	774	620	471
2	692	652	663	604	564	532
3	570	554	527	506	491	456
4	443	461	471	487	465	440
5	287	310	323	353	418	459
6	171	192	203	231	297	371
7	87	104	112	135	191	260
8	17	28	35	53	98	157

Table C-2: Moment (kip-ft.) for load cases 7 to 12 from Model 1 for one lane

Girder	Case 7	Case 8	Case 9	Case 10	Case 11	Case 12
1	342.54	242	163	103	57	19
2	442	349	266	196	140	90
3	469	449	376	303	236	176
4	445	427	462	422	359	292
5	426	444	440	467	490	447
6	444	465	453	489	504	569
7	342	435	526	559	601	687
8	235	333	460	607	760	864

Table C-3: Moment (kip-ft.) for load cases 1 to 8 from Model 1 for two lanes

Girder	Case 1	Case 2	Case 3	Case 4	Case 5	Case 6	Case 7	Case 8
1	1086	1016.49	972.21	899.35	693.49	511.04	356.91	238.03
2	996.10	934.82	930.08	844.4	736.68	645.01	514.93	393.18
3	855.75	852.81	821.89	819.78	764.21	673.64	623.61	552.85
4	743.51	748.92	775.95	765.66	759.31	747.19	706.27	636.23
5	611.07	628.6	622.23	643.54	712.95	743.08	750.15	768.65
6	473.7	511.52	532.25	578.68	636.9	700.25	792.39	823.89
7	311.28	349.34	370.14	423.41	547.33	670.36	751.41	892.52
8	163.99	197.38	215.76	265.46	391.14	551.66	746.8	937.31

Table C-4: Moment (kip-ft.) for load cases 1 to 8 from Model 1-R for two lanes

Girder	Case 1	Case 2	Case 3	Case 4	Case 5	Case 6	Case 7	Case 8
1	1063.25	980.97	933.76	848.47	637.97	463.89	325.17	225.43
2	1014.76	956.2	943.41	857.72	727.52	612.24	472.83	354.05
3	905.34	900.73	876.33	868.37	804.18	696.13	616.38	521.01
4	772.66	790.54	814.55	816.7	817.89	800.65	740.92	652.93
5	604.35	630.85	634.71	667.73	757.2	799.52	812.52	811.61
6	435.12	474.81	497.86	550.86	636.21	727	830.55	877.43
7	279.48	313.31	332.56	382.59	506.06	641.58	752.45	904.98
8	166.46	192.5	207.34	247.87	355.1	501.36	691.76	895.26

Table C-5: Moment (kip-ft.) for load cases 1 to 4 from Model 1 for three lanes

Girder	Case 1	Case 2	Case 3	Case 4
1	1009.25	891.45	814.31	611.35
2	1001.75	920.54	828.78	701.33
3	959.53	902.64	878.35	787.41
4	944.54	949.81	919.57	867.43
5	834.12	855.57	895.15	933.91
6	749.6	819.94	849.45	933.46
7	651.71	704.41	764.23	926.62
8	533.67	638.27	732.62	922.45

Table C-6: Moment (kip-ft.) for load cases 1 to 4 from Model 1-R for three lanes

Girder	Case 1	Case 2	Case 3	Case 4
1	984.56	858.25	774.61	576.37
2	996.93	914.16	825.52	686.87
3	979.09	925.34	896.69	802.64
4	963.42	968.5	944.03	893.9
5	864.06	887.08	921.33	957.42
6	757.88	830.63	866.79	950.85
7	634.18	696.01	759.56	926.01
8	504.09	603	693.95	889.99

Table C-7: Moment (kip-ft.) for load cases 1 to 6 from Model 2 for one lane

Girder	Case 1	Case 2	Case 3	Case 4	Case 5	Case 6
1	964	847	806	673	494	356
2	806	828	773	777	631	465
3	601	624	675	697	709	663
4	346	373	391	430	556	657
5	202	220	232	260	339	435
6	117	129	136	155	207	277
7	68	76	81	93	127	176
8	41	47	50	58	83	118

Table C-8: Moment (kip-ft.) for load cases 7 to 12 from Model 2 for one lane

Girder	Case 7	Case 8	Case 9	Case 10	Case 11	Case 12
1	250	177	122	85	60	42
2	344	252	180	131	95	70
3	528	383	282	211	158	119
4	624	613	443	345	266	206
5	608	622	660	561	436	352
6	375	521	657	707	699	605
7	246	336	456	623	773	805
8	171	243	346	482	658	948

Table C-9: Moment (kip-ft.) for load cases 1 to 8 from Model 2 for two lanes

Girder	Case 1	Case 2	Case 3	Case 4	Case 5	Case 6	Case 7	Case 8
1	1067.62	937.52	889	744.7	541.64	387.42	271.5	191.82
2	1023.83	1003.59	941.33	903.34	713.1	523.29	384.11	281.41
3	1028.06	987.79	1011.84	957.05	878.48	767.83	599.18	438.85
4	809.51	869.54	847.42	903.69	919.39	891.05	783.7	713.79
5	592.00	636.39	692.42	745.36	840.85	901.22	950.07	857.4
6	353.75	391.4	415.9	471.13	635.82	795.29	869.47	1003.14
7	221.00	247.8	264.39	305.2	416.14	558.36	790.63	914.84
8	145.78	165.81	178.2	209.57	296.69	417.95	593.92	841.42

Table C-10: Moment (kip-ft.) for load cases 1 to 8 from Model 2-R for two lanes

Girder	Case 1	Case 2	Case 3	Case 4	Case 5	Case 6	Case 7	Case 8
1	1068.41	938.14	889.51	745.05	541.6	387.03	270.93	191.08
2	1024.77	1004.21	941.86	903.61	712.96	522.87	383.33	280.32
3	1028.99	988.69	1012.65	957.82	878.88	767.81	598.87	438.29
4	809.95	870.11	848.07	904.45	920.21	891.75	784.04	713.84
5	591.84	636.32	692.39	745.45	841.28	901.92	950.89	858.06
6	352.96	390.75	415.31	470.64	635.56	795.38	869.97	1003.97
7	219.41	246.61	263.26	304.16	415.48	558	790.6	915.26
8	144.9	165	177.43	208.86	296.14	417.66	593.96	841.87

Table C-11: Moment (kip-ft.) for load cases 1 to 4 from Model 2 for three lanes

Girder	Case 1	Case 2	Case 3	Case 4
1	976.21	811.73	680.41	494.05
2	974.14	886.59	842.09	660.8
3	1040.06	1000.66	935.62	838.97
4	956.75	951.79	971.29	939.5
5	945.15	972.2	961.66	981.33
6	763.52	825.87	901.58	984.54
7	598.07	713.07	785.72	940.26
8	430.41	520.68	603.84	844.56

Table C-12: Moment (kip-ft.) for load cases 1 to 4 from Model 2-R for three lanes

Girder	Case 1	Case 2	Case 3	Case 4
1	976.64	811.89	680.4	493.57
2	974.43	886.45	841.75	660.16
3	1040.45	1000.86	935.73	838.77
4	957.25	952.37	971.79	939.82
5	945.39	972.51	962.06	981.87
6	763.19	825.75	901.58	984.81
7	597.32	712.46	785.25	940.19
8	430.00	520.00	603.63	844.8

Table C-13: Moment (kip-ft.) for load cases 1 to 6 from Model 4 for one lane

Girder	Case 1	Case 2	Case 3	Case 4	Case 5	Case 6
1	1093	940	882	714	474	298
2	896	911	850	845	671	473
3	629	667	725	759	785	732
4	320	364	391	448	613	737
5	145	175	193	235	347	477
6	54	70	80	104	172	265
7	12	19	23	35	68	121
8	--	--	1.86	2.13	16	42

Table C-14: Moment (kip-ft.) for load cases 7 to 12 from Model 4 for one lane

Girder	Case 7	Case 8	Case 9	Case 10	Case 11	Case 12
1	173	94	44	17	2.97	--
2	324	210	126	72	37	13
3	576	402	273	178	109	57
4	709	685	487	365	243	152
5	679	707	741	621	458	329
6	393	568	726	783	763	636
7	203	315	462	661	839	893
8	89	165	286	458	694	1071

Table C-15: Moment (kip-ft.) for load cases 1 to 8 from Model 4 for two lanes

Girder	Case 1	Case 2	Case 3	Case 4	Case 5	Case 6	Case 7	Case 8
1	1120.55	953.4	888.41	712.48	456.52	276.275	153.32	78.66
2	1097.5	1062.52	991.68	936.74	707.31	483.38	318.4	198.84
3	1104.6	1071.19	1096.38	1041.28	949.82	811.27	607.06	410.16
4	856.78	934.1	918.87	988.58	1021.09	985.81	854.41	746.18
5	589.33	651.92	717.43	789.19	920.25	999.48	1048.64	934.29
6	300.25	349.55	381.22	451.57	653.34	846.54	944.77	1087.46
7	131.37	160.61	179.53	225.79	355.49	526.76	794.87	958.5
8	41.09	56.53	66.87	94.35	178.29	312.72	521.36	828.68

Table C-16: Moment (kip-ft.) for load cases 1 to 4 from Model 4 for three lanes

Case 1	Case 2	Case 3	Case 4
970.69	764.67	610	386.2
995.77	887	829	615
1086.93	1045	975	858.31
1012.93	1014.85	1035	994.6
990.72	1029.91	1023.5	1043.73
771	848.98	933.88	1031
541	672	759.05	946.81
315	418	516.38	807.9

REFERENCES

AASHTO (2012). “AASHTO LRFD Bridge Design Specification”. American Association of State Highway and Transportation Officials, Washington, D.C.

Abendroth, R. E., Klaiber, F. W., and Shafer, M. W. (1995). “Diaphragm effectiveness in prestressed-concrete girder bridges”. *Journal of Structural Engineering*, *121*(9), 1362-1369.

Barr, P. J., Eberhard, M. O., and Stanton, J. F. (2001). “Live-load distribution factors in prestressed concrete girder bridges”. *Journal of Bridge Engineering*, *6*(5), 298-306.

Castine, S. (2017), "Development of High Early-Strength Concrete for Accelerated Bridge Construction Closure Pour Connections".*Masters Theses*. 498.

Cai, C. S. (2005). “Discussion on AASHTO LRFD load distribution factors for slab-on-girder bridges”. *Practice periodical on structural design and construction*, *10*(3), 171-176.

Cai, C. S., Shahawy, M., and Peterman, R. J. (2002). “Effect of diaphragms on load distribution of prestressed concrete bridges”. *Transportation research record*, *1814*(1), 47-54.

Chandolu, K. (2005) "Assessing the needs for intermediate diaphragms in prestressed concrete girder bridges". Master's Theses, 2829, Louisiana State University.

Culmo, M. (2011). “Accelerated Bridge Construction - Experience in Design, Fabrication and Erection of Prefabricated Bridge Elements and Systems”. FHWA-HIF-12-013, Federal Highway Administration.

Diversified Technology Consultants (2017). “Innovative Bridge Superstructure Cuts Construction Time”. *Teamdct*, (August 10, 2019)

Garcia, R. (2017). “Prefabricated Bridge Elements and Systems”. Center of Accelerating Innovation, U.S. DOT Federal Highway Administration.

Green, T., Yazdani, N., Spainhour, L., and Cai, C. S. (2002). “Intermediate diaphragm and temperature effects on concrete bridge performance”. *Transportation research record*, *1814*(1), 83-90.

Green, T., Yazdani, N., and Spainhour, L. (2004). “Contribution of intermediate diaphragms in enhancing precast bridge girder performance”. *Journal of performance of constructed facilities*, *18*(3), 142-146.

Li, L., and John Ma, Z. (2010). “Effect of intermediate diaphragms on decked bulb-tee bridge system for accelerated construction”. *Journal of Bridge Engineering*, *15*(6), 715-722.

Li, L., Ma, Z., Griffey, M. E., and Oesterle, R. G. (2009). “Improved longitudinal joint details in decked bulb tees for accelerated bridge construction: Concept development”. *Journal of Bridge Engineering*, *15*(3), 327-336.

Ma, Z., Chaudhury, S., Millam, J. L., and Hulsey, J. L. (2007). “Field test and 3D FE modeling of decked bulb-tee bridges”. *Journal of bridge engineering*, *12*(3), 306-314.

Milliam, J. L. (2004). “Single-lane live load distribution factor for decked precast, prestressed concrete girder bridges”. Master’s Theses, University of Alaska Fairbanks.

Millam, J. L., and Ma, Z. (2005). “Single-lane live load distribution factor for decked precast, prestressed concrete girder bridges”. *Transportation research record*, *1928*(1), 142-152.

PCI Northeast (2018). “Northeast Deck Bulb Tee Beam Details”. PCI Northeast Deck Bulb Tee Guidelines.

PCIMidwest. “Route 10 Northampton Street Bridge Over Manhan River”. *Pcimidwest-project*, (August 8, 2019).

Sengupta, S. and Breen, J. E., (1973). “The effects of diaphragms in prestressed concrete girder and slab bridges”. Research Report 158-1F, Project 3-5-71-158, Center for Highway Research, University of Texas at Austin, Texas.

Sithichaikasem, S., and Gamble, W. L. (1972). “Effects of diaphragms in bridges with prestressed concrete I-section girders”. University of Illinois Engineering Experiment Station, College of Engineering, University of Illinois at Urbana-Champaign.

Stanton, J., and Mattock, A. H. (1986) “Load Distribution and Connection Design for Precast Stemmed Multibeam Bridge Superstructures”. NCHRP Report 287.

Weeks, J. (2011). “Highways, Byways, And Bridge Photography”. *Johnweeks*, (August 8, 2019)

Wong, A. Y. C., and Gamble, W. L. (1973). “Effects of diaphragms in continuous slab and girder highway bridges”. University of Illinois Engineering Experiment Station, College of Engineering, University of Illinois at Urbana-Champaign.

Yousif, Z., and Hindi, R. (2007). “AASHTO-LRFD live load distribution for beam-and-slab bridges: Limitations and applicability”. *Journal of Bridge Engineering*, *12*(6), 765-773.

Zokaie, T. (2000). “AASHTO-LRFD live load distribution specifications”. *Journal of bridge engineering*, *5*(2), 131-138.